FINAL REPORT

PILOT PROJECT FOR MAXIMUM HEAT OF MASS CONCRETE

Mang Tia
Adrian Lawrence
Chris Ferraro
Tu Anh Do
Yu Chen

April 2013

Department of Civil and Coastal Engineering
Engineering School of Sustainable Infrastructure and Environment
College of Engineering
University of Florida
Gainesville, Florida 32611-6580

DISCLAIMER

The opinions, findings, and conclusions expressed in this publication are those of the authors and not necessarily those of the State of Florida Department of Transportation or the U.S. Department of Transportation.

Prepared in cooperation with the State of Florida Department of Transportation and the U.S. Department of Transportation.

SI (MODERN METRIC) CONVERSION FACTORS (from FHWA)

APPROXIMATE CONVERSIONS TO SI UNITS

SYMBOL	WHEN YOU KNOW	MULTIPLY BY	TO FIND	SYMBOL
LENGTH				
in	inches	25.4	millimeters	mm
ft	feet	0.305	meters	m
yd	yards	0.914	meters	m
mi	miles	1.61	kilometers	km

SYMBOL	WHEN YOU KNOW	MULTIPLY BY	TO FIND	SYMBOL
AREA				
in^2	square inches	645.2	square millimeters	mm^2
ft^2	square feet	0.093	square meters	m^2
yd^2	square yard	0.836	square meters	m^2
ac	acres	0.405	hectares	ha
mi^2	square miles	2.59	square kilometers	km^2

SYMBOL	WHEN YOU KNOW	MULTIPLY BY	TO FIND	SYMBOL
VOLUME				
fl oz	fluid ounces	29.57	milliliters	mL
gal	gallons	3.785	liters	L
ft^3	cubic feet	0.028	cubic meters	m^3
yd^3	cubic yards	0.765	cubic meters	m^3
NOTE: volumes greater than 1000 L shall be shown in m^3				

SYMBOL	WHEN YOU KNOW	MULTIPLY BY	TO FIND	SYMBOL
MASS				
oz	ounces	28.35	grams	g
lb	pounds	0.454	kilograms	kg
T	short tons (2000 lb)	0.907	megagrams (or "metric ton")	Mg (or "t")

SYMBOL	WHEN YOU KNOW	MULTIPLY BY	TO FIND	SYMBOL
TEMPERATURE (exact degrees)				
°F	Fahrenheit	5 (F-32)/9 or (F-32)/1.8	Celsius	°C

SYMBOL	WHEN YOU KNOW	MULTIPLY BY	TO FIND	SYMBOL
ILLUMINATION				
fc	foot-candles	10.76	lux	lx
fl	foot-Lamberts	3.426	candela/m^2	cd/m^2

SYMBOL	WHEN YOU KNOW	MULTIPLY BY	TO FIND	SYMBOL
FORCE and PRESSURE or STRESS				
lbf	poundforce	4.45	newtons	N
kip	kilo poundforce	4.45	kilo newtons	kN
lbf/in^2	poundforce per square inch	6.89	kilopascals	kPa

APPROXIMATE CONVERSIONS TO SI UNITS

SYMBOL	WHEN YOU KNOW	MULTIPLY BY	TO FIND	SYMBOL
LENGTH				
mm	millimeters	0.039	inches	in
m	meters	3.28	feet	ft
m	meters	1.09	yards	yd
km	kilometers	0.621	miles	mi

SYMBOL	WHEN YOU KNOW	MULTIPLY BY	TO FIND	SYMBOL
AREA				
mm^2	square millimeters	0.0016	square inches	in^2
m^2	square meters	10.764	square feet	ft^2
m^2	square meters	1.195	square yards	yd^2
ha	hectares	2.47	acres	ac
km^2	square kilometers	0.386	square miles	mi^2

SYMBOL	WHEN YOU KNOW	MULTIPLY BY	TO FIND	SYMBOL
VOLUME				
mL	milliliters	0.034	fluid ounces	fl oz
L	liters	0.264	gallons	gal
m^3	cubic meters	35.314	cubic feet	ft^3
m^3	cubic meters	1.307	cubic yards	yd^3

SYMBOL	WHEN YOU KNOW	MULTIPLY BY	TO FIND	SYMBOL
MASS				
g	grams	0.035	ounces	oz
kg	kilograms	2.202	pounds	lb
Mg (or "t")	megagrams (or "metric ton")	1.103	short tons (2000 lb)	T

SYMBOL	WHEN YOU KNOW	MULTIPLY BY	TO FIND	SYMBOL
TEMPERATURE (exact degrees)				
ºC	Celsius	1.8C+32	Fahrenheit	ºF

SYMBOL	WHEN YOU KNOW	MULTIPLY BY	TO FIND	SYMBOL
ILLUMINATION				
lx	lux	0.0929	foot-candles	fc
cd/m^2	candela/m^2	0.2919	foot-Lamberts	fl

SYMBOL	WHEN YOU KNOW	MULTIPLY BY	TO FIND	SYMBOL
FORCE and PRESSURE or STRESS				
N	newtons	0.225	poundforce	lbf
kPa	kilopascals	0.145	poundforce per square inch	lbf/in^2

*SI is the symbol for International System of Units. Appropriate rounding should be made to comply with Section 4 of ASTM E380.
(Revised March 2003)

1. Report No.	2. Government Accession No.	3. Recipient's Catalog No.

4. Title and Subtitle	5. Report Date
Pilot Project for Maximum Heat of Mass Concrete	April 2013
	6. Performing Organization Code

7. Author(s)	8. Performing Organization Report No.
Mang Tia, Adrian Lawrence, Chris Ferraro, Tu Anh Do & Yu Chen	00093793

9. Performing Organization Name and Address	10. Work Unit No. (TRAIS)
Department of Civil and Coastal Engineering Engineering School of Sustainable Infrastructure & Environment University of Florida 365 Weil Hall – P.O. Box 116580 Gainesville, FL 32611-6580	
	11. Contract or Grant No.
	BDK75 977-47

12. Sponsoring Agency Name and Address	13. Type of Report and Period Covered
Florida Department of Transportation 605 Suwannee Street, MS 30 Tallahassee, FL 32399	Final Report 03/28/11 – 5/01/13
	14. Sponsoring Agency Code

15. Supplementary Notes

16. Abstract

A 3-D finite element model was developed for prediction of early age behavior of mass concrete footing placed on a soil layer. Three bridge pier footings and one bridge pier cap in Florida were monitored for temperature development. The measured temperatures were compared with the results obtained from the model. Isothermal calorimetry testing was done on the cementitious materials of concrete mixtures to determine the energy released during hydration, which was then converted to temperature rise as inputs for the finite element model. Analysis of behavior of mass concrete placed directly on various types of soil was conducted. A user-friendly software called "DIANA Input File Generator" was developed to provide the needed input files to TNO DIANA software for modeling of typical mass concrete structures such as rectangular footings and columns.

The developed 3-D finite element model was found to be effective in predicting the thermal behavior of mass concrete structures at early ages, as the temperature predictions from the finite element modeling showed close agreement with those measured in the field. The in situ condition of the soil was found to have a great effect on the thermal behavior of the concrete footing and determines whether or not an insulation layer would be needed to reduce the temperature difference in the mass concrete and the likelihood for cracking. Dry soil with an R-value of 0.41 or greater (or thermal conductivity of 0.35 J/sec-m-°C or lower) would provide adequate insulation at the bottom of mass concrete footing in terms of preventing thermal cracking. However, for wet soil where its R-value is less than 0.41, an insulation layer between the soil and the concrete footing would be needed. The development of the user-friendly software "DIANA Input File Generator" provides a convenient and effective tool for generating the needed input files to the TNO DIANA software for analysis of typical mass concrete structures of rectangular footings and columns. It allows engineers and contractors who are not familiar with the detailed inputs to the TNO DIANA software to use this software conveniently and efficiently.

17. Key Words	18. Distribution Statement
Mass concrete; 3-D finite-element model; isothermal calorimetry; concrete footing; soil foundation; R-value; temperature differential; temperature monitoring; insulation; temperature logger; concrete at early age; TNO DIANA.	No restrictions.

19. Security Classif. (of this report)	20. Security Classif. (of this page)	21. No. of Pages	22. Price
Unclassified	Unclassified	168	

Form DOT F 1700.7 (8-72)   Reproduction of completed page authorized

ACKNOWLEDGMENTS

EXECUTIVE SUMMARY

Background and Research Needs

Florida Department of Transportation (FDOT) Standard Specification for Road and Bridge Construction requires that an analysis be made of the anticipated thermal developments in mass concrete elements for all the expected temperature ranges using the selected mix design, casting procedures, and materials. The current specification requires that a maximum allowable temperature of 180°F and differential between the concrete core and the exterior surface of 35°F not be exceeded. A previous FDOT-funded study based on laboratory mass concrete specimens has shown that finite element modeling could be used to predict the thermal behavior of mass concrete. Further research and development were needed to extend the finite element method to field applications such as columns, pier caps, and footings of various shapes, that are large enough to be classified as mass concrete. The developed testing and analysis procedures needed to be field-tested to verify their applicability and to make necessary modifications. After verification and proper adjustments, a user-friendly computer software with clear instructions should be developed so that the recommended testing and analysis procedures could be effectively implemented in the field.

Scope of Study

A finite element model using the commercially available TNO DIANA 9.4.4 software package (DIANA, 2012a) was developed for prediction of early age behavior of mass concrete footing placed on a soil layer. To evaluate the effectiveness of the model, four different mass concrete structures in Florida were monitored for temperature development. These four structures included three bridge pier footings and one bridge pier cap. The measured temperatures were compared with the results obtained from the model. Isothermal calorimetry testing was done on the cementitious materials of concrete mixtures to determine the energy

released during hydration, which was then converted to temperature rise as inputs for the finite element model. Analysis of behavior of mass concrete placed directly on various types of soil was conducted. A parametric study on the effects of dimensions of three types of rectangular footings on the maximum allowable temperature differential to prevent cracking in concrete was conducted. A user-friendly software called "DIANA Input File Generator" was developed to provide the needed input files to TNO DIANA software for modeling of typical mass concrete structures such as rectangular footings and columns.

Main Findings

The main findings from this study can be summarized as follows:

(1) The developed finite element model in this study was able to predict temperatures in mass concrete footings reasonably well, as observed from the fair agreement between the predicted and the measured temperatures in the field.

(2) The in situ condition of the soil upon which a concrete footing is directly placed affects the temperature development of the footing and determines whether or not an insulation layer would be needed to reduce the temperature difference in the mass concrete and the likelihood for cracking. Soil with an R-value of 0.41 or greater (or thermal conductivity of 0.35 J/sec-m-°C or lower) would provide adequate insulation at the bottom of concrete footing using a conventional concrete mix with 100% Portland cement (Mix 1) and with a volume-area ratio (V/A) of 13 ft or less to prevent thermal cracking. Thus, an insulating layer between the mass concrete and the soil would not be needed in such situation.

(3) With a V/A of less than 4.5 ft, under the same insulation condition and using the same concrete mix (Mix 1), a larger footing had a higher maximum temperature

difference, and lower crack index. However, with a V/A of 4.5 ft or greater, a larger

footing had a similar or slightly smaller maximum temperature difference, and an

almost constant crack index. Thus, cracking potential was not dependent on how

large a footing was when its V/A was 4.5 ft or greater.

(4) Rectangular footings that had the same V/A but different shapes (dimensional

proportions) would develop a similar maximum temperature, a similar maximum

temperature difference, and a similar crack index under the same insulation

condition.

(5) When the concrete of Mix 1 was used, footings with a V/A from 1.1 ft to 1.6 ft

reached a maximum temperature differential of 25.2°C before cracking. Footings

with a V/A from 1.7 ft to 4.4 ft reached a maximum temperature differential of

21.6°C, and footings with a V/A from 4.5 ft to 13.1 ft reached a maximum

temperature differential of 20.1°C before cracking. Thus, the required maximum

allowable temperature differential of 20 °C in mass concrete appears to be a

conservative and appropriate criterion.

(6) When Styrofoam with an R-value of 5.0 per inch was used, 0.5 inch would provide

adequate insulation for a footing with a V/A of around 1.0 ft; 1.0 inch would provide

adequate insulation for a footing with a V/A less than 4.0 ft; 1.25 inches would

provide adequate insulation for a footing with a V/A up to 13.0 ft. If another type of

insulating material is used, the required insulation thickness can be determined from

the material's R-value.

(7) The development of the user-friendly software "DIFG" provides a convenient tool

for generating the needed input files to the TNO DIANA software for analysis of

typical mass concrete structures of rectangular footings and columns. It allows engineers and contractors who are not familiar with the detailed inputs to the TNO DIANA software to use this software conveniently and efficiently.

Recommendations

Based on the findings from this study, the following recommendations are made:

(1) Bottom insulation should be used in concrete footings in the following cases: (a) Presence of water at the bottom of footing. (b) Footings with a V/A of 2.0 ft or less placed on soil with an R-value of less than 0.29 per in. (c) Footings with a V/A of greater than 2.0 ft and placed on soil with an R-value of less than 0.41 per in.

(2) The required insulation thickness method presented in this report should be used for footings to be constructed in the field.

(3) A database of rate of heat production of different cement blends should be developed. Isothermal calorimetry testing should be performed on the cementitious materials used in typical FDOT mass concrete mix designs to build a database of adiabatic temperature rise tables that can be used in the DIANA software for the modeling of mass concrete structures. The concrete mix designs that are to be analyzed consist of Type I/II Portland cement, ground-granulated blast furnace slag, Class F fly ash, ultra-fine fly ash, and silica fume, in various combinations and proportions.

(4) Thermal properties of soil in different in situ conditions should be evaluated and monitoring of footings directly placed on soil is needed to evaluate the predicted results. Since the properties of the soil upon which a mass concrete footing is placed greatly influence the thermal behavior of the concrete footing, further investigation

needs to be conducted to determine the R-values for different types of soil and under

different in situ conditions.

(5) Further development of the user-friendly software for mass concrete analysis should

be made. The present developed software is capable of generating input files of

rectangular footings on soil with options of insulation and with concrete properties

loaded from a file. Additional capabilities with further development of the software

can provide input files for pier caps and columns with rectangular or octagonal

shape. It should also have the capability of inputting the concrete properties from the

database to be developed.

TABLE OF CONTENTS

LIST OF TABLES

LIST OF FIGURES

CHAPTER 1
INTRODUCTION

1.1 Background and Research Needs

Section 346-3.3 of the Florida Department of Transportation (FDOT) Standard Specification for Road and Bridge Construction requires that an analysis be made of the anticipated thermal developments in mass concrete elements for all the expected temperature ranges using the selected mix design, casting procedures, and materials. The current approved method for this analysis is the procedure outlined in Section 207 of the ACI Manual of Concrete Practice. The specification requires that a maximum allowable temperature of 180°F and differential between the concrete core and the exterior surface of 35°F be not exceeded. A previous FDOT-funded study has shown that finite element modeling of laboratory mass concrete specimens is a viable option. The specimens studied were rectangular concrete monoliths. Further research and development is needed to extend the finite element method to field applications such as columns, pier caps, and footings of various shapes and are large enough to be classified as mass concrete. The developed testing and analysis procedures need to be field-tested to verify their applicability and to make necessary modifications. After verification and proper adjustments, a user-friendly computer software with clear instructions needs to be developed so that the recommended testing and analysis procedures can be effectively implemented in the field.

Although the FDOT Standard Specifications for Road and Bridge Construction require that the maximum temperature differential between the concrete core and the exterior surface does not exceed 35°F (20°C), it is not clear whether or not this limiting value is dependent on a footing's dimensions. This research investigates the effects of a footing's dimensions on the maximum allowable temperature differential to prevent cracking in the concrete. This study also

1

investigates the thermal performance and cracking risk of mass concrete footings placed directly and indirectly on soil, and determines the required insulation to prevent early-age cracking in the concrete.

1.2 Objectives of Research

The specific objectives of the research are:

- To develop a 3-D finite element model of mass concrete footings and compare the predicted temperatures from the model with measured temperatures from selected mass concrete structures in Florida.

- To evaluate the effects of thermal properties of soil on the temperature development and thermal cracking in mass concrete footings placed directly on soil.

- To investigate the effects of a footing's dimensions on the maximum allowable temperature differential to prevent cracking induced by thermal contraction.

- To provide FDOT with user-friendly and effective computer software and laboratory testing procedure for analysis of mass concrete structures.

1.3 Research Approach

The research is an analytical study supplemented by laboratory testing and field testing. The overall research approach is presented in a flow chart in Figure 1-1. The main tasks performed are as follows:

- Literature review on the behavior of mass concrete at early age and review of finite element method for predicting temperatures, thermal stresses, and cracking potential in mass concrete structures.

- Finite Element Modeling of Mass Concrete Structures: The selected mass concrete structures including rectangular footings, columns and pier caps were modeled. The analyses involved thermal analysis, stress analysis, and cracking prediction. The temperature predictions from the finite element model were compared with the temperatures measured in the field.

- Laboratory Testing Program: The material properties which were needed as input parameters for the finite element modeling were obtained in this laboratory testing program. The input parameters needed for the envisioned finite element modeling included the following:

  (1) Cement Heat of Hydration: Obtained via Isothermal Calorimetry Testing (University of Florida Method (Tia et al., 2010))

(2) Specific Heat Capacity (University of Florida Method (Tia et al., 2010))

(3) Activation Energy of Cementitious Material (ASTM 1074)

(4) Coefficient of Thermal Expansion of Concrete (AASHTO TP 60)

(5) Modulus of Elasticity for Concrete (ASTM C469)

(6) Splitting Tensile Strength of Concrete (ASTM C496)

(7) Poisson's Ratio of Concrete (ASTM C469)

(8) Conductivity of Construction Materials
   a) Concrete
   b) Formwork
   c) Insulating Material

(9) Heat Capacity of Construction Materials
   a) Concrete
   b) Formwork
   c) Insulating Material

- Instrumentation and Monitoring of Selected Mass Concrete Structures: Temperature sensors were installed on the selected mass concrete structures.

- Comparison of Predictions from Finite Element Modeling with Field Measurements: Comparisons were made between the predicted temperatures from the finite element model and the measurements from the instrumented mass concrete structures. Necessary adjustments in the finite element modeling were made as needed. The results from the finite element modeling were used to identify areas where cracking was likely to occur.

- Development of Computer Software for Mass Concrete Structures in Florida: As a by-product, a user-friendly computer program was developed for generating inputs to the DIANA software for analysis of some common mass concrete structures such as rectangular footings, columns and pier caps.
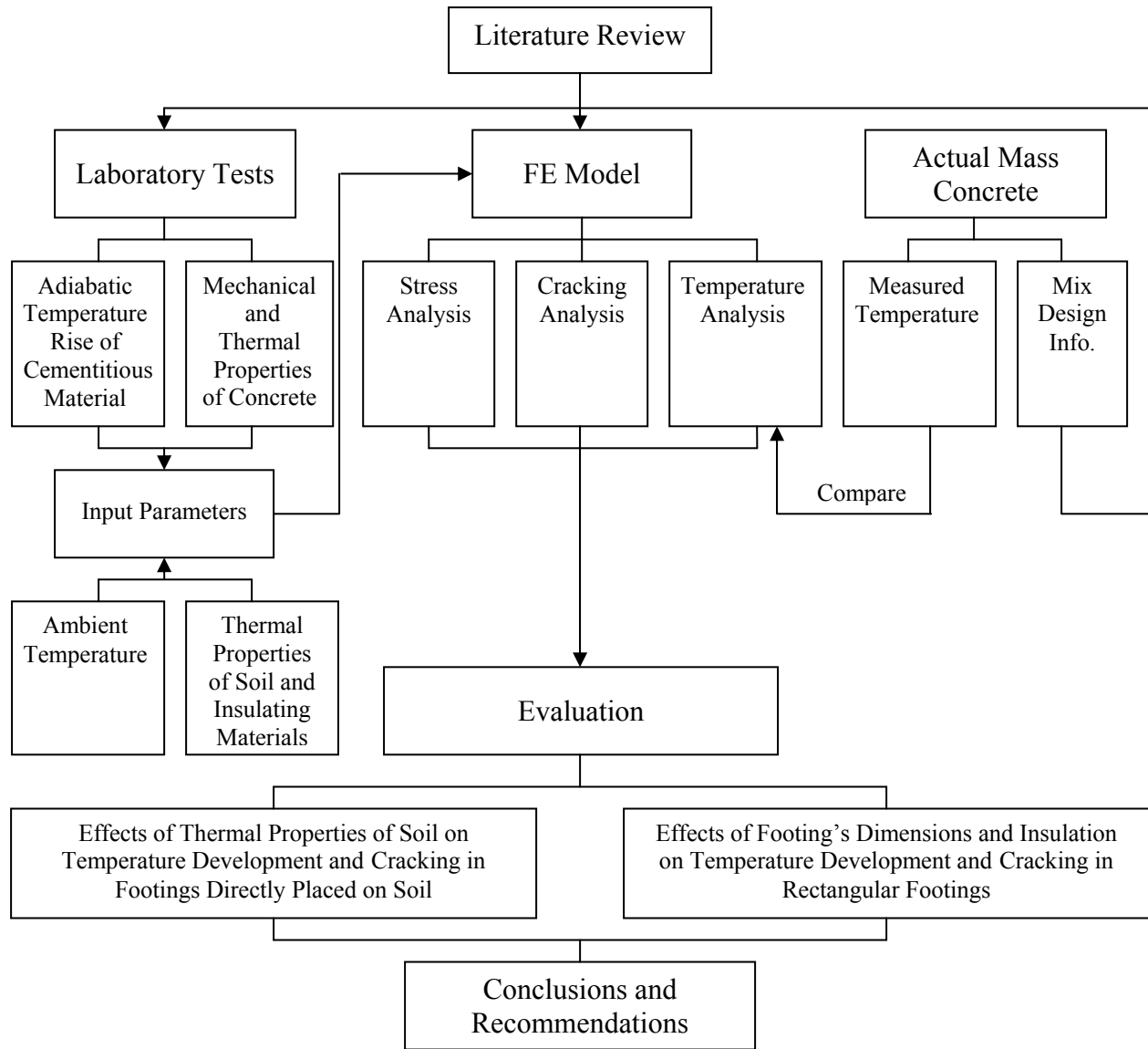
Figure 1-1. Research approach diagram.

1.4 Outline of Report

Chapter 2 presents a literature review on the behavior of mass concrete at early ages and a review of finite element modeling for predicting temperatures, thermal stresses, and cracking potential in mass concrete structures.

Chapters 3 and 4 discuss the finite element modeling including input parameters, material model, structural model, element types, and boundary conditions used in the thermal and stress analyses.

Chapter 5 describes instrumentation and monitoring of selected mass concrete structures and discusses the measured results.

Chapter 6 presents the comparisons of the finite element results with the field measurements.

Chapter 7 presents the analysis on the effects of thermal properties of soil on temperature development and thermal cracking in mass concrete footings.

Chapter 8 presents the investigation on the effects of a footing's dimensions on temperature development and thermal cracking in the concrete, and the determination of the required insulation thickness for footings.

Chapter 9 presents the development of computer program for generating inputs to the DIANA software for analysis of some common mass concrete structures such as rectangular footings, columns and pier caps in Florida.

Chapter 10 presents the findings and conclusions from this study, and recommendations for future research.

CHAPTER 2
LITERATURE REVIEW

2.1 Overview of Literature Review

Mass concrete is defined by the American Concrete Institute (ACI) as "any volume of concrete with dimensions large enough to require that measures be taken to cope with generation of heat from hydration from cement and attendant volume change to minimize cracking." Increasingly, this definition refers to a larger spectrum of structures, but most importantly applies to concrete dams and large concrete foundations, the failure of which can have disastrous consequences to human life and property. For this reason, the study and understanding of mass concrete has been of interest to engineers for the last 70 years.

Along with the observation of mass concrete experiments at early ages, numerical models have been developed in the past decades to investigate the early-age behavior of mass concrete and predict thermal cracking potential in mass concrete structures.

This chapter presents a literature review on the methods for analysis of mass concrete structures.

2.2 Two-Dimensional Finite Element and Finite Difference Analyses

In 1998, Radovanovic conducted a 2-D finite element (FE) analysis with the aid of the commercial software ANSYS to predict the early stage behavior of concrete of a dam structure. The analysis consisted of two theoretical models, namely a transient thermal model and a transient stress model. The finite element analysis sought to investigate whether the residual thermal stresses caused by the heat of hydration of the massive concrete pour were responsible for the apparent loss of strength in the construction joints. The early thermal behavior of a 0.6-m × 0.6-m laboratory concrete specimen and a dam structure model consisting of an upper and lower block cast 102 hours apart were modeled and observed. The thermal characteristics of

interest were the temperature field, thermal flux and thermal gradient. The Long Spruce Dam in northern Manitoba, Canada, that was found to have a crack that runs from the downstream side to the upstream side of the structure, was used as a case study. The thermal properties of the concrete in the laboratory specimen model were assumed to be independent of time and temperature during hydration. The thermal conductivity was assigned a constant value of 4.1 KJ/m-hr-°C, and the specific heat was assigned a value of 1971 KJ/m^3 -°C, obtained from literature. The ambient temperature in the laboratory analysis was also kept constant at 23°C to represent a controlled environment. For the dam structure model, the thermal properties were slightly different to reflect the use of larger aggregate. The initial temperature of the concrete was set at 10°C because of the use of ice water to pre-cool the large blocks. The boundary condition of convection is imposed on all sides except the bottom where a prescribed temperature is described. For the stress analysis, the bottom surface is constrained in all directions, representing the contact friction of the block resting on the floor. The analysis for the laboratory specimen model was conducted in six-hour load steps. The beginning of thermal process in the dam structure model was analyzed every six hours, and then increased to every 12 hours, then finally every 24 hours. The adiabatic temperature rise resulting from the heat of hydration was calculated using the expression developed and presented by Tanabe et al. (1986). The highest temperature was found to occur in the middle section of the specimen and decreased as it got closer to the sides of the model. This confirms the theory that the outer section of the concrete loses heat more quickly than the middle because of its greater exposure to the atmospheric conditions.

Radovanovic (1998) found that the 0.6-m × 0.6-m laboratory specimen was too small to realistically predict the behavior of massive concrete structures. This led to the enlargement of

the FE model by two, five and ten orders of magnitude. The size that came closest to a realistic

characterization of the behavior of the Long Spruce Dam was the 6-m × 6-m model. However

the maximum temperature for this size model was much higher than the dam specimen. The

reason given by Radovanovic (1998) was that the dam specimen was cast in September, when

the outside temperature was much lower than the initial temperature used for the laboratory

specimen. Radovanovic (1998) concluded that assumptions made in the calculation of the heat

generation rates, material properties and boundary conditions were reasonable and that the finite

element algorithm was accurate enough to predict the early age thermal behavior of the

laboratory concrete specimen and dam. Afterwards, a finite element stress analysis of the

laboratory specimen and the dam were conducted. As a worse-case scenario, the maximum stress

occurring in the models were considered as the residual stress. The process of hardening was

implemented by calculating the development of the modulus of elasticity of the concrete with

time based on the ACI charts. Radovanovic (1998) concluded that the results of the analysis

showed that the stresses produced by the thermal gradients were significant enough to cause

cracking in the early age concrete.

Riding (2007) developed a software package named ConcreteWorks based on a plane

strain finite-difference scheme that involved calculations of the temperature development for

several types of concrete members and the thermal stress cracking probability for several mass

concrete members. A temperature prediction model was developed to predict the concrete

temperature development, including the interaction between the concrete edges and the

environment. Over 12 mass concrete members, a bridge deck, and several precast concrete

beams were instrumented for temperature to calibrate the temperature prediction module in

ConcreteWorks. According to Riding (2007), rectangular footings had some unique features that

required special considerations for modeling. When footings were modeled in 2-D, ConcreteWorks assumed a vertical cross-section of the footing as shown in Figure 2-1 with no heat transfer perpendicular to the cross section. The heat exchange between the footing and the environment was dependent on: the formwork, cure blankets and plastic used, soil conditions, weather, orientation of the footing, shading from scaffolding and embankments, and heat conduction from the concrete interior. Solar radiation, atmospheric radiation, irradiation from the footing, and the radiation exchange between the vertical surface and form horizontal cross bracing models were used in the side and top boundary condition calculations. Radiation emitted by the ground surface was assumed to be incident on the side surface only. If the user chose to shade the sides of the footing because of scaffolding or the embankment, then the solar radiation was set to zero. Conduction to or from the soil underneath the footing was modeled by assuming a constant depth of soil. The initial temperature of the soil was set to the user-defined average soil temperature. The temperature at the bottom of the modeled soil was set to the user-defined average soil temperature. Figure 2-2 shows how the rectangular footing was modeled. Symmetry was assumed in the model in the width and length (when calculated in three dimensions) direction.

Riding (2007) concluded that from the concrete member temperature data measured, the concrete temperature prediction performed well. The average absolute error for the measured temperatures to the predicted member temperatures ranged from 0.5 to 4.6°C (1.0 – 8.4°F). However, the footing model might deviate from the actual member stresses because the stress in the third dimension might not be small relative to the other two dimensions.

2.3 Three-Dimensional Finite Element Analysis

A very early 3-D FE model was introduced by Machida and Uehara (1987) for forecasting thermal cracking in massive concrete using the ADINAT and ADINA programs. A

wall structure consisting of reinforced concrete measuring 1.0 m thick, varying height of 3.9 m to

4.73 m, and 15.0 m long cast on a 1.5-m thick basemat concrete slab, was instrumented with

thermocouples, effective stress meters, mold type strain gauges, and non-stress strain gauges, to

capture the temperatures, strain and stress responses at different locations within the wall, as

shown in Figure 2-3. The finite element thermal model consisted of half of the concrete wall,

basemat slab, and the soil beneath as shown in Figure 2-4. The heat transfer analysis of the

exothermic phenomenon cement's heat of hydration, and the phenomena of heat conduction and

convection was performed, then followed by a thermal stress analysis for the mechanical

characteristics. The heat generation rate for the concrete used in the wall was calculated by

differentiating with respect to time the equation for adiabatic temperature rise developed by

Tanabe et al. (1986). A comparison of the thermal analysis results with the experimental results

revealed that the maximum measured temperature occurred along the mid-length of the wall and

was 2.1°C higher than the maximum analytical temperature which also occurred along the mid-

length of the wall model. After the peak temperature was obtained, the analytical temperature

decrease was larger than the experimental, but after 12 days, the temperature of the structure

equaled the ambient temperature. The difference in the estimation of temperature decrease was

attributed to the difference in the assumed heat convectivity in the model and the actual

convection and to the variance in atmospheric temperature of the experimental wall instead of

the assumed constant temperature in the model. The stress analysis model was similar to the one

used in the thermal analysis. It was assumed that no sliding took place between the basemat and

the subsoil. The degrees of freedom were constrained in the direction perpendicular to the

structural symmetry plane and perpendicular to the subsoil's outside surface plane. The

compressive and tensile strengths and elastic modulus of the wall were calculated using

empirical formulas that related their development to the temperature of the hydrating concrete. Constant values for the Poisson's ratio and coefficient of thermal expansion were also assumed. The results showed that the maximum compressive stress occurred in the mid-length one day after concrete placement in both the experiment and finite element analysis. The compressive stress became a tension stress in the middle and bottom of the wall as the concrete aged. The upper mid-length of the structure experienced a small compression peak at 18 hours, which then became a tensile stress, peaking after about 2 days and becoming a compressive stress again peaking at 8 days after placement. On the other hand, the finite element analysis results showed no clear compressive stress peak but a tensile peak at 60 hours, after which it began to decrease but remained in the tensile stress region. Again, the difference in the measured and analytical results for the mid-length point close to the surface was attributed to the real atmospheric conditions of the structure being different than the assumed constant values assigned in the finite element model.

Ayotte et al. (1997) focused on developing a methodology, based on finite elements, that could be used to predict the heat generated and resulting thermal stresses in mass concrete. The study included both an experimental component and a modeling component. Three concrete monoliths were built directly on bedrock in the St. James Bay Territory in Northern Quebec, Canada, on the site of a major hydroelectric project. The dimensions of the monoliths were 2 m wide, 10 m long, and 2 to 3 m high, with the height depending on the bedrock profile. Each monolith was instrumented with 26 T-type (Copper-Constantan alloy) thermocouples to monitor temperature distribution with time, and 8 pairs of mechanical strain targets on the skin reinforcement to measure the induced strain (see Figure 2-5). To observe the performance of the concrete when subjected to severe freeze thaw cycles, the monoliths were cast in February inside

large individual heated shelters in which the temperature was maintained at 30 to 32°C during the construction phase.

The 2-D and 3-D FE modeling conducted by Ayotte et al. (1997) consisted of the concrete thermal behavior using the finite element software ADINA-T and the mechanical response (stresses and strains) using ADINA. To accommodate simultaneous changes of temperature and mechanical property, a modeling technique which employed a step-by-step incremental approach of calculating the thermally induced strains was developed to bypass the link between ADINA-T and ADINA. The cement type used was Portland cement Type 20M which was specially made for Hydro-Quebec, so a generic function for the heat of hydration as a function of time was obtained by interpolating between the known functions of Type 20 and Type 50 cements, which was then calibrated by comparing the calculated temperatures with the temperatures measured by the thermocouples. The values for other concrete thermal properties, which included specific heat, the thermal conductivity and convection coefficient, were obtained from various literature sources. Radiation was not considered because the monoliths were built inside shelters which blocked the heat radiation. Convection boundary conditions were used to model the heat loss to the ambient air, while rock elements were added below the concrete elements for the heat dissipation through the rock foundation. The structural model for the monolith was identical to the three-dimensional model used in the thermal analysis. Displacements were restricted in the directions of the planes of symmetry, and in all directions at the bottom of the rock elements. The mechanical properties, which included elastic modulus, compressive and tensile strength, were modeled as varying with time, while the coefficient of thermal expansion was given a constant value of 10 $\mu\varepsilon$/°C. To include creep and relaxation, an effective reduced elastic modulus that accounts for the reduction in stresses was adopted.

Ayotte et al. (1997) found that the calculated temperature at the center of the monolith model followed almost perfectly the temperatures measured experimentally. However there was a gap between the temperatures calculated at a point near the top of the monolith and those experimentally measured. In the structural analysis, it was found that the largest strains were located at the top of the monolith where there was the least restraint, while the strains at the base were very small due to the restraint of the foundation. It was also observed that the stress variation on the top surface of the monolith was in tension while compressive stresses were computed on the vertical faces due to the insulating effect of the formwork which limited the temperature difference between this surface and the core.

Lawrence et al. (2012) used a 3-D finite element analysis to study the effects of the variation in hydration rates on the distribution of temperatures, the thermal gradients, and resulting stresses. His finite element model was successfully verified by performing analyses on eight 1.07-m × 1.07-m × 1.07-m (3.5 ft × 3.5 ft × 3.5 ft) concrete blocks containing four different concrete mixtures. The finite element model of one-fourth of the concrete block with insulation is illustrated in Figure 2-6. All of the concrete mixes used in this study had water to cementitious material ratio of 0.5. Mix 1 consisted of 100% Type I Portland cement concrete; Mix 2 had 50% of the Portland cement mass replaced by ground granulated blast-furnace slag; Mix 3 contained 35% Class F fly ash; and Mix 4 was a blend of 50% Portland cement, 30% granulated blast furnace slag, 20% Class F fly ash. The concrete blocks were cast in a controlled laboratory environment in which the ambient temperature remained constant and the flow of air kept at a minimum for the duration of the monitoring period. The model of the blocks was constructed using the adiabatic temperature rise data for each concrete mixture. These adiabatic temperatures were obtained by measuring the hydration energy produced when the various combinations of

13

the cementitious components are mixed with water in an adiabatic calorimetric chamber. The

other properties used to model the thermal behavior of the concrete blocks were the activation

energy, the specific heat, and the thermal conductivity (which was derived from diffusivity

testing on cylinders made from sampling the concrete used in each block mixture), which were

also measured experimentally. The models also utilized the thermal material properties of the

formwork and insulation, as well as the mechanical properties of each concrete block measured

from cylindrical and prismatic test specimens. The predicted temperature profiles in his model

closely agreed with those from the experiment, and thermal cracking which occurred in the

concrete blocks, as shown in Figure 2-7, were very similar in location to those predicted in the

finite element models. The results of his study also show that cracking in mass concrete is more

dependent on the attained early age strength of concrete than the magnitude of the maximum

temperature differential.

2.4 Adiabatic Temperature Rise Model

Past research leading to the creation of numerical models for the prediction of

temperature distribution in mass concrete primarily focused on using generic heat generation

functions for the calculation of adiabatic temperature rise (Machida and Uehara, 1987;

Radovanovic, 1998; Ayotte et al., 1997). The adiabatic temperature rise resulting from the heat

of hydration was calculated using the expression developed and presented by Tanabe et al.

(1986):

$$T(t) = K(1 - e^{-\alpha t}) \tag{2-1}$$

where   T = temperature (°C)

t = time (days)

K = constant based on casting temperature (°C)

α = constant based on casting temperature

The values for K and α are obtained from the plots in Figure 2-8.

The total amount of heat generated was then calculated by the following equation:

$$Q(t) = C_P \rho(t) = KC_P \rho(1 - e^{-\alpha t}) \qquad (2\text{-}2)$$

where C_p = specific heat capacity of the concrete (J/g-°C)

ρ = density of the concrete (g/m^3)

t = time (days)

K = constant based on casting temperature (°C)

α = constant based on casting temperature

And the rate of heat generation calculated as:

$$R(t) = KC_P \rho \alpha e^{-\alpha t} \qquad (2\text{-}3)$$

Recently, consideration of supplementary cementitious materials has been taken, and calculated adiabatic energy rise obtained from laboratory or field tests has been used as inputs for finite element models to account for better prediction of behavior of concrete at early ages (Riding, 2007; Ferraro, 2009; Tia et al., 2010; Lawrence et al., 2012). Tia et al. (2010) investigated three calorimetry methods for the measurement of heat generation in concrete materials: isothermal conduction calorimetry (Evju, 2003), semi-adiabatic calorimetry, and Sure-Cure/adiabatic calorimetry. Tia et al. (2010) found that of the three methods investigated, the isothermal calorimetry method was determined to be the most appropriate method for the quantification and modeling of heat generation of cementitious materials at early ages.
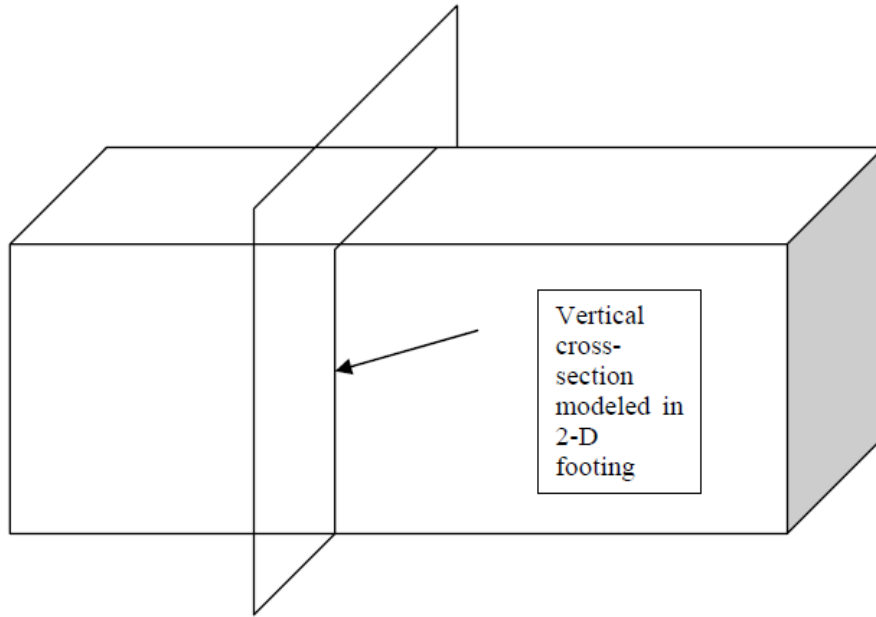
Figure 2-1. Diagram of the vertical cross-section assumed in modeling a 2-D footing (Riding, 2007).
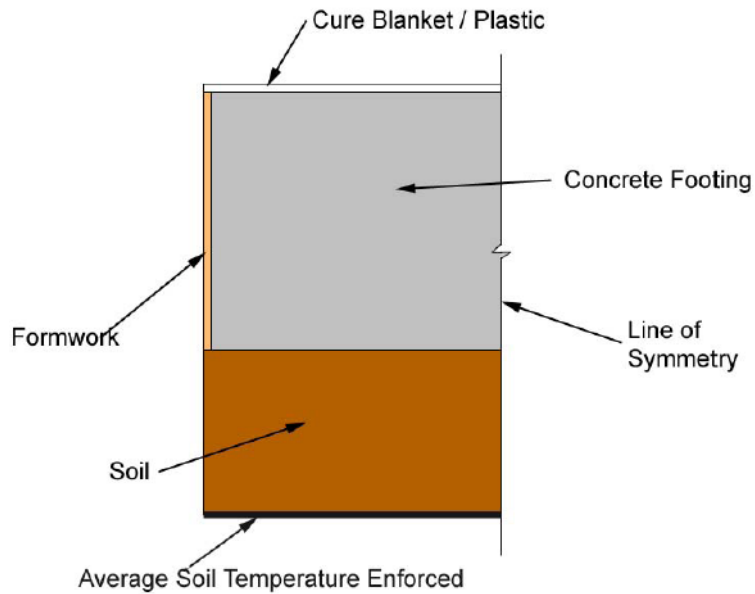
Figure 2-2. Rectangular footing model (Riding, 2007).
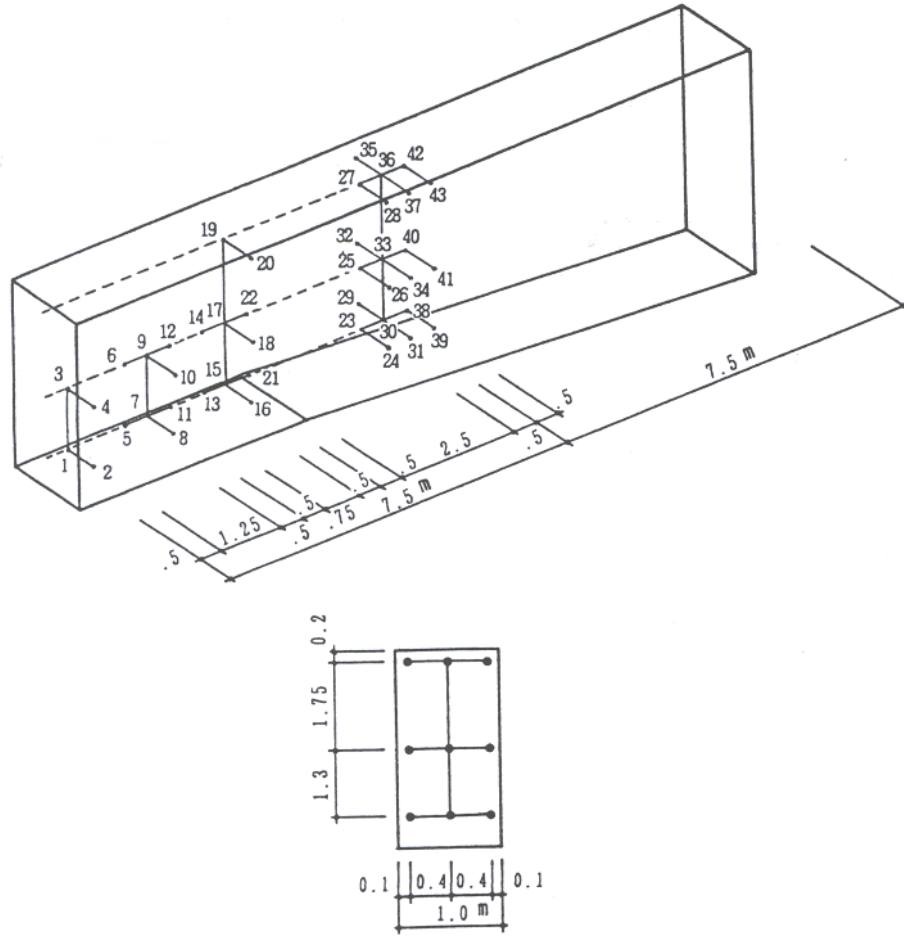
Figure 2-3. Locations for temperature and stress measurements in a reinforced concrete wall (Machida and Uehara, 1987).
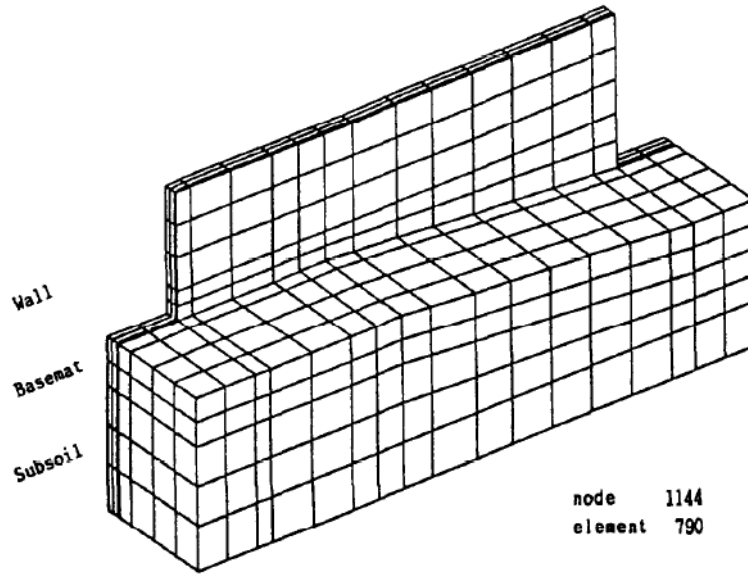
Figure 2-4. Finite element mesh (Machida and Uehara, 1987).
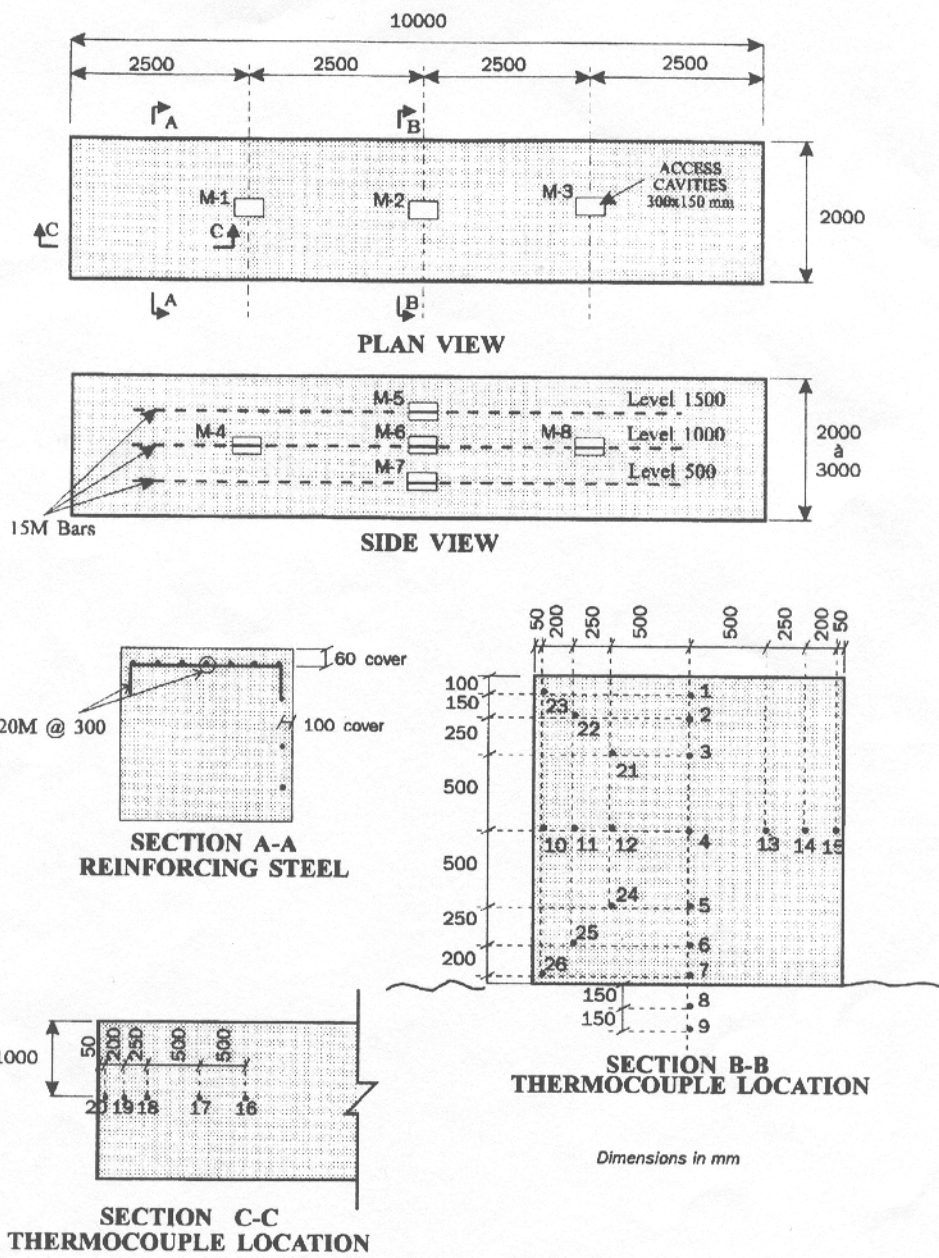
Figure 2-5. Thermocouple and strain gauge locations in the James Bay concrete monolith (Ayotte et al., 1997).

19
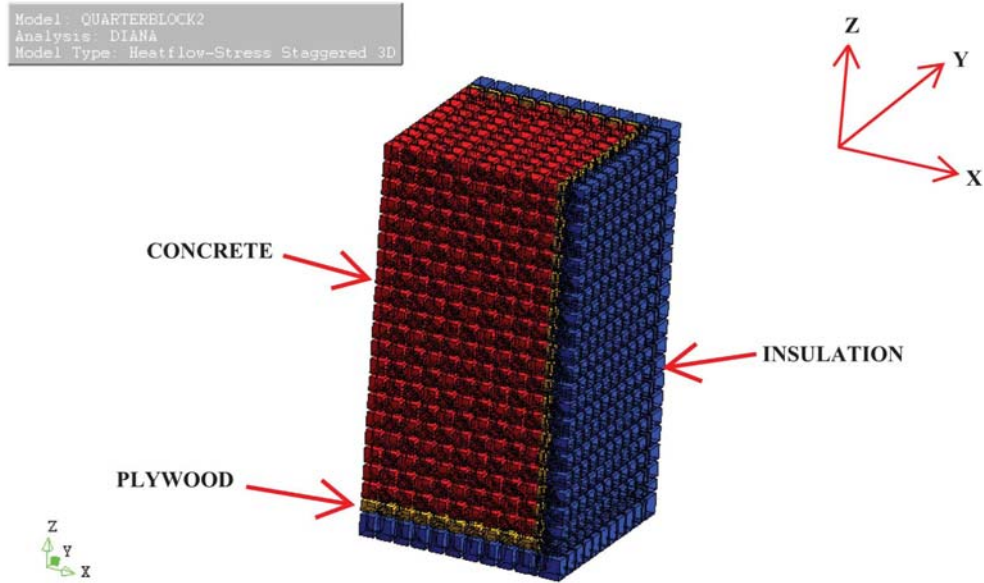
Figure 2-6. Finite element model of one fourth of the concrete block with insulation (Lawrence et al., 2012).

Figure 2-7. Typical location and distribution of cracking found in experimental blocks (Lawrence et al., 2012).
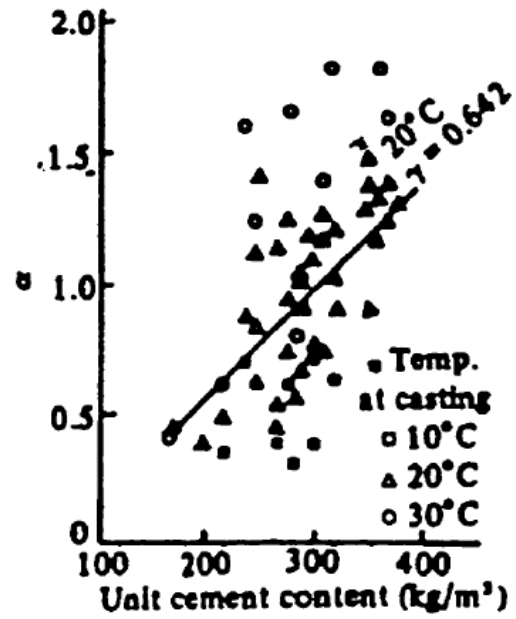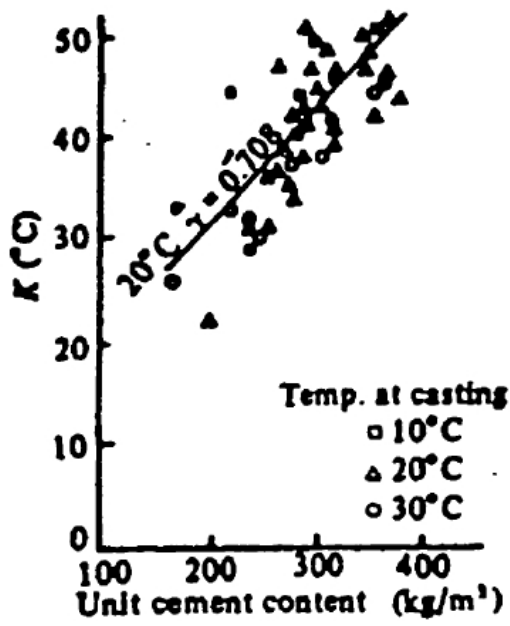
Figure 2-8. K and α values of adiabatic temperature rise (Radovanic, 1998).

CHAPTER 3
FINITE ELEMENT THERMAL MODEL

3.1 Overview of Finite Element Thermal Model

The modeling of the early age thermal behavior of concrete was conducted with the aid

of the commercially available TNO DIANA 9.4.4 (2012a) software package. This software

package was chosen because it offers a wide range of material models for the analysis of

nonlinear concrete material behavior, including the behavior of young hardening concrete. It can

make the assessment of the temperature development due to the cement hydration and the

computation of the associated stress development within the concrete mass (Lawrence, 2009;

Lawrence et al., 2012). Main modeling features utilized are:

- Equivalent age calculation;
- Temperature and time dependent material properties; and
- Crack index calculation to assess risk of cracking.

The finite element analysis utilized DIANA's 'Heatflow-Stress Staggered 3D' feature, in

which the thermal analysis is combined with a subsequent structural analysis. The model

comprises two domains: one for the thermal flow analysis; and one for the structural analysis.

These domains overlap for a considerable part of the analysis and so reside in a domain called

the 'flow-stress domain'.

Formwork used in the construction of massive concrete structures, including plywood

and polystyrene foam, was explicitly modeled. Since researchers were interested only in their

effects on the transfer of the thermal energy generated by the concrete, these materials were

modeled with flow elements, and thus, are only active in the thermal analysis. The concrete,

however, is active in both the thermal analysis and structural analysis, and therefore, lies in the

flow-stress domain. For this reason, the concrete is modeled with a quadratically interpolated

structural element that is converted during the thermal analysis to a linearly interpolated flow element.

Although the reinforcing steel in the concrete conducts heat rapidly, it was not modeled in the thermal model due to its complexity of geometry.

3.2 Element Selection

As stated above, the concrete in this analysis is active in the flow-stress domain and therefore is modeled with a structural element. For this, we selected the structural element CHX60, a three dimensional twenty-node brick element that is converted to the three dimensional eight-node HX8HT isoparametric brick element for the thermal analysis. Both types of elements, shown in Figure 3-1, have coinciding corner nodes. However, because the structural CHX60 element is quadratically interpolated and element HX8HT is a linearly interpolated element, the mid-nodes of the CHX60 are disregarded in the thermal analysis. The basic theory and required material properties needed for the structural analysis with element CHX60 will be discussed in further detail in Chapter 4.
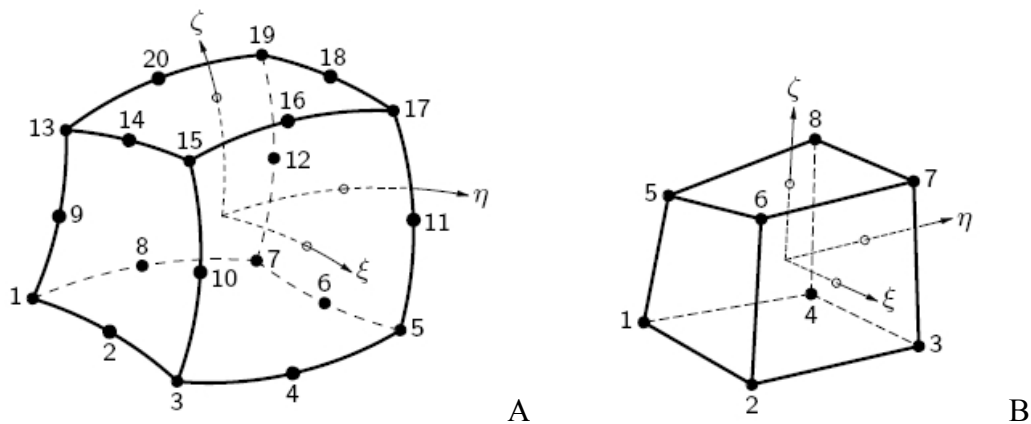
Figure 3-1. Elements used to model early age concrete behavior. A) Twenty-node isoparametric solid brick element CHX60. B) Eight-node isoparametric brick element HX8HT.

23

Element HX8HT is effective in simulating the phenomenon of convection-diffusion, and is especially useful for the analysis of heat transfer problems. It utilizes linear interpolation and Gauss integration with a 2 x 2 x 2 integration scheme. Heat transfer is modeled by assigning the thermal conductivity and heat capacity of the concrete, where the conductivity can be modeled as isotropic, orthotropic or anisotropic, while the heat capacity is always isotropic. Both the conductivity and capacitance may be constant or depend on temperature, or time or both. For the model described in this research, both the conductivity and heat capacity were modeled as constant.

Additional properties used to model the internal heat generation of the concrete are the Arrhenius constant (activation energy divided by the universal gas constant), and the heat generation function, which can either be a table that provides a direct description of the heat production rate with respect to the degree of hydration, or a table that describes the adiabatic temperature rise, in degrees Celsius (°C), with respect to time.

The plywood and polystyrene were directly modeled with element HX8HT, using each of its conductivity and heat capacity to describe the way the heat would be transferred between the concrete, plywood and polystyrene.

The boundary convection was modeled using the BQ4HT element, shown in Figure 3-2, which is a four-node isoparametric quadrilateral element specially used to describe boundaries in three-dimensional thermal analyses. It uses linear interpolation and Gauss integration in its computational scheme. The four nodes in this element were modeled to coincide with the corner nodes of the surface of the brick elements they lie on.

24
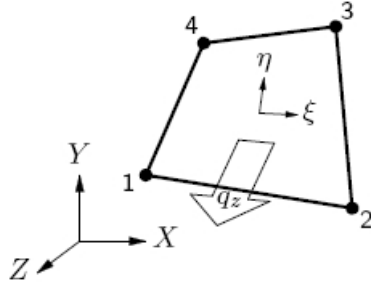
Figure 3-2. Four-node isoparametric boundary element (BQ4HT).

3.3 Input Parameters

3.3.1   Heat of Hydration

To properly model the behavior of hydrating concrete, knowledge of the heat produced during the hydration reaction, as well as both the material properties of the concrete itself and the environmental conditions in which it is placed are needed.

As previously stated, the heat produced during hydration is a function of the temperature history of the concrete. The momentary heat production rate is defined as (DIANA, 2012b):

$$q_v(r, T) = \alpha q_r(r) q_T(T) \tag{3-1}$$

where q_v = momentary heat production rate (J/m^3-s)

   r = degree of reaction

   T = temperature (°C)

   α = maximum value of the heat production rate (J/m^3-s)

   q_r = degree of reaction dependent heat production (scaled to one)

   q_T = temperature dependent heat production, and,

$$q_T(T) = \exp\left(\frac{\dfrac{E_a}{R}(r, T)}{T + 273}\right) \tag{3-2}$$

where E_a = the activation energy of the concrete (J/mol)

R = the universal gas constant (8.3144 J/mol-°C)

The heat production rate, q_r, which is dependent on degree of reaction can also be determined by DIANA using preprocessing. The temperature history produced under adiabatic hydration conditions is used as the input in this case. DIANA derives the heat production q(t) from

$$q(t) = c(T,r)\frac{\partial T}{\partial t}$$ (3-3)

where c(T,r) = the capacitance dependent on temperature and degree of reaction.

DIANA then approximates the degree of reaction and the temperature dependent heat production,

$$r_m = \frac{Q_m}{Q_n}$$ (3-4)

$$Q_m \approx \sum_{i=1}^{m} c(T_i^*, r_i^*)\Delta T_i$$ (3-5)

where n = specified time points

m = 1,…,n

and $\Delta T_i = T_i - T_{i-1}$ (3-6)

$$r_i^* = \frac{r_{i-1} + r_i}{2}$$ (3-7)

$$T_i^* = \frac{T_{i-1} + T_i}{2}$$ (3-8)

Finally, DIANA approximates $\partial T/\partial t$ numerically at m = 1,…,n points and uses equations (3-1) and (3-2) to calculate the corresponding degree of reaction dependent heat production rate $q_{r,m}$

$$q_m = c_m \frac{\partial T}{\partial t} \approx c \frac{T_{m+1} - T_{m-1}}{t_{m+1} - t_{m-1}} \tag{3-9}$$

$$\alpha q_{r,m} = \frac{q_m}{q_{T,m}} \tag{3-10}$$

The preprocessing method was utilized in this research. This method was chosen because the adiabatic temperature rise with respect to time could be conveniently input into DIANA directly.

Power data obtained from isothermal calorimetry testing on a cementitious mixture, as illustrated in Figure 3-3, can be integrated with respect to time to obtain the energy rise,

$$Q = \int_{t=0}^{t} Pdt \tag{3-11}$$

which is then approximated to the energy rise of the hydrating concrete made from the mixture.

Finally, the adiabatic temperature rise, presented in Figure 3-4, is calculated from the energy using the relationship described by the first law of thermodynamics and expressed in Equation 3-12. This method was used to maintain consistency in the type of input used to describe the concrete hydration.

$$\Delta Q = mC_p \Delta T \qquad \text{or} \qquad \Delta T = \frac{\Delta Q}{mC_p} \tag{3-12}$$

where ΔQ = energy rise (J)

m = mass of concrete (g)

C_p = specific heat capacity (J/g-°C)

ΔT = the change in temperature or temperature rise (°C)
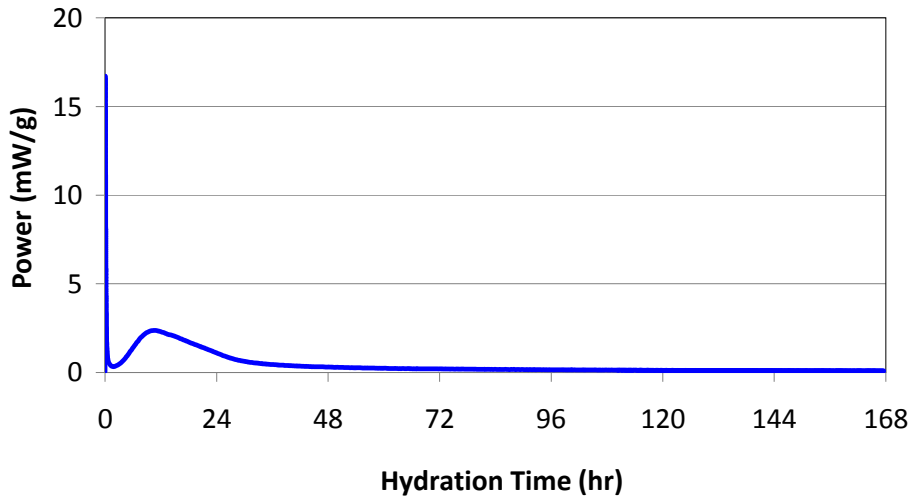
Figure 3-3. Hydration power of cementitious mixture (used in Footing at I-4 US-192 Braided Ramp, Orlando, FL) obtained from isothermal calorimetry testing.
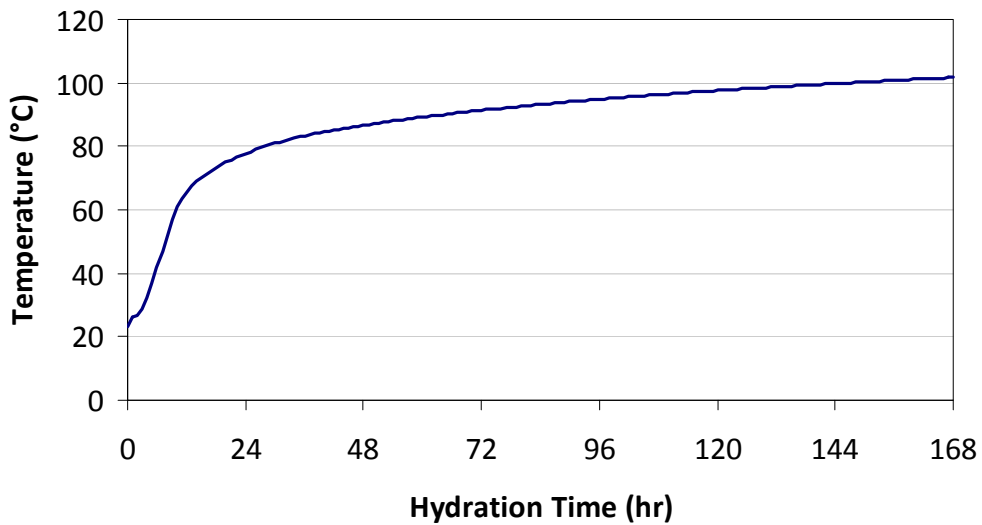
Figure 3-4. Adiabatic temperature rise of a concrete mixture calculated from the hydration power obtained in the isothermal calorimetry testing.

3.3.2 Conductivity and Heat Capacity

Heat energy transferred by way of conduction is caused by the physical interaction between adjacent molecules that have different temperatures. Experimental observations have shown that in the one dimensional plane, the rate of heat transfer through a finite area can be

28

expressed by what is known as Fourier's law of heat conduction, expressed by Equation 3-13, and illustrated in Figure 3-5,

$$\dot{Q}_x = -kA_x \frac{\partial T}{\partial x} \qquad (3\text{-}13)$$

where $\dot{Q}_x$ = heat flow (J/s)

k = the thermal conductivity (J/m-s-°C)

A_x = The surface area (m^2)

T = Temperature (°C)

x = coordinate (m)

The thermal conductivity of a solid is its ability or the ease with which it transmits heat. The minus sign denotes a negative temperature gradient reflecting the fact that the heat flows in the direction of decreasing temperature.
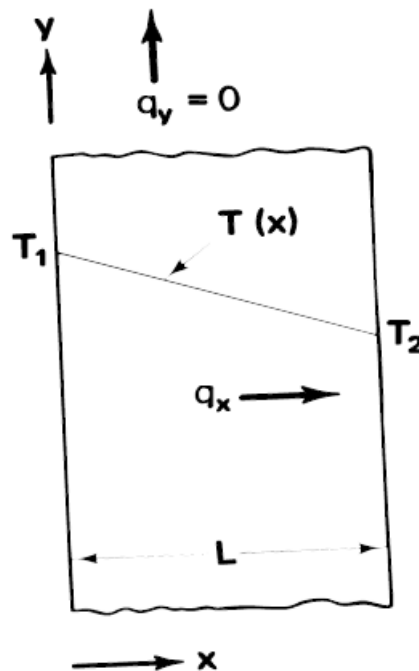
Figure 3-5. One-dimensional conduction heat transfer.

It is often convenient to divide Equation (3-13) by the area to give:

$$q_x \equiv \frac{\dot{Q}_x}{A_x} = -k\frac{\partial T}{\partial x}$$

(3-14)

where q_x is the heat flux (J/s-m^2).

Expanded to the three-dimensional case, as shown in Figure 3-6, the Fourier equation for heat transfer becomes (Mills, 1995):

$$q'' = -k\nabla T = -k\left(i\frac{\partial T}{\partial x} + j\frac{\partial T}{\partial y} + k\frac{\partial T}{\partial z} \right)$$

(3-15)

where x, y, z = coordinates

i, j, k = the unit vectors in the x, y, and z directions, respectively
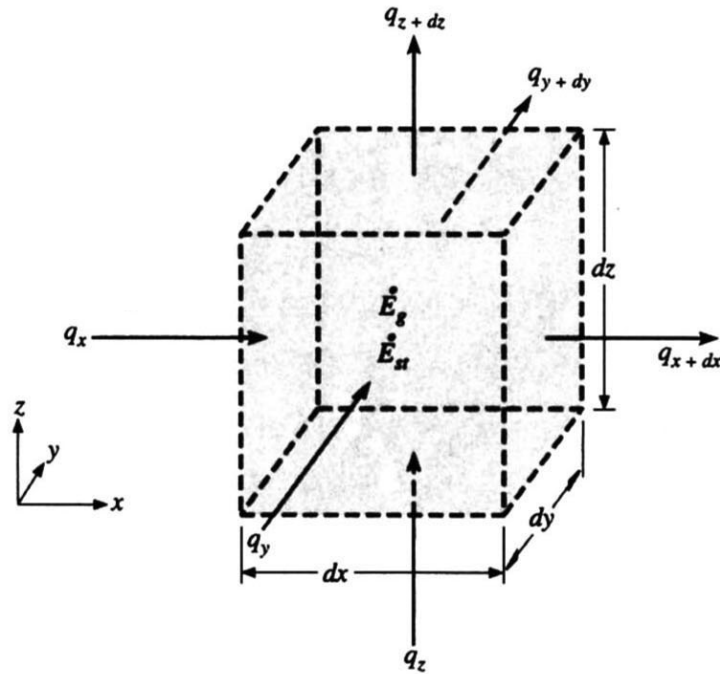
Figure 3-6. Differential volume for a rectangular solid.

Consider the case of a heat-conducting solid such as mass concrete which also has an internal source of heat generation. If $q*$ is used to denote the rate at which heat is being internally generated per unit volume, then

rate of total heat generated $= q*(dxdydz)$ (3-16)

The principle of conservation of energy requires that

{rate of thermal energy in} − {rate of thermal energy out}

+ {rate of total heat generated} = {rate of accumulation of thermal energy}   (3-17)

The rate of heat inflow across the face at x is $q_x dydz$, and the outflow across the face at x+dx is

$$q_{x+dx}dydz = \left(q_x + \frac{\partial q_x}{\partial x} dx \right) dydz \qquad (3-18)$$

The net inflow in the x direction is then

$$q_x dydz - q_{x+dx}dydz = -\frac{\partial q_x}{\partial x} dxdydz$$

Similar terms arise from conduction in the y and z directions. Thus, the net heat transfer into the volume by conduction is

$$\left(-\frac{\partial q_x}{\partial x} - \frac{\partial q_y}{\partial y} - \frac{\partial q_z}{\partial z} \right) dxdydz$$

Substituting in Equation (3-17) and dividing by dxdydz gives

$$\left(-\frac{\partial q_x}{\partial x} - \frac{\partial q_y}{\partial y} - \frac{\partial q_z}{\partial z} \right) + q^* = \rho c_p \frac{\partial T}{\partial t} \qquad (3-19)$$

Introducing Fourier's law, Equation (3-14), for q_x, q_y, and q_z,

$$\rho c_p \frac{\partial T}{\partial t} = \frac{\partial}{\partial x}\left(k \frac{\partial T}{\partial x} \right) + \frac{\partial}{\partial y}\left(k \frac{\partial T}{\partial y} \right) + \frac{\partial}{\partial z}\left(k \frac{\partial T}{\partial z} \right) + q^* \qquad (3-20)$$

This equation represents a volumetric heat balance which must be satisfied at each point in the body, and describes the dependence of the temperature in a solid on the spatial coordinates and on time.

Assuming thermal conductivity, specific heat and density of concrete being relatively constant values (Faria et al., 2006), the conductivity of concrete created based on the cementitious mixtures can be calculated using the relationship:

$$k = \alpha \rho c_p \tag{3-21}$$

where α = diffusivity (m^2/s)

ρ = density (kg/m^3)

c_p = heat capacity (J/kg-°C)

3.3.3 Convection

Convection refers to the energy transported as a result of macroscopic motion. In other words, the transfer of heat from the surface of a material to a fluid that is moving over it. Figure 3-8 presents an approach to the analysis of convection heat transfer from a surface from which equation 3-22 is derived.

$$q_c = \bar{h} A_s (T_s - T_F) \tag{3-22}$$

where q_c = rate of heat transfer (W/m^2 -°C)

T_s = temperature at the surface (°C)

T_F = Fluid temperature (°C)

A_s = surface area (m^2)

$\bar{h}$ = mean coefficient of heat transfer
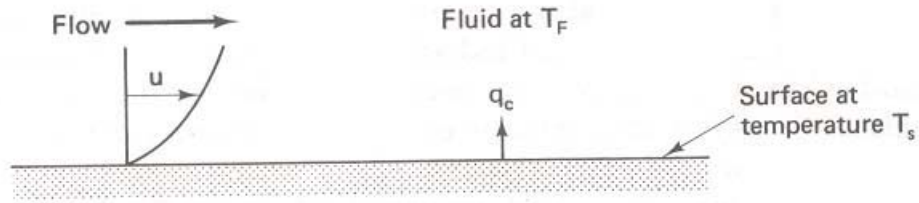
Figure 3-7. Convection heat transfer (Thomas, 1980).

The heat lost and gained to the surrounding environment by the hydrating concrete's exposed surface and also the interaction of the foam with ambient conditions is modeled by imposing boundary convection elements. This is conveniently done using the convection element found in DIANA to specify the convection and boundary conditions. The heat flow through the surface of the elements, q^S, due to convection is modeled by the following equation:

$$q^S = h_c(\theta_e - \theta^S) \tag{3-23}$$

where q^S = heat flow through surface (W/m^2)

h_c = convection coefficient (W/m^2-°C)

θ_e = external environment temperature (°C)

θ^S = surface temperature of the concrete block (°C)

The convection coefficient can be constant, temperature-dependent, or time dependent. The convection coefficient was calculated using the equation (similar to Ali and Urgessa (2012)):

$$h_c = \begin{cases} 5.6 + 3.95v, v \le 5\text{m/s} \\ 7.6v^{0.78}, v \ge 5\text{m/s} \end{cases} \tag{3-24}$$

where v = wind speed, m/s.

The assumed convection coefficient values for the thermal model in this research range from 9.0 W/m^2-°C to 50.0 W/m^2-°C.

33

3.4 Model Geometry

The general finite element model developed in this study consists of a rectangular mass concrete footing lying on a soil layer. The concrete is insulated at the top, bottom, and all the sides. Based on the double symmetry of the rectangular footing, only one-quarter of the whole structure was to be modeled to reduce the computation time and the output file size from the DIANA software. The finite element mesh of one-quarter of the footing is illustrated in Figure 3-8.
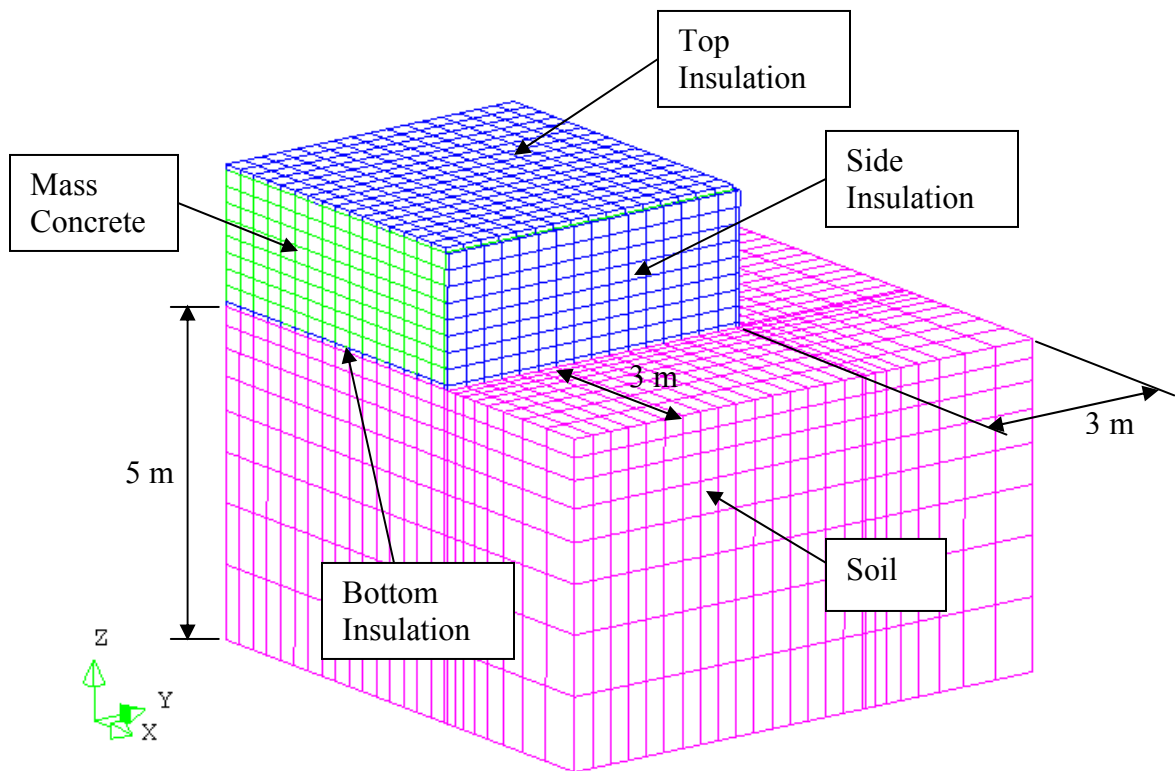
Figure 3-8. General finite element mesh of one-quarter of footing.

The polystyrene insulation, plywood and concrete were explicitly discretized and modeled according to their corresponding thermal properties.

The modeled concrete had the full depth but half length and half width of the actual concrete of the footing. The model soil layer beneath the footing extended 5 m deeper and 3 m wider on each side of the footing in order to ensure adequate medium for heat transfer from the footing concrete.

3.5 Boundary Conditions

The boundary conditions imposed for the thermal analysis consist of an initial temperature of the model and the external temperature. The initial temperature was set at the placement temperature of the concrete whereas the external temperature was set at mean environmental temperature recorded in the field during the monitoring period of the footing.

Figure 3-9 illustrates the boundary temperatures imposed on the finite element model. The external temperature is applied to the surfaces of the structure that are exposed to the environment including the outer surfaces of the concrete-insulation structure and the top surface of the soil layer. The fixed temperature is applied to the bottom and the sides of the soil layer. The fixed temperature is the same in magnitude as the external temperature, the only difference between these two loads is that there is air convection at the surface where the external temperature is applied while there is no convection at the surface where the fixed temperature is imposed.

Figure 3-10 presents the temperature history of the environment during the monitoring of a pier footing at S.R. 826 and S.R. 836 Interchange, Miami, FL. The description of the field testing is presented in Chapter 5.
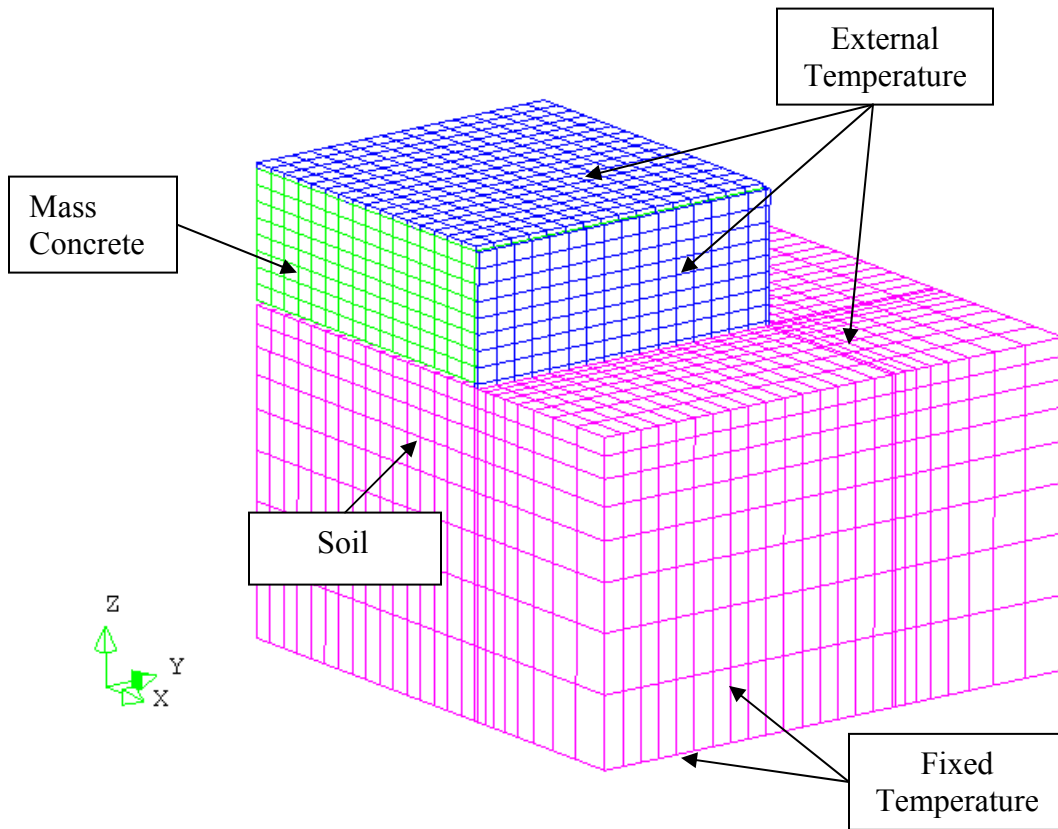
Figure 3-9. External temperatures imposed on finite element model representing the ambient conditions.
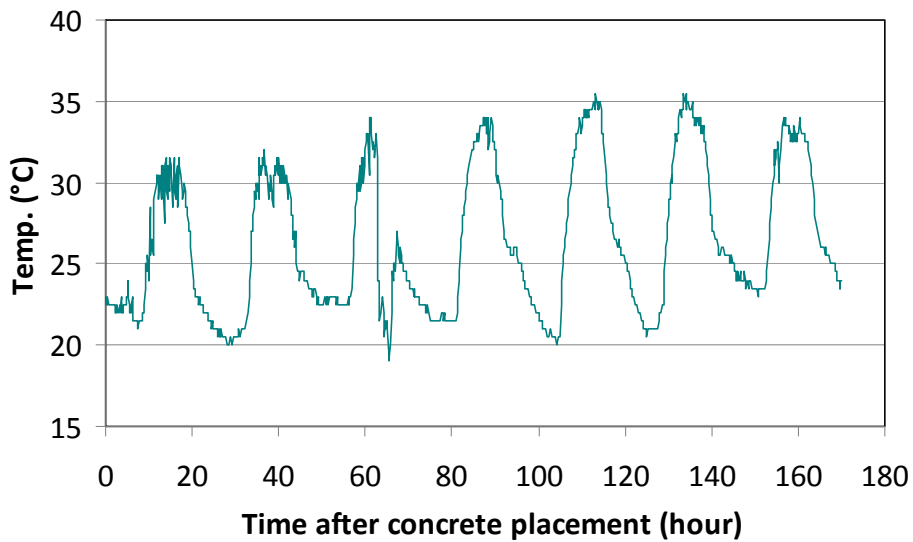
Figure 3-10. Ambient temperature during the monitoring of a pier footing at S.R. 826 and S.R. 836 Interchange, Miami, FL.

CHAPTER 4
FINITE ELEMENT STRUCTURAL MODEL

4.1 Overview of Finite Element Structural Model

Heat produced during the hydration of concrete causes an increase in its temperature. However, because of the inhomogeneous hydration within the concrete element and the inhomogeneous loss of heat to the surrounding environment, temperature differences will occur throughout the concrete element. These temperature differences can induce thermal strains and stresses that could potentially initiate cracking if they exceed the early age tensile strength of the concrete.

The temperature distribution solution obtained from the thermal analysis is imposed as a thermal load in the structural analysis of the concrete. The mechanical response to the stresses induced by the thermal gradient is greatly dependent on the physical characteristics of the concrete.

This chapter describes the elements used in DIANA to model the concrete and the physical input parameters required to measure the mechanical behavior.

4.2 Element Selection

As stated in Chapter 3, the structural behavior of a concrete footing was modeled using the three dimensional twenty-node CHX60 isoparametric solid brick element reproduced here in Figure 4-1. The stress and strain distribution is approximated over the volume of the element. Stress σ_{xx} and strain ε_{xx} vary linearly in the x direction and quadratically in the y and z directions. Stress σ_{yy} and strain ε_{yy} vary linearly in the y direction and quadratically in the x and z directions. Stress σ_{zz} and strain ε_{zz} vary linearly in the z direction and quadratically in the x and y directions. It utilizes linear interpolation and Gauss integration in its computational scheme.
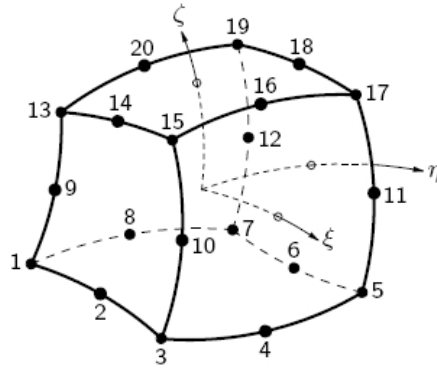
Figure 4-1. Twenty-node isoparametric solid brick element CHX60.

4.3 Material Model

The modeling of the structural behavior presented a few challenges as early age concrete exhibits both an elastic component and a viscous component.

Although the actual reinforcing steel in the concrete can hold potential cracks caused by thermal contraction, it was not modeled in the structural model due to its complexity of geometry. Shrinkage of concrete was also not considered in this study.

To model the elasticity of the concrete, the Young's modulus E, Poisson's ratio v, and coefficient of thermal expansion α, were directly input into the model. The viscoelastic behavior was modeled based on a Maxwell chain which is also in the form of the direct input of the progression of the Young's modulus with age.

The potential for cracking is tracked by specifying the tensile strength evolution by way of a discrete function that is dependent on time.

4.4 Input Parameters

4.4.1 Modulus of Elasticity

Cracking in mass concrete occurs when the tensile stresses induced by the thermal gradients are greater than the tensile strength. The modulus of elasticity of concrete is the ratio between the stress and reversible strain and is important because it influences the rigidity of the

38

concrete structure. This linear relationship is known as Hooke's Law and is expressed in Equation 4-1,

$$\sigma = E\varepsilon \hspace{4cm} (4\text{-}1)$$

where σ = stress (MPa)

E = Young's Modulus (MPa)

ε = linear strain.

The elastic limit represents the maximum allowable stress before the concrete will crack and undergo permanent deformation.

In heterogeneous multiphase materials like concrete, the modulus of elasticity increases as it hydrates, which is detrimental to the concrete because the probability of cracking increases as the modulus increases.

To correctly model the thermal stresses in young concrete, it is essential to include the variation of the mechanical properties with time of the concrete (De Schutter, 2002; Lawrence et al., 2012), most importantly the elastic modulus. Therefore, testing for the tensile modulus of elasticity of concrete at early ages is needed for input parameters of modeling.

4.4.2 Poisson's Ratio

Poisson's ratio is the ratio of the lateral strain to the axial strain within the elastic range of the concrete. According to Mehta and Monteiro (2006), Poisson's ratio has no consistent relationship with the curing age of the concrete. Values obtained during the testing for compression modulus of elasticity were consistently 0.2, which is within the universally accepted range of 0.15 and 0.20 for concrete.

4.4.3 Coefficient of Thermal Expansion

The coefficient of thermal expansion is used to describe the sensitivity of concrete expansion or contraction to changes in temperature. It is defined as the change in unit length per

degree of temperature change (Mehta and Monteiro, 2006). The value of the coefficient of thermal expansion is particularly important in mass concrete because the strain induced during the cooling period is dependent on both the magnitude of the change in temperature and the coefficient of thermal expansion.

4.4.4 Tensile Strength

In normal concrete applications, the low tensile strength of concrete is usually of little concern because reinforcing steel bars, which have high tensile strength values, are used to increase the overall strength of the structure. However, in mass concrete applications, the use of steel is either impractical, such as in the case of dams, or due to the size of the structure, the spaces between the steel are large creating elements that are weak in tension.

4.5 Symmetry and Boundary Conditions

The boundary conditions imposed for the structural analysis of the quarter footing consisted of the restriction of displacements against the symmetry planes. Since the depth of footing was relatively thick, it was assumed that there was no curling in the footing. Therefore, the base of the footing was modeled as being constrained against displacements along the z direction, but was free in the x and y directions as friction between the base of footing and soil was neglected. Both conditions are presented in Figure 4-2.
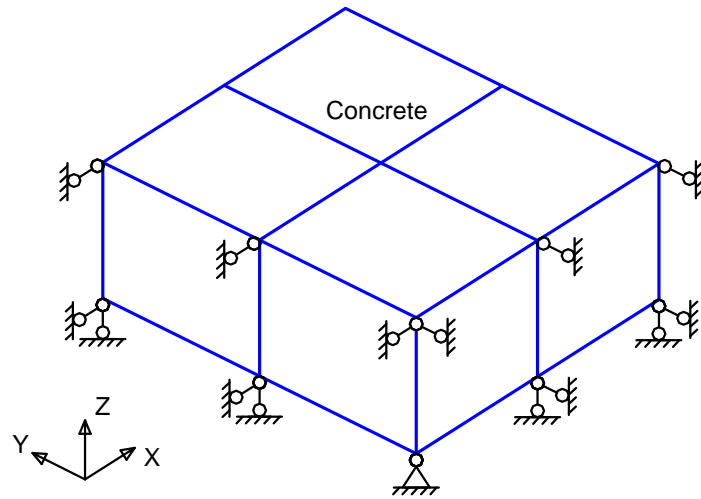
Figure 4-2. Symmetry conditions and supports of model.

CHAPTER 5
INSTRUMENTATION AND MONITORING OF MASS CONCRETE

5.1 Overview

An FDOT-funded study (Tia et al., 2010) has successfully verified the developed finite element model by performing and monitoring concrete specimens in the laboratory conditions. It is needed to extend monitoring of actual concrete structures such as columns, pier caps, and footings of various shapes that are large enough to be classified as mass concrete. To achieve this task, some of substructures that were constructed in the field in Florida were selected for temperature monitoring after concrete placement. The temperature measurements were then compared with the results obtained from the finite element modeling developed in Chapter 3.

5.2 Selected Mass Concrete Structures

During November 2011 and July 2012, four different mass concrete structures were monitored for temperature developments in Florida, including three bridge pier footings and one bridge pier cap as listed in Table 5-1. Measurements of the temperature in these structures were recorded 7 days from placement of concrete.

Table 5-1. Selected Mass Concrete Structures

Name of Structure	Dimensions (m)	Location	Placement Date
Footing 1	14.02×8.53×2.13	S.R. 826 and S.R. 836 Interchange, Miami, FL	11/2011
Pier Cap	4.72×4.42×3.2	S.R. 826 and S.R. 836 Interchange, Miami, FL	01/2012
Footing 2	10.36×10.36×2.03	S.R. 826 and S.R. 836 Interchange, Miami, FL	03/2012
Footing 3	6.71×3.05×1.75	I-4 US-192 Braided Ramp, Orlando, FL	07/2012

The concrete mix design used in Footing 1, Pier Cap, and Footing 2 was a Class IV concrete mix with a total cementitious content of 666 lbs/yd^3, 48% of which is Type F fly ash as a replacement of Portland cement, and water-to-cementitious content ratio of 0.36.

The concrete mix design used in Footing 3 was a Class IV concrete mix with a total cementitious content of 700 lbs/yd^3, of which 64.3% was Portland cement, 32.1% Type F fly ash, and 3.6% Boral Micron 3 Ultra-Fine Fly Ash. The water-to-cementitious content ratio of this concrete mixture was 0.38.

5.3 Instrumentation

5.3.1 Proposed Locations for Temperature Sensors

Temperature sensors were installed on the selected mass concrete structures. The proposed locations for the temperature sensors are described in the following sections.

5.3.1.1 Footings

The FDOT specifications require that the temperature sensors be placed at the center, top, and bottom of the footing placements, in the shortest direction. The top and bottom temperature sensors should be located two inches, inside the concrete, from the outer surfaces. For this research, it was proposed that in addition to the locations required by the specifications, temperature sensors should be placed at six inch intervals between the center and top and bottom of the footing. It was further proposed that temperature sensors be placed at one corner, and along the side furthest from the center of the footing, spaced six inches apart and two inches within the top, bottom and side surface.

5.3.1.2 Columns and Pier Cap

The FDOT specifications require that the temperature sensors be placed at the center and sides of the column and cap placements, in the shortest direction. The temperature sensors placed at the sides should be located two inches, inside the concrete, from the outer surfaces.

5.3.2 Data Acquisition Equipment

There were 2 types of temperature sensor used in this research: thermocouples and data loggers. Thermocouples were used to measure temperatures for Footing 1 and Pier Cap, whereas

data loggers, as illustrated in Figure 5-1, were used to record temperatures for Footing 2 and Footing 3.

For Footing 2 and Footing 3, an advanced data acquisition system was used to measure and record the temperatures. This data acquisition system, called the Command Center, consists of temperature data loggers that allow for pre-programming to start recording temperatures at a specific time (usually set at the scheduled placement time) before being placed at the monitoring locations, as shown in Figure 5-2. The system also does not require an external power source, therefore eliminates the need for intermittent changing of batteries. Once the sensors are installed and programmed, they can be left in place unattended, and the data would be downloaded at the end of the monitoring period.
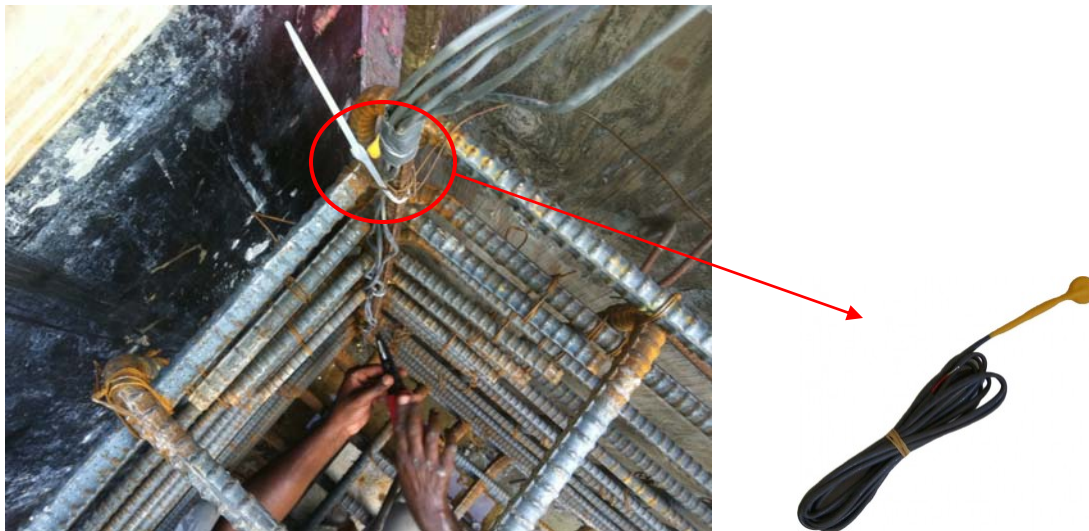
Figure 5-1. Data logger attached to reinforcing steel bar of footing.

Figure 5-2. Data acquisition equipment used in Footing 2 and Footing 3.

5.4 Monitoring of Selected Mass Concrete Structures

5.4.1 Footing 1 (at S.R. 826 and S.R. 836 Interchange, Miami, FL)

Concrete for the bridge pier footing located at the S.R. 826 (or Palmetto Expressway) and S.R. 836 (or Dolphin Expressway) interchange was placed in November 2011. The dimensions of the footing are 14.02 m (46 ft.) long, 8.53 m (28 ft.) wide and 2.13 m (7 ft.) deep. The pier footing was insulated on top with insulating blankets, while the bottom was insulated with polystyrene foam boards. The footing was formed on the sides by plywood panels as illustrated in Figure 5-3.

The thermocouples were installed at the top, middle and bottom elevations of the centroidal axis of the horizontal plan view. Figure 5-4 shows the concrete being placed into the bridge pier footing, while Figure 5-5 shows the data acquisition equipment that was used to record the temperatures in the pier footing during the hydration of the concrete. The temperatures

recorded by the thermocouples placed at the top, middle and bottom of the footing are shown in Figure 5-6.
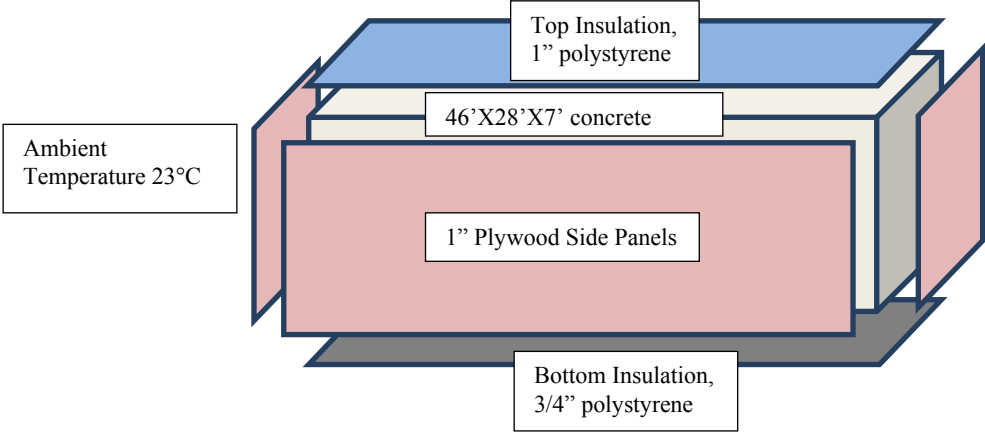
Figure 5-3. Mass concrete block, plywood panels, bottom and top insulation.

Figure 5-4. Concrete being placed for Footing 1.

Figure 5-5. Data acquisition equipment with thermocouple wiring.
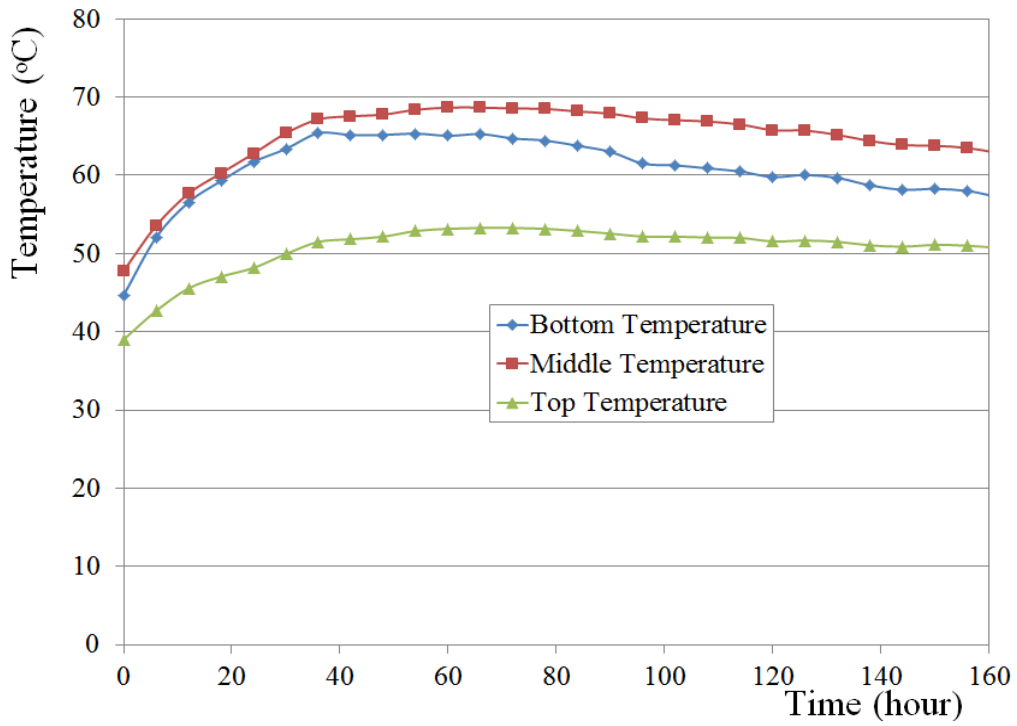
Figure 5-6. Temperatures measured at bottom, middle and top of Footing 1.

5.4.2 Pier Cap (at S.R. 826 and S.R. 836 Interchange, Miami, FL)

A 4.72 m (15'-6") long, by 4.42 m (14'-6") wide, by 3.2 m (10'-6") deep bridge pier cap was placed in January 2012. This pier cap would act as one of the seats for a segmental bridge at the interchange. Details of the pier cap are shown in Figure 5-7, Figure 5-8, and Figure 5-9.

The pier cap being placed on top of a previously casted concrete column was not insulated on its bottom surface. It was insulated at the top and sides with insulating blankets.
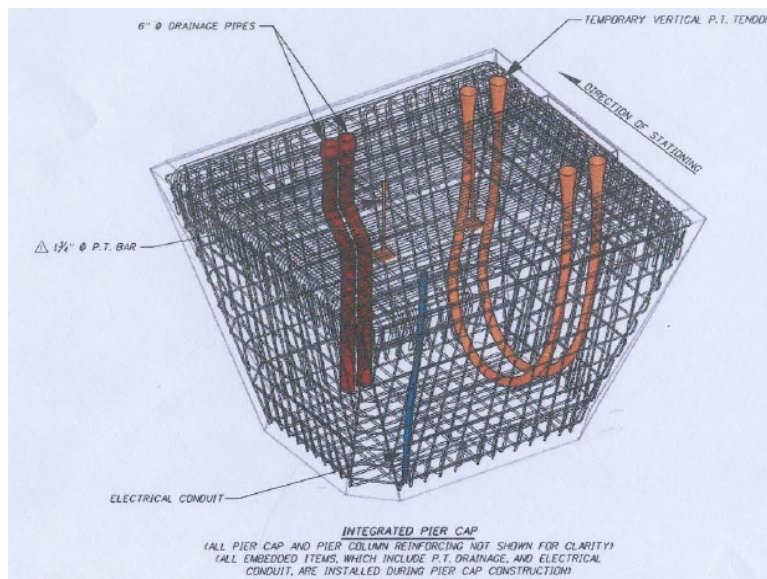
Figure 5-7. Pier cap details.
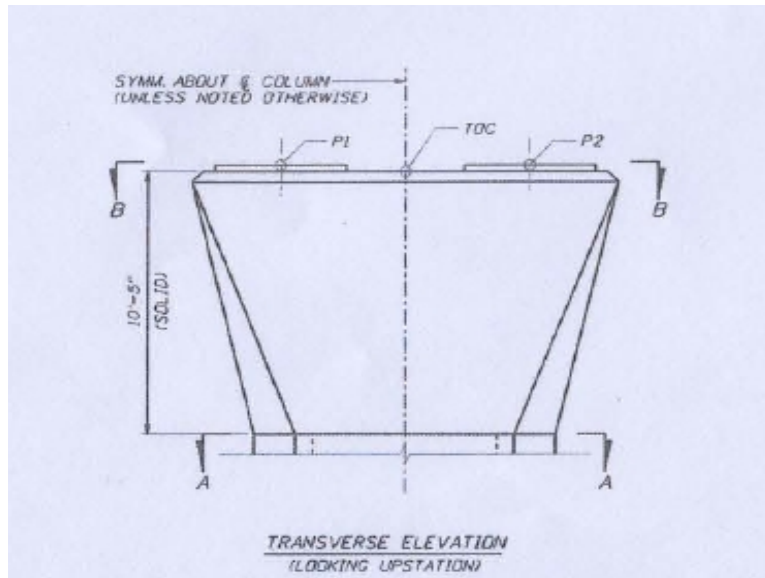
Figure 5-8. Transverse elevation of pier cap.
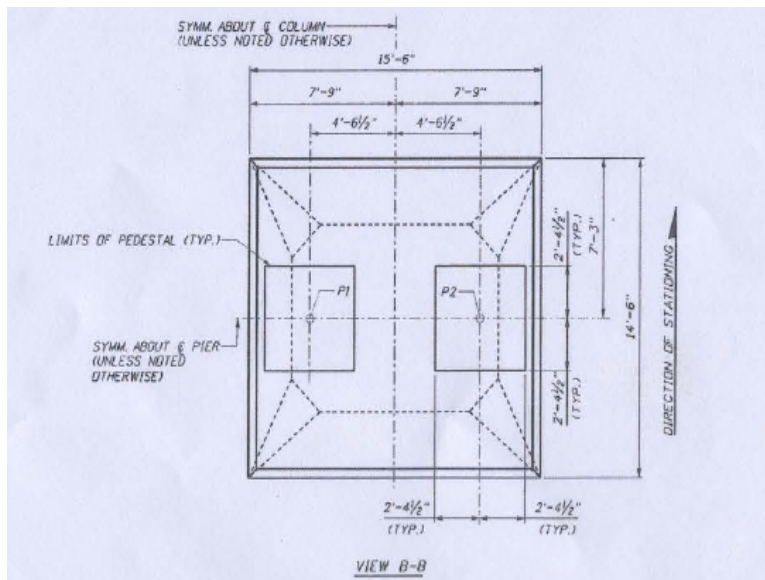
Figure 5-9. Pier cap section B-B.

To measure the temperature development during the hydration of the concrete in the pier cap, thermocouples were installed at the centroidal axis of the pier cap as well as at the side in the shortest direction. The side temperature sensors were located at two inches, inside the

49

concrete, from the outer surface, in a horizontal line with the center sensor, as shown in Figure 5-10. The temperatures measured by the thermocouples in the pier cap are shown in Figure 5-11.
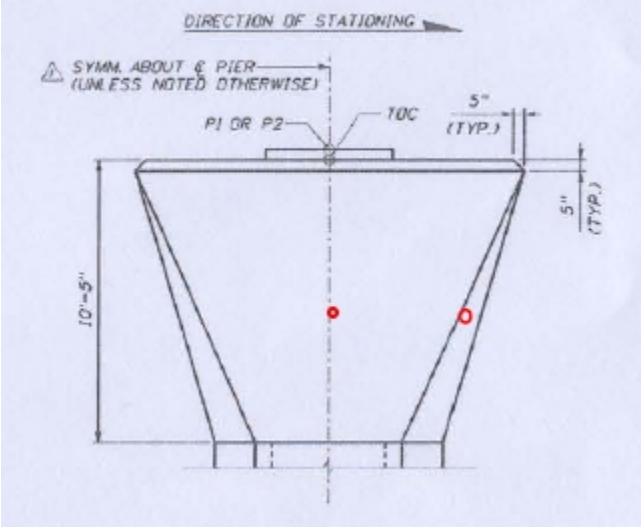
Figure 5-10. Location of thermocouples in pier cap.
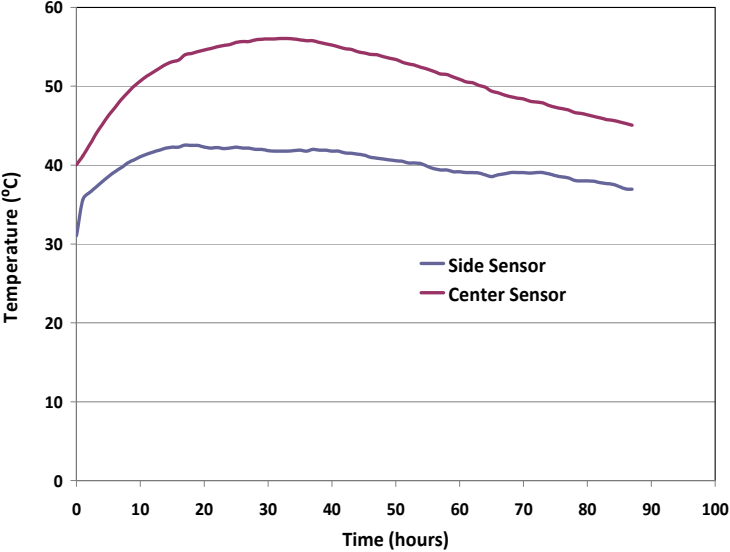
Figure 5-11. Profile of temperatures measured by thermocouples in pier cap.

5.4.3 Footing 2 (at S.R. 826 and S.R. 836 Interchange, Miami, FL)

Concrete of this footing was intended to be placed on top of a seal concrete slab. However, due to the contractor's inability to completely stop the flow of ground water into the footing area, a 3-inch layer of gravel was placed on top of the seal concrete prior to pouring the concrete for the footing to prevent the water from contacting the bottom of the footing. Figure 5-12 shows view of the footing with reinforcement before concrete was placed.

Figure 5-12. View of Footing 2.

Temperatures in the footing were measured and stored using the Command Center data acquisition system. The locations of the temperature sensors installed in the pier footing are shown in Figure 5-13. Sensors 1 through 5 were placed along the vertical centerline; Sensors 6 through 10 and Sensors 16 through 20 were placed 50 mm (2 in.) from mid-sides of the footing;

and Sensors 11 through 15 were placed 50 mm from the corner of the footing. Details of sensor elevation are given in Table 5-2.

The pier footing was insulated at the top with a 25-mm (1-in.) thick insulating blanket. The concrete was directly placed on top of the sand without any insulation in between. The thermal properties of the insulating blanket, concrete and sand are given in Table 5-3.
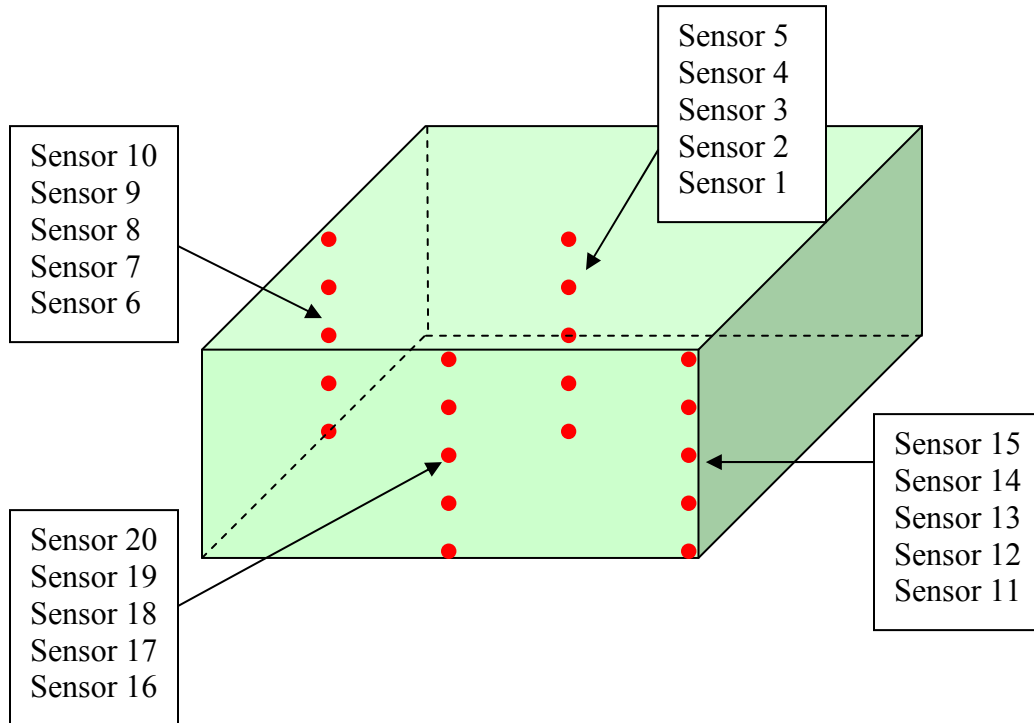
Figure 5-13. Locations of temperature sensors in Footing 2.

Table 5-2. Temperature Sensor Elevation in Footing 2

Sensor	Distance from Bottom (mm)	Distance from Top (mm)
1, 6, 11, and 16	100	1,930
2, 7, 12, and 17	406	1,624
3, 8, 13, 18, and 21	965	1,065
4, 9, 14, and 19	1,422	608
5, 10, 15, and 20	1,930	100

Table 5-3. Thermal Properties of Concrete, Sand, Insulating Blanket, Plywood and Polystyrene Foam

Material	Conductivity (J/sec-m-°C)	Heat Capacity (J/m³-°C)
Insulating Blanket	0.058	1.45×10^5
Polystyrene Foam	0.029	2.84×10^4
Plywood	0.15	8.54×10^5
Concrete	2.2	2.676×10^6
Sand	0.27	1.212×10^6

The ambient temperature at the time of placement was 23°C (73°F) and the concrete had a placement temperature of 25.5°C (78°F). During the monitoring of the temperature development of the footing, the ambient temperature was recorded as shown in Figure 5-14.

The temperatures measured in the sensors are presented in Figure 5-15, 5-16, 5-17, and 5-18. Interestingly, the temperatures measured 407 mm (16 in.) above the centroid (Sensor 4) were always higher than the temperatures measured at the centroid of the footing (Sensor 3) during cement hydration. An explanation for this is that the footing was insulated at the top while there was no insulation at the bottom. The peak temperature in the pier footing was measured as 66°C (151°F) in Sensor 4, at 55 hours after placement of concrete. Sensors 1, 6, 11, and 16, which were located 100 mm (4 in.) above the bottom surface of the pier footing at the center, western side, corner, and southern side, respectively, each recorded a peak temperature of approximately 35°C (95°F) as a result of the ground water infiltrating the footing area, rising to a level that resulted in these sensors being submerged. The maximum temperature difference recorded was 34°C between Sensor 4 and Sensor 12.
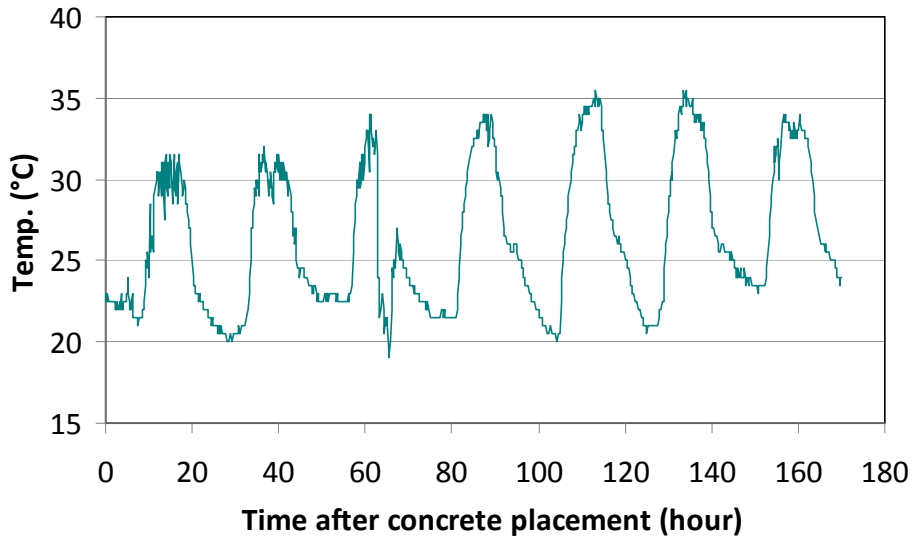
Figure 5-14. Ambient temperature during the monitoring of Footing 2.
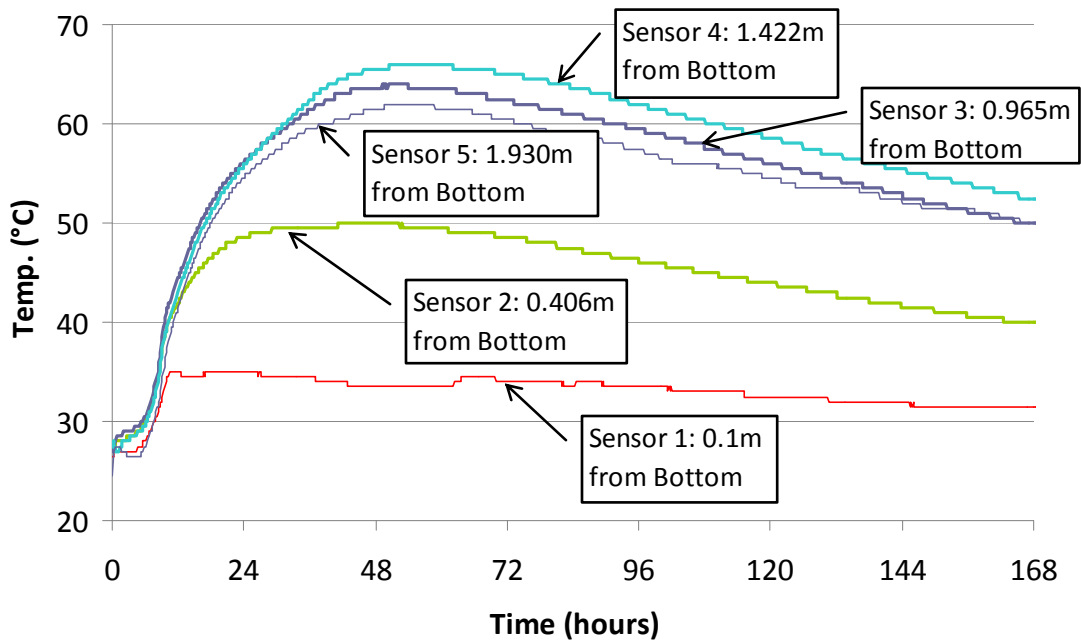
Figure 5-15. Profile of temperatures measured along vertical centerline of Footing 2.
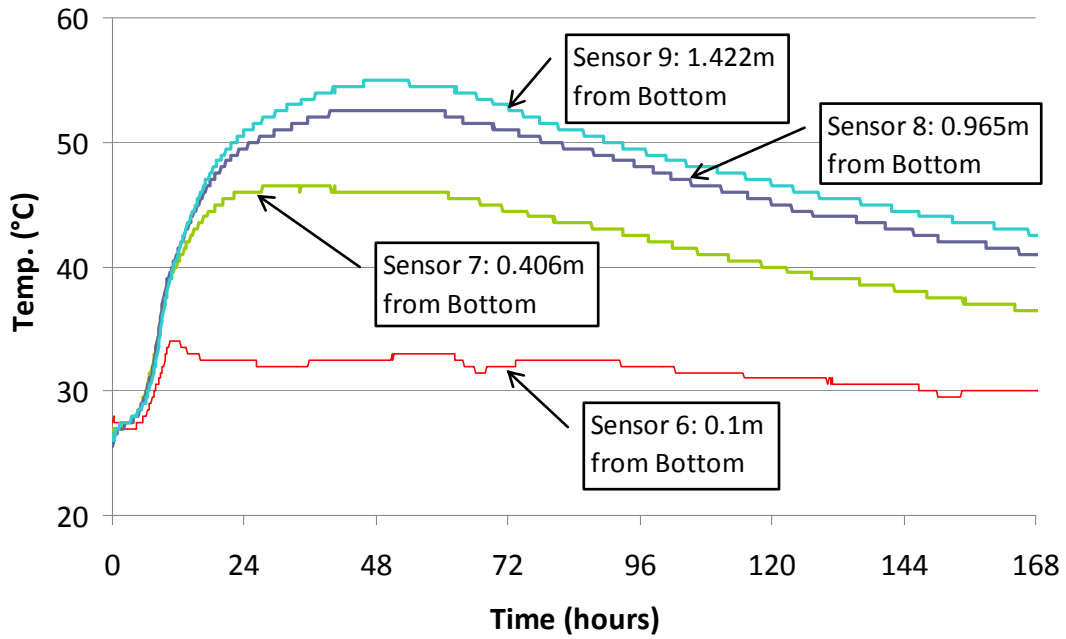
Figure 5-16. Profile of temperatures measured at mid-side of Footing 2.
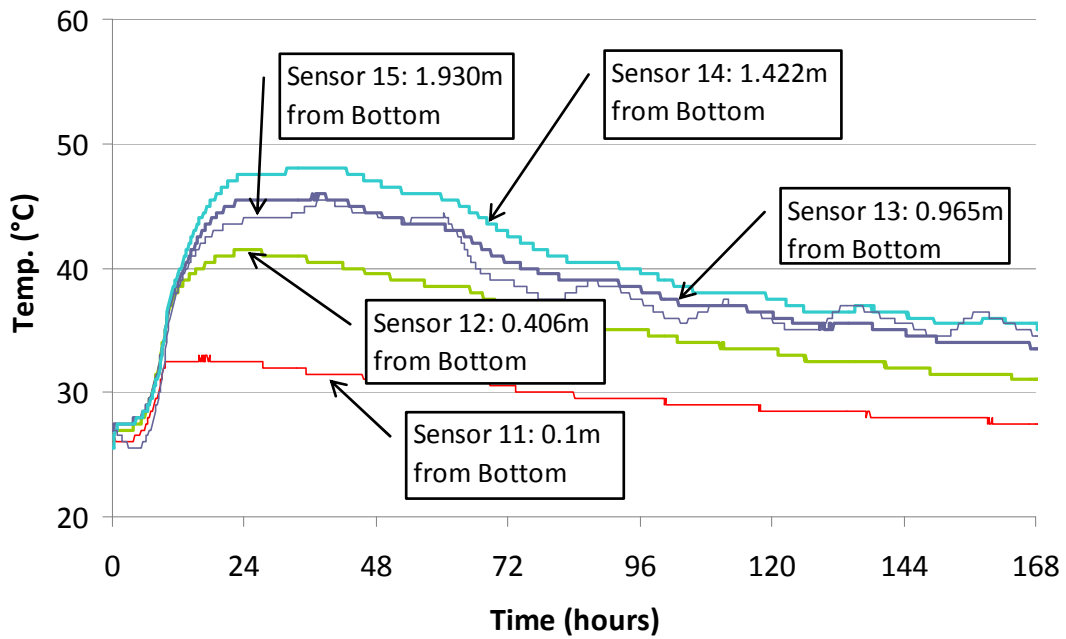
Figure 5-17. Profile of temperatures measured at the corner of Footing 2.
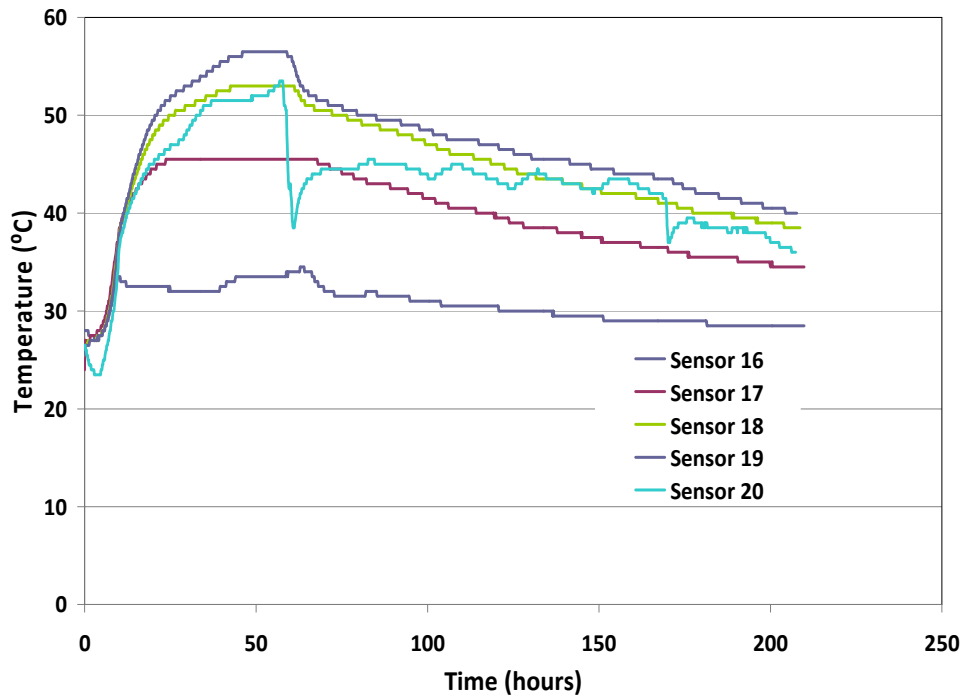
Figure 5-18. Profile of temperatures measured by sensors 16 to 20 in Footing 2.

The erratic behavior observed in sensors 15 and 20, which were located beneath the top surface of the footing, could be attributed to the fact that the elevations of the rebar to which the sensors at these locations were attached were raised to compensate for the change in the bottom elevation of the footing caused by the placement of gravel over the seal concrete. This change in elevation caused the sensors to be so close to the top surface of the footer that whenever the insulation blanket was lifted to inspect the concrete, sharp reductions in the temperature measurement occurred.

5.4.4   Footing 3 (at I-4 US-192 Braided Ramp, Orlando, FL)

A mass concrete structure at the I-4 US-192 Braided Ramp was monitored for temperature development in July 2012. The mass concrete structure was a 6.71-m (22') long, by 3.05-m (10') wide, by 1.75-m (5'-9") deep pier footing as shown in Figure 5-19 and Figure 5-20.

Figure 5-19. Footing at I-4 US-192 Braided Ramp, Orlando, FL.
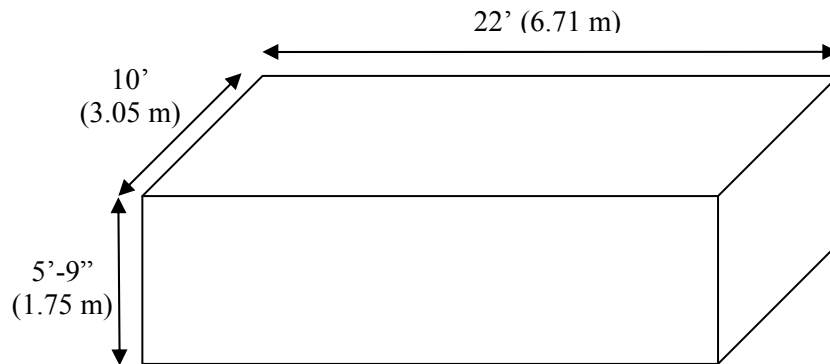
Figure 5-20. Dimensions of Footing 3.

The temperature sensors were placed 2 inches below the top surface, at the center, and 2 inches above the bottom surface of the footing (on the vertical axis of symmetry).

The concrete was placed at 7:30 AM and had a placement temperature of 32.2°C (90°F), while the average ambient temperature during monitoring period was 30.8°C (87.4°F). The temperatures recorded in the sensors are presented in Figures 5-21. The peak temperature in the pier footing was measured as 74°C (165°F) at the center of the footing 42 hours after concrete

placement. The maximum temperature difference recorded was 15°C (27°F) between the middle sensor and the top sensor.
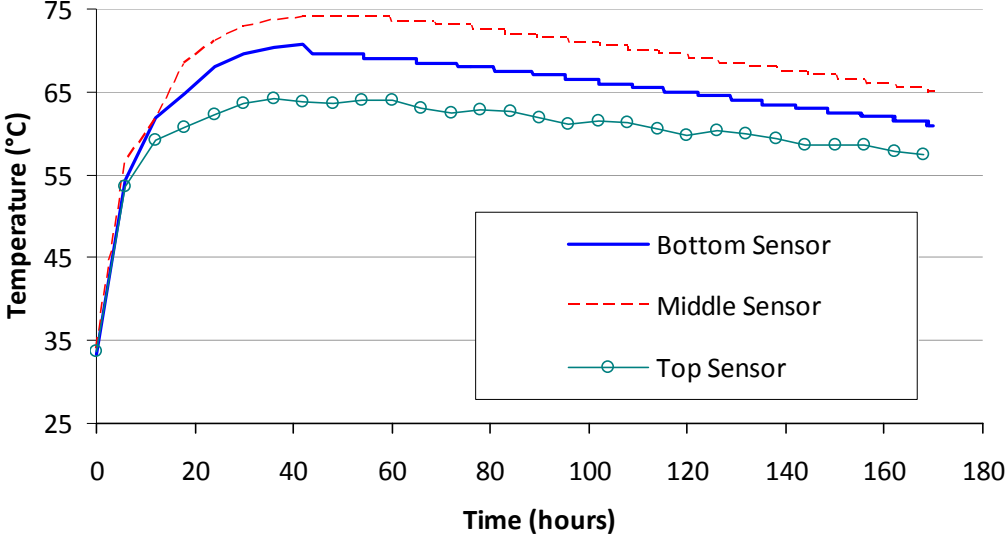
Figure 5-21. Measured temperatures at top, middle, and bottom of footing.

CHAPTER 6
COMPARISONS OF FINITE ELEMENT RESULTS WITH FIELD MEASUREMENTS

6.1 Overview

The finite element model described in Chapter 3 was used to predict temperature developments in each monitored mass concrete structure presented in Chapter 5. The computed temperatures from the finite element model were then compared with the recorded temperatures in the field. Each finite element model corresponding to each structure to be analyzed had different boundary conditions from one another.

6.2 Footing 1 (at S.R. 826 and S.R. 836 Interchange, Miami, FL)

The finite element model predicted the temperature profiles at the top, middle, and bottom elevations along the central line as indicated in Figure 6-1. The results at Nodes 1849 (top surface), 2719 (middle), and 862 (bottom surface) were compared with field test results as shown in Figure 6-2. The experimental and predicted temperatures were relatively close, especially in the latter half of the field results.
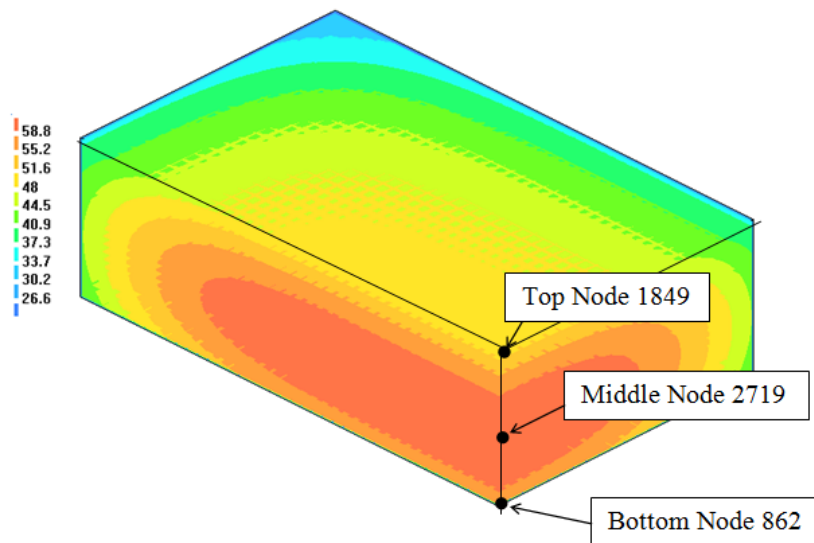
Figure 6-1. Temperature contour at 7th day in Footing 1 model.
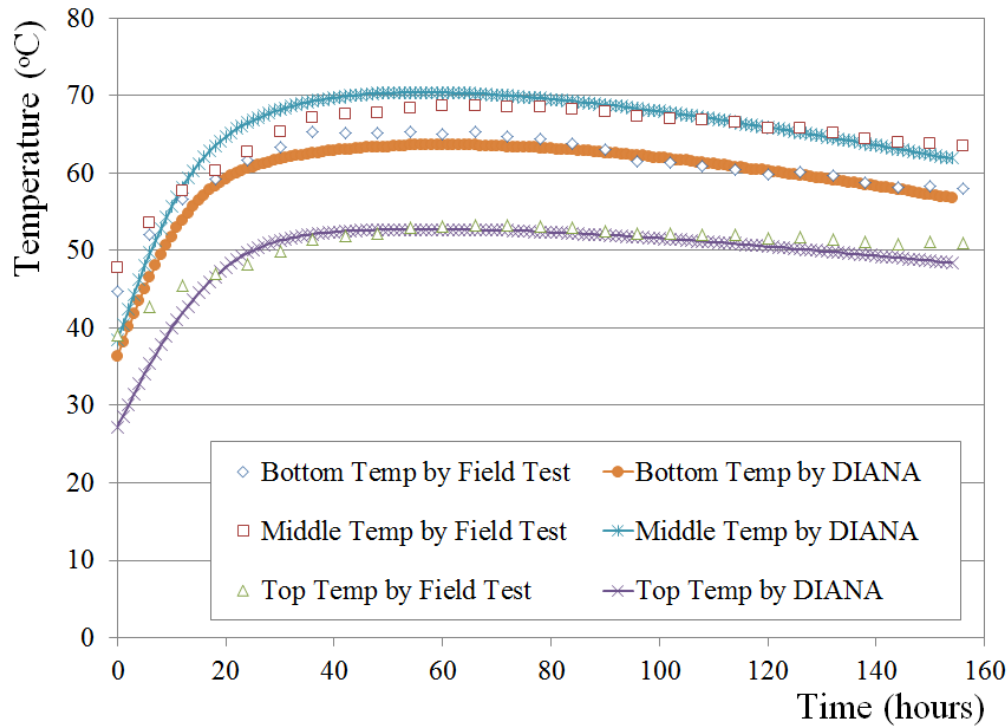
Figure 6-2. Comparison between measured temperatures and FE results of Footing 1.

6.3 Pier Cap (at S.R. 826 and S.R. 836 Interchange, Miami, FL)

The finite element model of the pier cap with the predicted temperature distribution contours is presented in Figure 6-3. The model includes insulation on the top and side surfaces only, as the bottom surface of the pier cap is cast directly on top of a previously constructed concrete column. Figure 6-4 shows the comparison of the temperature profiles at center and side of the pier cap calculated by the finite element model with the measured temperatures obtained in the field. The calculated temperature predictions at the side of the pier cap were fairly close to those recorded in the thermal sensors in the field. The temperatures calculated at the center of the pier cap were similar to those recorded in the field for the first 50 hours of monitoring. However, the temperatures in the field taper off more rapidly. This difference can perhaps be attributed to

more rapid changes in the material properties of the concrete at the center of the pier cap than is accounted for in the model.
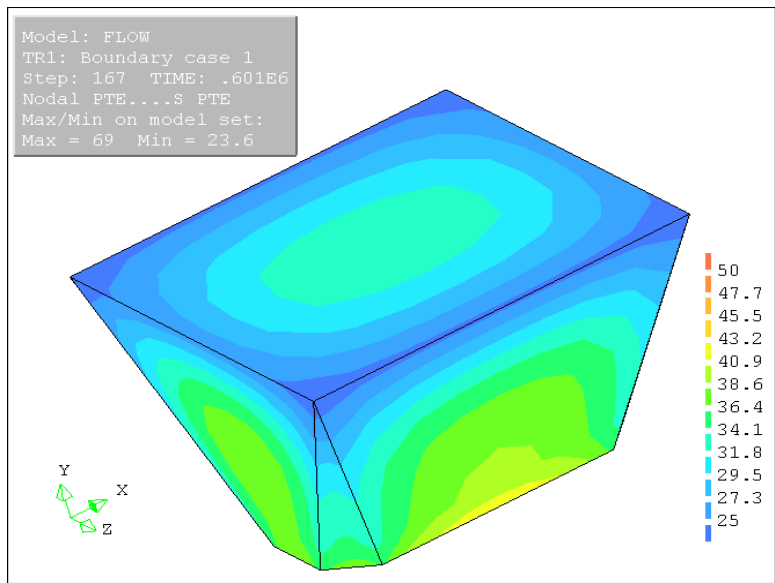
Figure 6-3. Temperature distribution at 7th day of the pier-cap model.
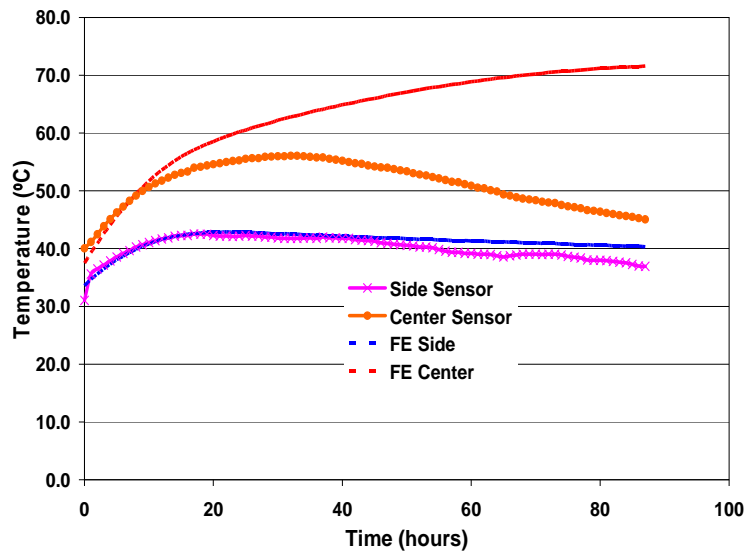
Figure 6-4. Comparison between measured temperatures and FE results of Pier Cap.

6.4 Footing 2 (at S.R. 826 and S.R. 836 Interchange, Miami, FL)

The finite element model of the pier footing with the predicted temperature distribution contours is presented in Figure 6-5. The highest temperature was found to occur in the middle section of the model and decreased as it got closer to the surfaces of the model.

Figures 6-6 through 6-15 present the comparisons of the predicted temperature time histories of the pier footing model with the measured temperatures obtained in the field at the respective locations. The trend of the temperature increases obtained from the model is relatively close to the trend of those recorded in the sensors. Most of the temperatures predicted in the finite element model closely match with the temperatures measured in the field. However, the computed temperatures near the top surface were lower than the measured ones (in Sensors 5 and 15). This is probably due to factors that impact the surface temperature of the concrete in the field such as ambient temperature change with time, solar radiation and radiation from the atmosphere.
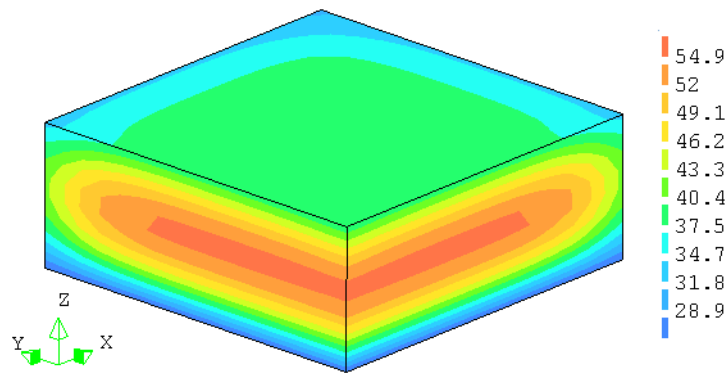
Figure 6-5. Predicted temperature distribution 7 days after concrete placement in Footing 2.
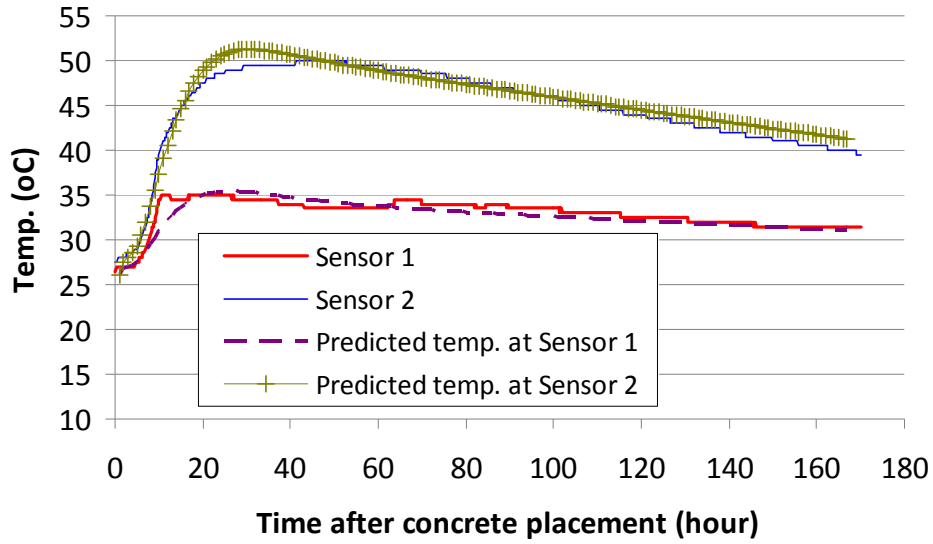
Figure 6-6. Predicted and measured temperatures in Sensors 1 and 2 along vertical centerline of Footing 2.
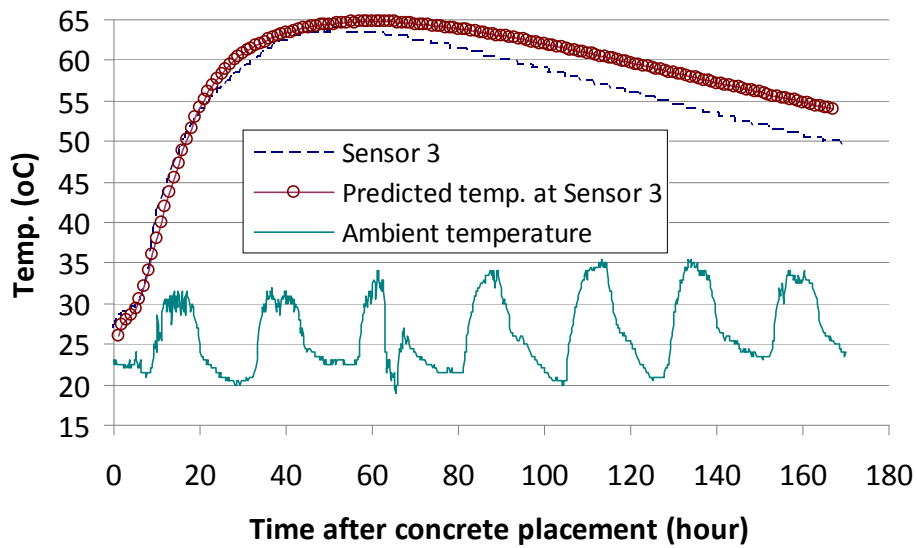
Figure 6-7. Predicted and measured temperatures in Sensor 3 along vertical centerline of Footing 2.
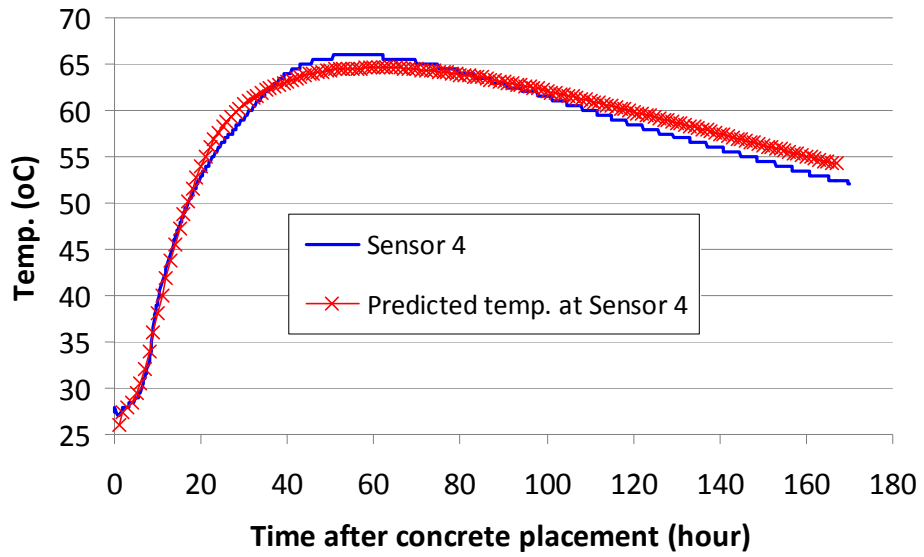
Figure 6-8. Predicted and measured temperatures in Sensor 4 along vertical centerline of Footing 2.
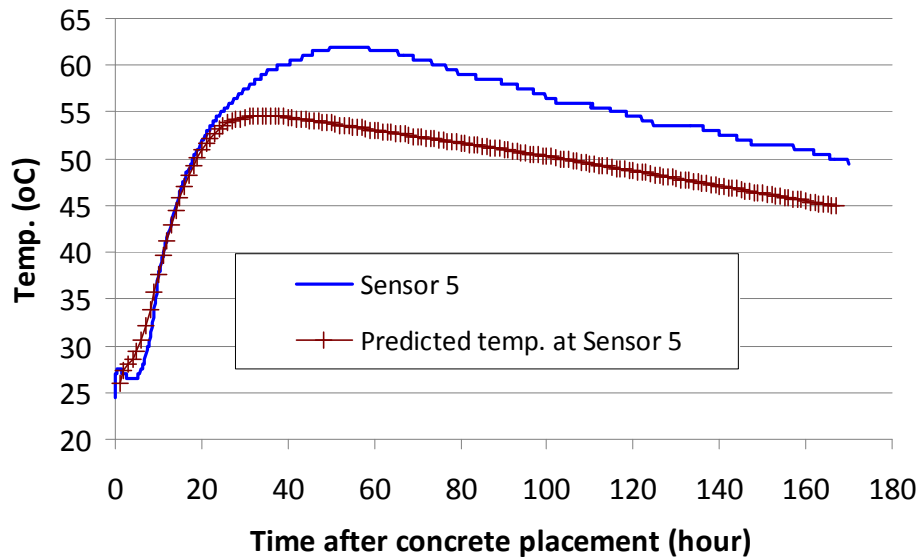
Figure 6-9. Predicted and measured temperatures in Sensor 5 along vertical centerline of Footing 2.
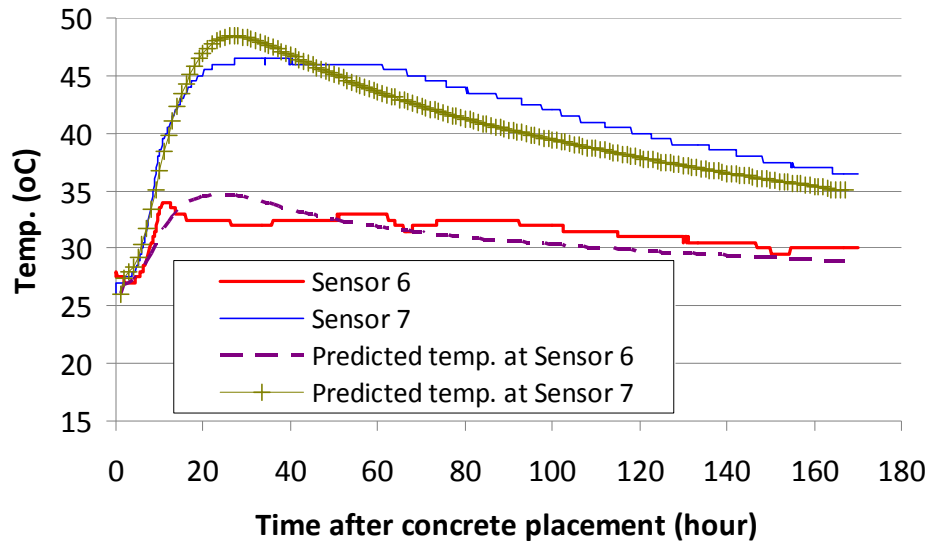
Figure 6-10. Predicted and measured temperatures in Sensors 6 and 7 at mid-side of Footing 2.
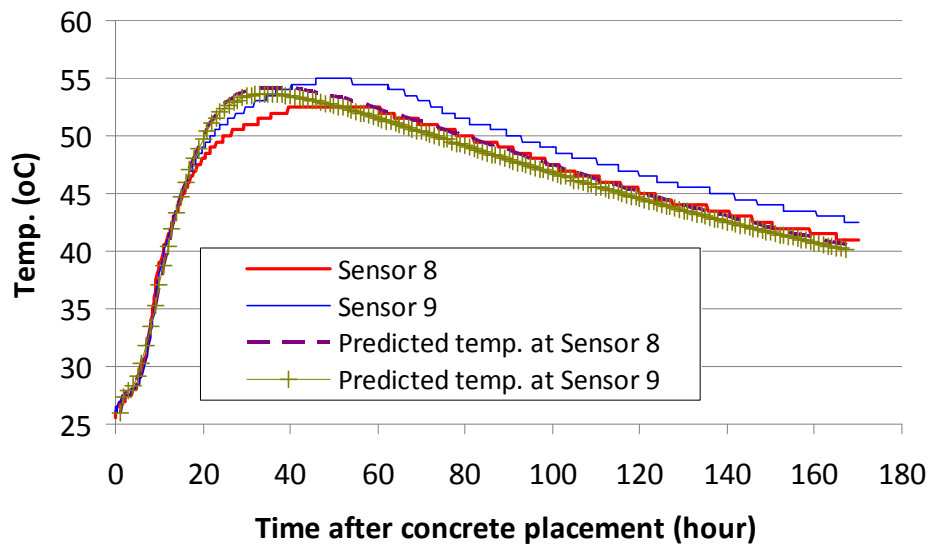
Figure 6-11. Predicted and measured temperatures in Sensors 8 and 9 at mid-side of Footing 2.

65
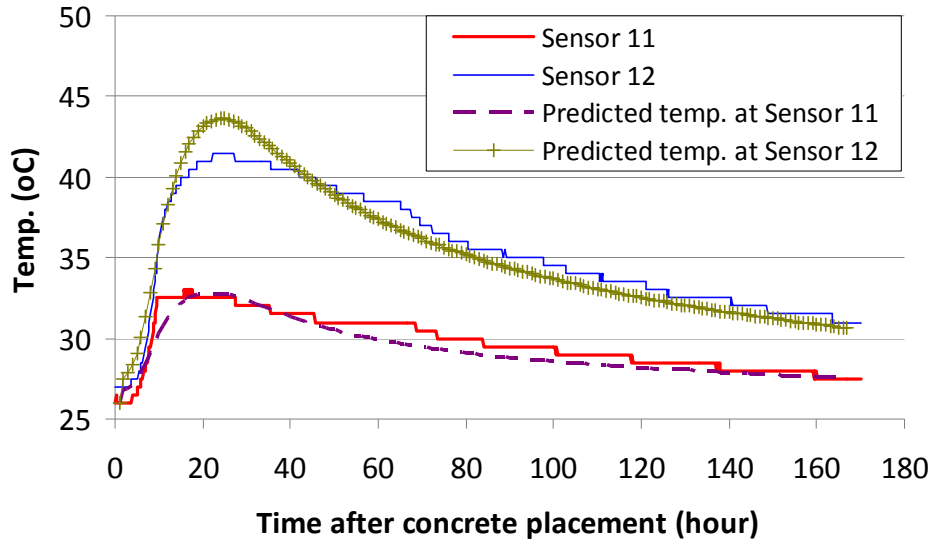
Figure 6-12. Predicted and measured temperatures in Sensors 11 and 12 at the corner of Footing 2.
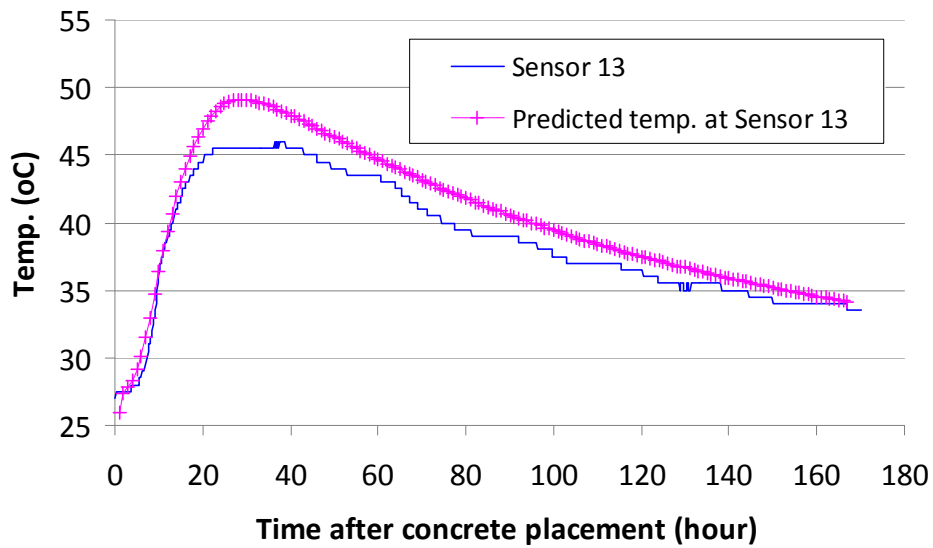
Figure 6-13. Predicted and measured temperatures in Sensor 13 at the corner of Footing 2.
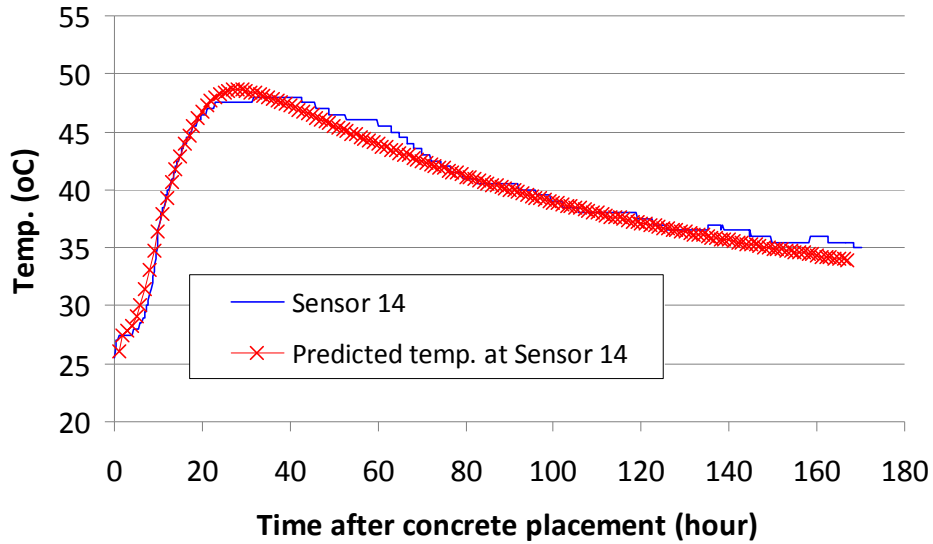
Figure 6-14. Predicted and measured temperatures in Sensor 14 at the corner of Footing 2.
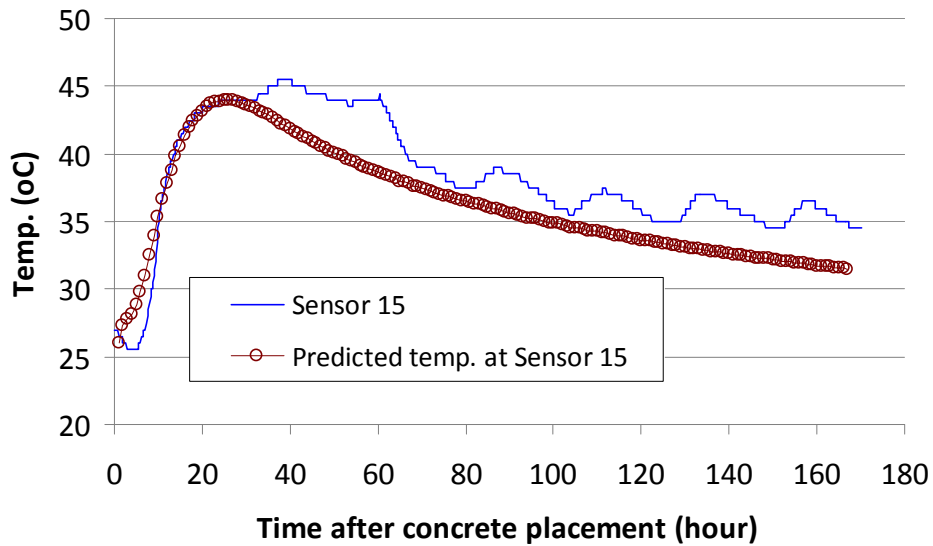
Figure 6-15. Predicted and measured temperatures in Sensor 15 at the corner of Footing 2.

6.5 Footing 3 (at I-4 US-192 Braided Ramp, Orlando, FL)

The finite element model of the pier footing with the predicted temperature distribution contours is presented in Figure 6-14. The model included full insulation at the top, side, and bottom surfaces using Styrofoam. Figures 6-15 through 6-17 show the comparisons of the

temperature profiles at the top, center and bottom of the pier footing calculated by the finite element model with the measured temperatures obtained in the field. The computed temperatures at the top of the pier footing were fairly close to those recorded in the top sensor. The temperatures calculated at the center and bottom of the footing were close to those recorded in the field for the first 40 hours of monitoring. However, the temperatures in the field dropped more rapidly after 40 hours. This difference can be explained by the fact that there were variables affecting the actual temperature development in the concrete in the field, which were not accounted for in the model. First, the time of placement of the top insulation was delayed after concrete placement due to strike-off of the concrete surface, resulting in heat loss in the concrete which was not considered in the finite element model. The second reason is that the formwork used for this footing was a steel formwork and it was in direct contact with the concrete surface (Styrofoam was placed outside of the steel formwork), causing more rapid heat transfer from the concrete to the steel formwork and thus more rapid heat dissipation, while the steel formwork was not modeled for temperature predictions.

Figure 6-17. Predicted and measured temperatures at the top of Footing 3.

Figure 6-18. Predicted and measured temperatures at the center of Footing 3.
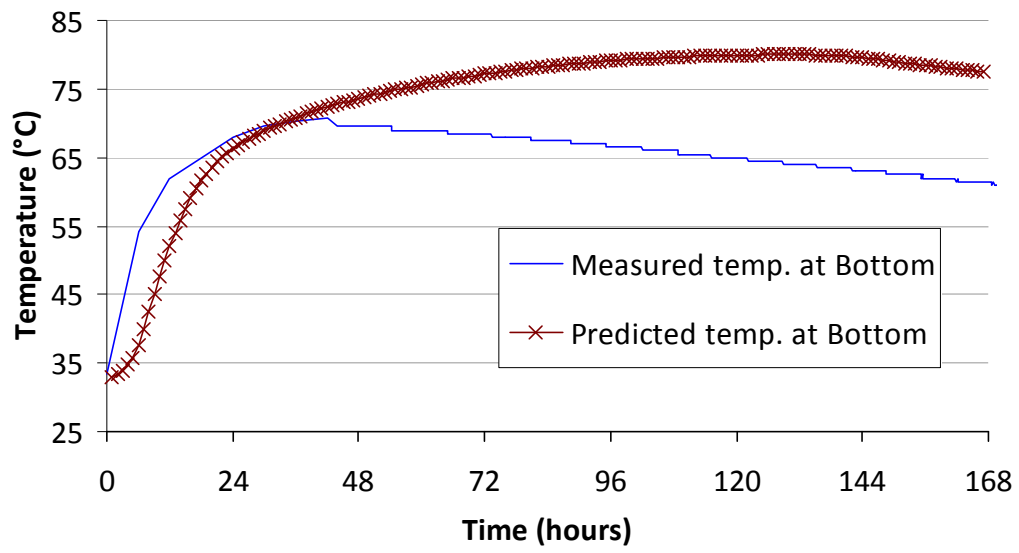
Figure 6-19. Predicted and measured temperatures at the bottom of Footing 3.

CHAPTER 7
EFFECTS OF THERMAL PROPERTIES OF SOIL ON TEMPERATURE DEVELOPMENT AND CRACKING IN FOOTINGS DIRECTLY PLACED ON SOIL

7.1 Description of Analysis Method

Many times, when mass concrete is placed directly on top of a soil layer, an insulation layer is not used at the bottom of the concrete. The rationale for this practice is that the soil on which the concrete is placed is already an insulating material. This chapter presents the investigation on the question of whether or not the absence of an insulating layer between the mass concrete and the soil may cause a problem with cracking of the concrete at early ages.

A finite element analysis was conducted to investigate the thermal behavior of a mass concrete footing placed directly on a soil layer. The modeled concrete was insulated at the top and sides while there was no insulation at the bottom, which was in direct contact with the soil. The model footing had the dimensions of 10.36 m ×10.36 m × 2.03 m (the same as Footing 2 (Table 5-1)). The concrete properties used were the same as those of Concrete Mix 1 that had water to cementitious material ratio of 0.5 and consisted of 100% Type I Portland cement concrete (Lawrence et al., 2012).

The model soil layer beneath the footing extended 5 m deeper (close to Kim (2001)), and 3 m wider on each side of the footing in order to ensure adequate medium for heat transfer from the footing. The initial temperature and the ambient temperature were set at 25.5°C and 26°C, respectively.

Several soils were modeled in this study, including sand and clay, each in three states of hydration, dry, moist, and saturated, and four other soils. Thermal conductivities, R-values, and heat capacities of these soils are given in Table 7-1. Note that the model moist sand and moist clay here were assumed based upon their thermal conductivities but not on their moisture

contents. The thermal conductivity of soil was determined from the R*-value of the soil layer by the following equation:

$$k = \frac{t}{R^*} \qquad (7\text{-}1)$$

where k = thermal conductivity (W/m-°C)

t = thickness of the layer (m)

R^* = thermal resistance (m^2-°C/W)

The R*-value can be converted to the commonly used R-value which has the units of ft^2-°F-h/(BTU-in).

Table 7-1. Thermal Properties of Sand and Clay

Material	Conductivity (J/sec-m-°C)	R-value (ft^2-°F-h/BTU-in)	Heat Capacity (J/m³-°C)
Dry Sand	0.27	R-0.53	1.212×10^6
Moist Sand	2.0	R-0.072	1.56×10^6
Saturated Sand	4.0	R-0.036	1.92×10^6
Dry Clay	0.15	R-0.96	1.285×10^6
Moist Clay	0.9	R-0.16	1.285×10^6
Saturated Clay	2.5	R-0.058	1.285×10^6
Soil 1	0.35	R-0.41	1.212×10^6
Soil 2	0.4	R-0.36	1.212×10^6
Soil 3	0.5	R-0.29	1.285×10^6
Soil 4	0.6	R-0.24	1.212×10^6
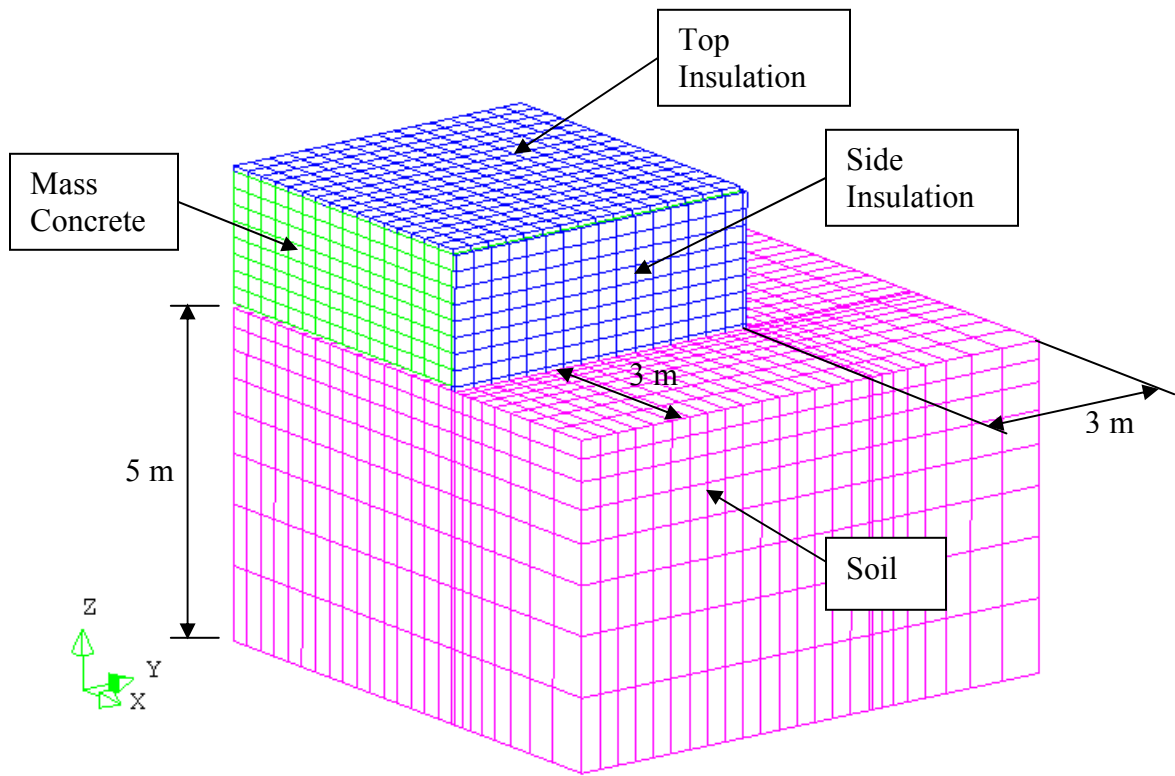
Figure 7-1. Finite element mesh of concrete footing in direct contact with soil.

7.2 Soil Temperature Distribution

To investigate the temperature in soil caused by heat of hydration generated from a mass concrete footing placed directly on it, two cases of soil, including dry sand and saturated sand, were analyzed. The thermal conductivity and R-value of each type of sand are listed in Table 7-1.

The temperature contours in dry and saturated sand are illustrated in Figure 7-2. Figures 7-3 and 7-4 show plots of temperature with respect to depth in dry and saturated sand at 3 locations: center, mid-side and corner of the footing. It can be seen that among the 3 locations, the temperature in soil at the center of footing was highest while the temperature in soil at the corner was lowest. This was due to the large contact area between the concrete and the soil at the

bottom middle allowing more heat to transfer to the soil, and the small contact area at mid-sides

and corner allowing less heat to transfer. The top layer of dry sand had a higher temperature than

that of saturated sand. The surface of the dry soil at the center, mid-side, and corner of footing

had temperatures of 77.4°C, 68.4°C, and 59.8°C, respectively, whereas that of the saturated soil

had lower temperatures of 64.3°C, 44.9°C, and 35.1°C, respectively. However, due to the lower

R-value, the saturated sand allowed heat from the concrete to transfer to a lower depth of around

5 m as compared with a depth of 1 m in the dry sand. It was also noted from the figures that heat

from the concrete transferred downwards better than sidewards in soil.
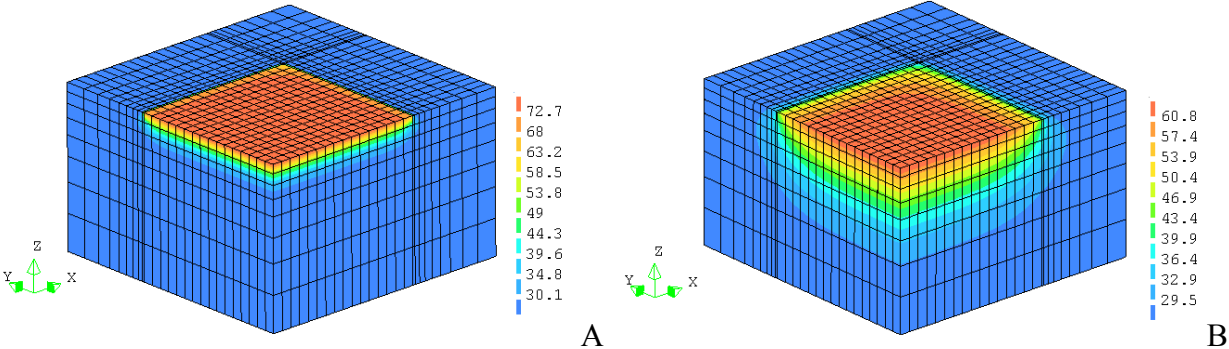
**Figure 7-2. Temperature distribution in soil 7 days after concrete placement. A) Dry sand.
B) Saturated sand.**
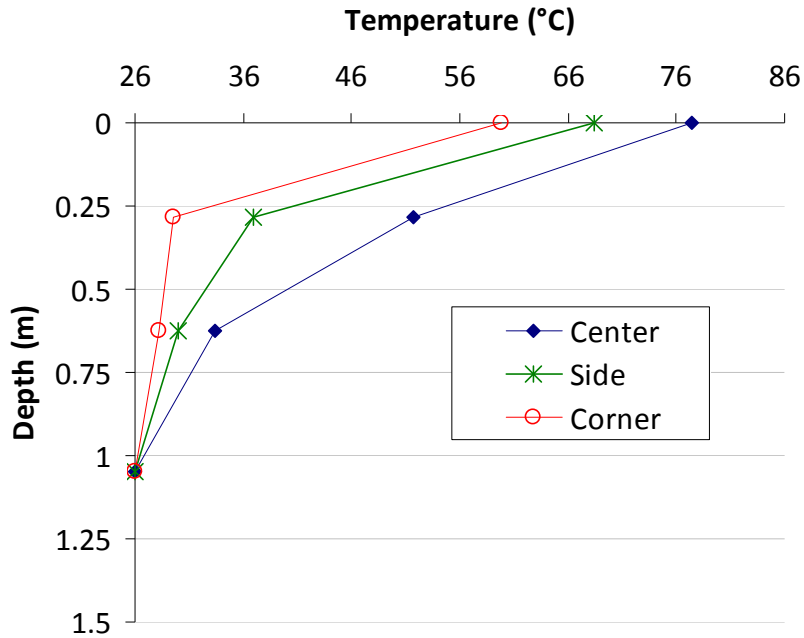
Figure 7-3. Temperature with respect to depth in dry sand 7 days after concrete placement.
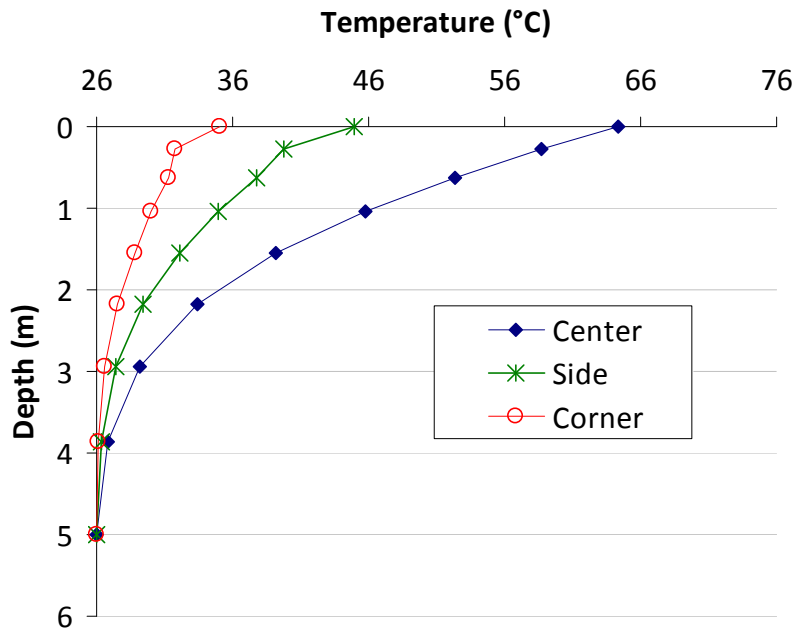
Figure 7-4. Temperature with respect to depth in saturated sand 7 days after concrete placement.

7.3 Temperature Development in Concrete

Figures 7-5 and 7-6 show the temperature developments in the concrete placed directly on dry sand and saturated sand, respectively. The center of concrete in the two cases had similar temperature profiles as it peaked 81°C in the case of dry sand and 77.5°C in the case of saturated sand at 7th day. However, the obvious difference between the 2 cases occurred in the concrete at the bottom corner. For the dry sand, the concrete temperature at this location gradually increased after 30 hours before it reached a high point of 59.8°C at 168th hour, while for the saturated sand, it remained constant at 35°C throughout this time period. The temperature differential, therefore, in the concrete on the dry sand was 21.2°C while it was doubled (42.5°C) in the concrete on the saturated sand. This sign revealed that the concrete on the saturated sand was likely to crack while the cracking probability in the concrete on the dry sand needed to be investigated.
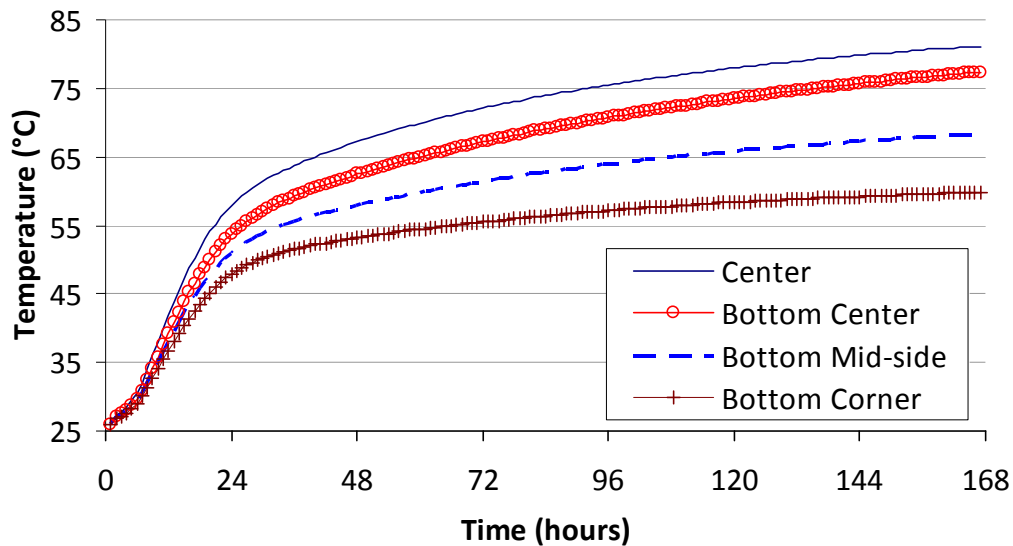
Figure 7-5. Temperature development in concrete footing placed on dry sand.
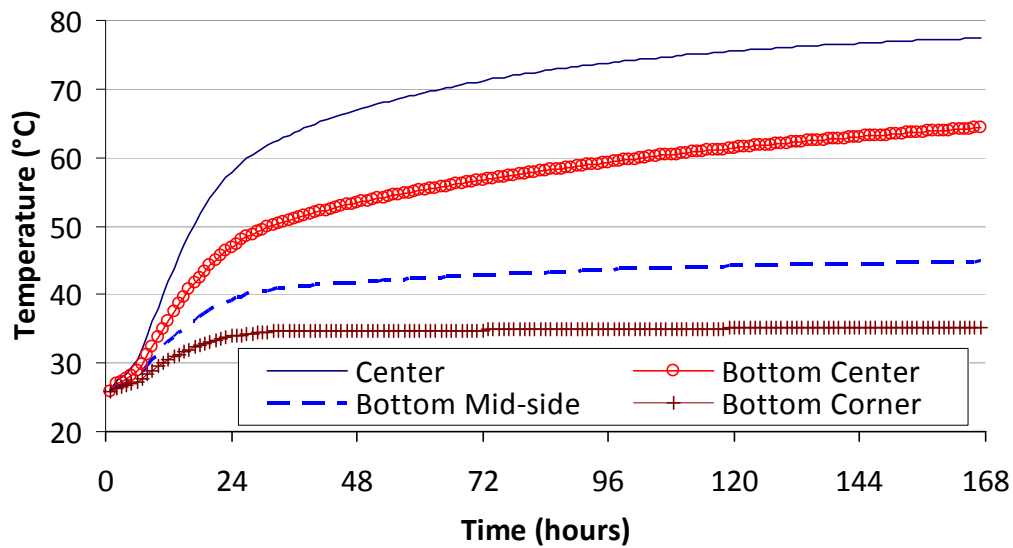
Figure 7-6. Temperature development in concrete footing placed on saturated sand.

7.4 Thermal Cracking Analysis

The probability of cracking is measured by the function called the crack index:

$$I_{cr}(t) = \frac{f_t(t)}{\sigma_I(t)}$$ (7-2)

where I_{cr} = crack index (if I_{cr} falls below 1.0, cracking has been initiated)

f_t = tensile strength

σ_I = maximum principal stress

t = time from concrete placement (hour)

The physical properties of the concrete were obtained from laboratory testing as shown in Table 7-2 (Lawrence et al., 2012). The concrete had density of 2,248 kg/m^3, Poisson's ratio of 0.2, and coefficient of thermal expansion of 9.16×10^{-6} mm/mm-°C.

Figure 7-7 illustrates the performance of the concrete with respect to the crack index for dry, moist, and saturated sand. As stated earlier, a crack index value less than 1.0 occurs when the induced tensile stress exceeds the early-age tensile strength of the concrete and indicates the

77

initiation of cracking. The results in this figure show that for the saturated and moist sands, the

crack index dropped to a value less than 1.0 within the first 24 hours while for the dry sand, the

crack index remained above 1.4. Therefore, this suggested that the dry sand provided good

protection against heat loss at the concrete bottom leading to low thermal gradients and thus low

tensile stresses.

Table 7-2. Physical Properties of Concrete

Time (day)	1	2	3	7
Tensile Strength (MPa)	1.25	1.66	1.93	2.206
Young's Modulus (MPa)	13,445	16,892	18,064	20,202

Thermal cracking analysis was also conducted for dry, moist, and saturated clays in this

chapter and the minimum calculated crack indices are plotted in Figure 7-8. This figure shows a

similar trend observed in Figure 7-7 as the crack index for the dry clay stayed above 1.9 while it

fell below 1.0 for the saturated and moist clays.

It was needed to extend analysis to moist sand and moist clay with different R-values in

order to investigate the threshold of R-value of soil that provides adequate insulation for the

concrete to prevent early-age thermal cracking. Figure 7-9 shows the minimum calculated crack

indices of the concrete on the soil with R-values ranging from 0.53 to 0.072. It is clearly seen

that the crack index decreased with the decrease of R-value. At an R-value of 0.29, the crack

index remained slightly above 1.0 throughout 7 days of cement hydration, therefore indicating

that cracking did not initiate in the concrete of the 10.36-m ×10.36-m × 2.03-m footing.

Analyses on 4-m × 4-m × 1-m, 20-m × 20-m × 5-m, 32-m × 32-m × 8-m, and 48-m × 48-

m × 12-m footings, as listed in Table 7-3, were also conducted. Soil with R-values of 0.29 and

0.41 were analyzed for each analysis. The minimum calculated crack index in these footings with respect to footing's volume-to-surface area ratio (V/A) are presented in Figure 7-10. It was found that soil with an R-value of 0.29 did not provide adequate insulation for a footing with a V/A of greater than 2.4, as the minimum calculated crack index dropped below 1.0. However, with an R-value of 0.41, the soil provided adequate insulation for a footing with a V/A up to 13.0.

Therefore, it could be concluded that soil (sand/clay) with an R-value of 0.41 or greater would provide adequate insulation at the bottom of mass concrete footing in terms of preventing thermal cracking.

Table 7-3. Footing Dimensions and Volume-to-Surface Area Ratio

Length (m)	4	10.36	20	32	48
Width (m)	4	10.36	20	32	48
Depth (m)	1	2.03	5	8	12
Volume:Surface Area Ratio (ft)	1.09	2.39	5.47	8.75	13.12
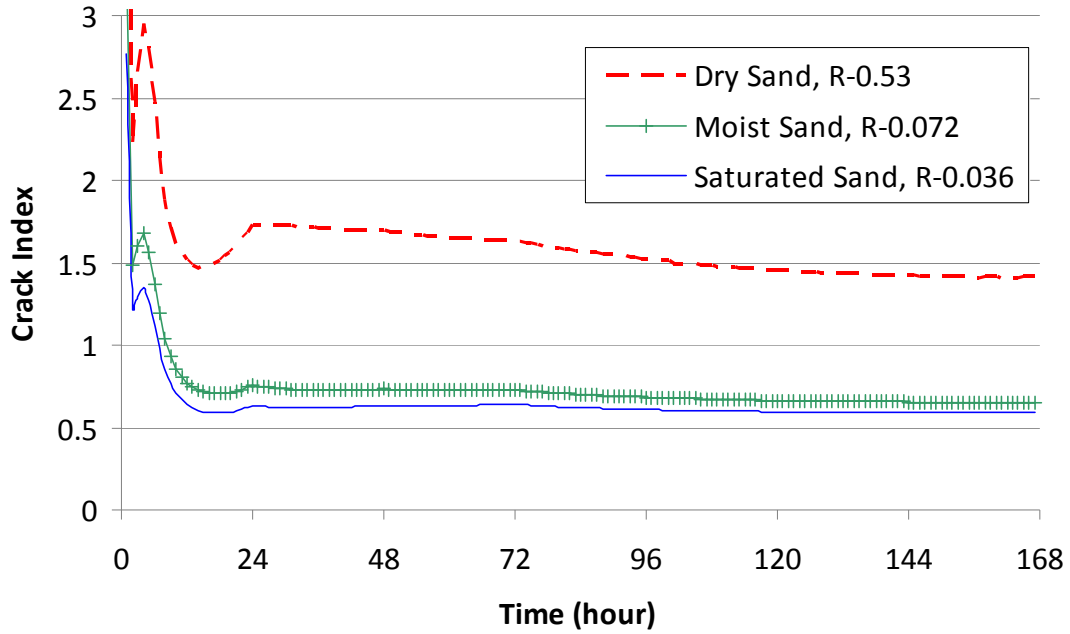
Figure 7-7. Minimum calculated crack index in concrete on sand.
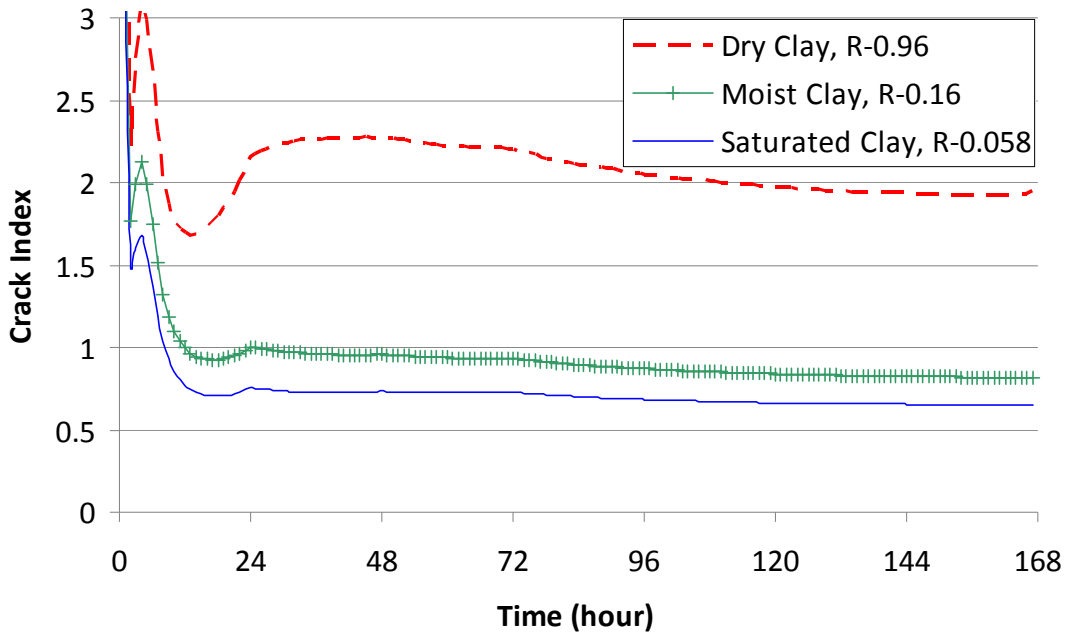
Figure 7-8. Minimum calculated crack index in concrete on clay.
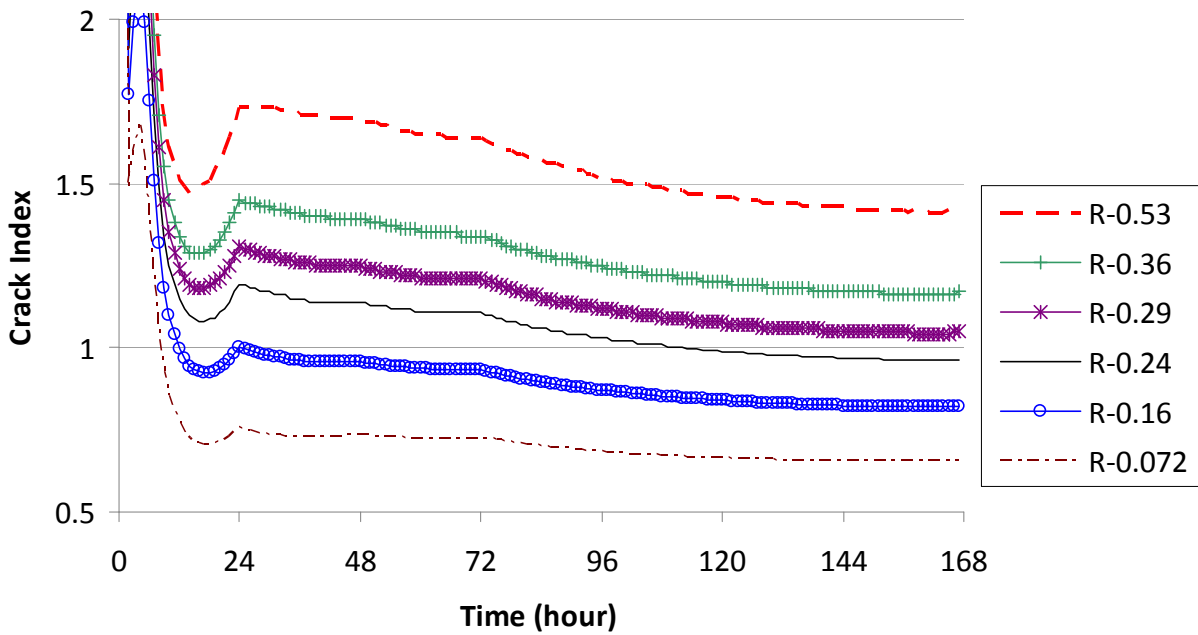
Figure 7-9. Minimum calculated crack index in concrete on soil with varying R-value.

81

7.5 Summary of Findings

The main findings from the parametric study in this chapter can be summarized as

follows:

- At the contact surface between the mass concrete footing and soil, dry soil had higher temperatures than wet or saturated soil. This was because wet soil allowed the heat of hydration generated from the concrete to transfer to a greater depth than dry soil did.

- The concrete footing on soil had the highest temperatures at its bottom center and had the lowest temperatures at its bottom corner.

- Mass concrete footing developed similar temperatures at its center regardless of whether it was placed on dry or saturated soil. However, the temperatures at its corner were quite different for the case of dry soil as compared with the case of saturated soil.

- Dry sand and dry clay provided good insulation at the bottom of mass concrete footing, as indicated from the crack indices obtained from the thermal cracking analysis performed.

- Soil with an R-value of 0.41 or greater (or thermal conductivity of 0.35 J/sec-m-°C or lower) would provide adequate insulation at the bottom of concrete footing using Mix 1 to prevent cracking. For footings with a V/A of less than 2.4 ft, soil with an R-value of 0.29 would be adequate to prevent cracking. Thus, an insulating layer between the mass concrete and the soil would not be needed in such situations.

CHAPTER 8
EFFECTS OF FOOTING'S DIMENSIONS AND INSULATION ON TEMPERATURE DEVELOPMENT AND CRACKING IN CONCRETE

8.1 Description of the Parametric Study

Although the FDOT Standard Specifications for Road and Bridge Construction require that the maximum temperature differential between the concrete core and the exterior surface does not exceed 35°F (20°C), it is not clear whether or not this limiting value is dependent on a footing's dimensions. This research investigates the effects of a footing's dimensions on the maximum allowable temperature differential to prevent cracking in concrete. The study also determines the required insulation to prevent early-age cracking in concrete footings.

For this task, a parametric study consisting of 63 finite element analyses (63 cases) was conducted. Three different shapes of rectangular footings were considered: cubic shape; length:width:depth ratio = 4:4:1; and length:width:depth ratio = 4:2:1. The dimensions of footing for all the cases studied are given in Tables 8-1 through 8-9.

The modeled concrete footing was fully insulated at its top, sides, and bottom with Styrofoam that had an R-value of 5.0 per inch. The insulation thicknesses modeled were 0.5 in., 1 in., and 1.25 in. The concrete properties used were the same as those of Concrete Mix 1 that had water to cementitious material ratio of 0.5 and the cementitious material consisted of 100% Type I Portland cement (Lawrence et al. 2012).

Table 8-1. Temperatures and Crack Index in Cubic Footings Insulated with 0.5-in Styrofoam

Length (m)	2	3	4	8	12	16	24
Width (m)	2	3	4	8	12	16	24
Depth (m)	2	3	4	8	12	16	24
Volume:Surface Area Ratio (ft)	1.09	1.64	2.19	4.37	6.56	8.75	13.12
Max. Temperature (°C)	71.4	78.8	82.6	83.9	83.9	84.1	84.6
Max. Temperature Difference (°C)	21.5	30.2	32.9	35.2	35.1	35	34.8
Crack Index	1.22	0.864	0.727	0.628	0.605	0.588	0.576

Table 8-2. Temperatures and Crack Index in Cubic Footings Insulated with 1-in Styrofoam

Length (m)	2	3	4	8	12	16	24
Width (m)	2	3	4	8	12	16	24
Depth (m)	2	3	4	8	12	16	24
Volume:Surface Area Ratio (ft)	1.09	1.64	2.19	4.37	6.56	8.75	13.12
Max. Temperature (°C)	74.9	80.9	83.1	83.9	83.9	84	84.3
Max. Temperature Difference (°C)	15	20.4	22.5	23.2	23	22.9	22.4
Crack Index	1.77	1.24	1.07	0.973	0.953	0.933	0.929

Table 8-3. Temperatures and Crack Index in Cubic Footings Insulated with 1.25-in Styrofoam

Length (m)	2	3	4	8	12	16	24
Width (m)	2	3	4	8	12	16	24
Depth (m)	2	3	4	8	12	16	24
Volume:Surface Area Ratio (ft)	1.09	1.64	2.19	4.37	6.56	8.75	13.12
Max. Temperature (°C)	76.3	81.5	83.3	83.9	83.9	84	84.3
Max. Temperature Difference (°C)	13	17.6	19.3	19.5	19.6	19.4	19
Crack Index	2.04	1.43	1.25	1.15	1.13	1.11	1.11

Table 8-4. Temperatures and Crack Index in 4:4:1 Footings Insulated with 0.5-in Styrofoam

Length (m)	4	6	8	16	24	32	48
Width (m)	4	6	8	16	24	32	48
Depth (m)	1	1.5	2	4	6	8	12
Volume:Surface Area Ratio (ft)	1.09	1.64	2.19	4.37	6.56	8.75	13.12
Max. Temperature (°C)	72.3	77.9	80.3	83.6	84	84.3	84.9
Max. Temperature Difference (°C)	25.2	29.9	31.9	34.9	35	34.7	33.9
Crack Index	1.05	0.838	0.753	0.634	0.599	0.583	0.581

Table 8-5. Temperatures and Crack Index in 4:4:1 Footings Insulated with 1-in Styrofoam

Length (m)	4	6	8	16	24	32	48
Width (m)	4	6	8	16	24	32	48
Depth (m)	1	1.5	2	4	6	8	12
Volume:Surface Area Ratio (ft)	1.09	1.64	2.19	4.37	6.56	8.75	13.12
Max. Temperature (°C)	76.3	80	81.5	83.7	83.9	84.1	84.6
Max. Temperature Difference (°C)	17.6	20.1	21.1	22.9	22.9	22.6	21.8
Crack Index	1.53	1.29	1.19	1.01	0.958	0.937	0.953

Table 8-6. Temperatures and Crack Index in 4:4:1 Footings Insulated with 1.25-in Styrofoam

Length (m)	4	6	8	16	24	32	48
Width (m)	4	6	8	16	24	32	48
Depth (m)	1	1.5	2	4	6	8	12
Volume:Surface Area Ratio (ft)	1.09	1.64	2.19	4.37	6.56	8.75	13.12
Max. Temperature (°C)	77.4	80.5	81.8	83.8	83.9	84	84.5
Max. Temperature Difference (°C)	15.2	17.1	17.9	19.6	19.4	19.1	18.4
Crack Index	1.79	1.54	1.41	1.2	1.14	1.12	1.14

Table 8-7. Temperatures and Crack Index in 4:2:1 Footings Insulated with 0.5-in Styrofoam

Length (m)	4.6	7	9.4	20	28	36	56
Width (m)	2.3	3.5	4.7	10	14	18	28
Depth (m)	1.15	1.75	2.35	5	7	9	14
Volume:Surface Area Ratio (ft)	1.08	1.64	2.20	4.69	6.56	8.44	13.12
Max. Temperature (°C)	71.5	78.2	81.2	83.9	84	84.2	84.6
Max. Temperature Difference (°C)	23.4	30	32.6	35.1	35.1	35	34.2
Crack Index	1.2	0.868	0.73	0.619	0.595	0.582	0.576

Table 8-8. Temperatures and Crack Index in 4:2:1 Footings Insulated with 1-in Styrofoam

Length (m)	4.6	7	9.4	20	28	36	56
Width (m)	2.3	3.5	4.7	10	14	18	28
Depth (m)	1.15	1.75	2.35	5	7	9	14
Volume:Surface Area Ratio (ft)	1.08	1.64	2.20	4.69	6.56	8.44	13.12
Max. Temperature (°C)	75.5	80.2	82.1	83.9	83.9	84	84.3
Max. Temperature Difference (°C)	16.4	20	21.6	23.1	22.9	22.7	21.9
Crack Index	1.79	1.27	1.11	0.972	0.94	0.925	0.936

Table 8-9. Temperatures and Crack Index in 4:2:1 Footings Insulated with 1.25-in Styrofoam

Length (m)	4.6	7	9.4	20	28	36	56
Width (m)	2.3	3.5	4.7	10	14	18	28
Depth (m)	1.15	1.75	2.35	5	7	9	14
Volume:Surface Area Ratio (ft)	1.08	1.64	2.20	4.69	6.56	8.44	13.12
Max. Temperature (°C)	76.8	80.7	82.4	83.9	83.9	84	84.2
Max. Temperature Difference (°C)	14.2	17	18.5	19.7	19.5	19.3	18.4
Crack Index	2.09	1.49	1.31	1.15	1.12	1.1	1.12

8.2 Effects of Footing's Dimensions on Temperature Development and Cracking

Figure 8-1 presents the maximum temperatures in cubic footings for 3 cases of insulation thickness: 0.5, 1.0, and 1.25 in. For a cubic footing that had a volume-to-surface area ratio (V/A) between 1.0 ft and 4.0 ft, the maximum temperature developed in concrete increased with the increase in insulation thickness. For instance, a 2-m × 2-m × 2-m footing had a maximum temperature of 71.4°C, 74.9°C, and 76.3°C when insulated with 0.5 in., 1.0 in., and 1.25 in. of Styrofoam, respectively. However, the maximum temperature developed in a cubic footing that had a V/A greater than 4.0 ft was not dependent on thickness of insulation. It was also observed that the maximum temperature in a footing with V/A greater than 4.0 ft nearly remained unchanged at 84°C.

Figure 8-2 clearly shows the influence of insulation thickness on the temperature difference in cubic footings. The temperature difference in the concrete decreased with the increase in insulation thickness. With a V/A of less than 4.5 ft, and under the same insulation condition, a larger cubic footing had a higher maximum temperature difference. Interestingly, with a V/A of 4.5 ft or greater, a larger cubic footing had a similar or slightly smaller temperature difference under the same insulation condition.

Crack indices in cubic footings with different V/As and insulation thickness levels are shown in Figure 8-3. With a V/A of less than 4.5 ft, and under the same insulation condition, a larger cubic footing had a lower crack index. However, with a V/A of 4.5 ft or greater, a cubic footing had an almost constant crack index under the same insulation condition. This means that cracking potential no longer increased with increasing size after V/A exceeded 4.5 ft.

Figures 8-4 through 8-6 show the maximum temperatures, maximum temperature differences, and crack indices in 4:4:1 footings while those for 4:2:1 footings are shown in Figures 8-7 through 8-9. There was a similar trend in the maximum temperatures developed in

these footings as in cubic footings: the maximum temperature rapidly increased as the V/A increased from 1.0 ft to 4.5 ft, then it grew only slightly as the V/A became larger than 4.5 ft. The temperature difference increased as the V/A rose from 1.0 ft to 4.5 ft, then it slightly decreased as V/A became larger than 4.5 ft. The crack index dropped as the V/A grew from 1.0 ft to 4.5 ft, however, it leveled off as the V/A became larger than 4.5 ft.

As shown in Figures 8-5 and 8-6, the 4:4:1 footing insulated with 0.5 in. of Styrofoam, with a V/A of 1.09 ft, had a maximum temperature difference of 25.2°C and a crack index of 1.05 indicating no occurrence of cracking. The footing insulated with 1.0 in. of Styrofoam, with a V/A of 4.37 ft, had a maximum temperature difference of 22.9°C and a crack index of 1.01. Of these two footings, the smaller one had a higher maximum temperature difference but lower likelihood of cracking than the larger one, thus the smaller footing did not require a smaller maximum allowable temperature to prevent cracking. With a V/A of 4.5 ft or greater and with the same insulation thickness, a larger footing had a similar or slightly smaller maximum temperature difference but similar cracking potential (a similar crack index). The same results were drawn from the observations of cubic footings and 4:2:1 footings. Therefore, smaller footings do not require a smaller maximum allowable temperature than larger footings to prevent cracking.
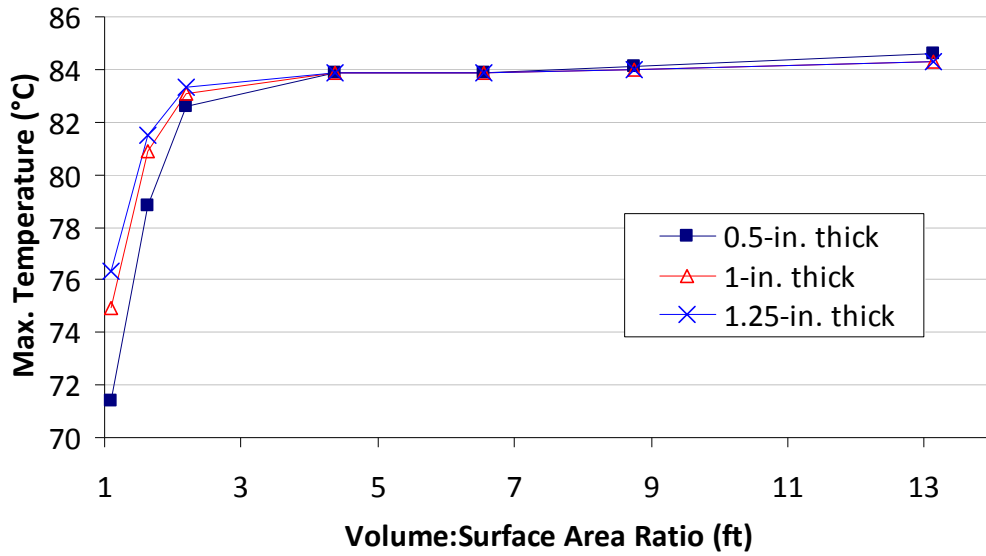
Figure 8-1. Maximum temperature in cubic footings.
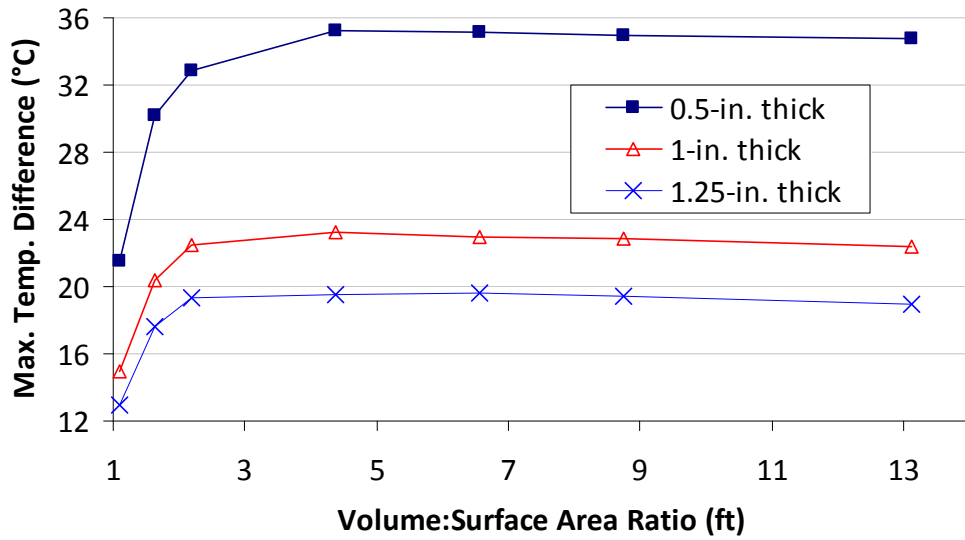
Figure 8-2. Maximum temperature difference in cubic footings.
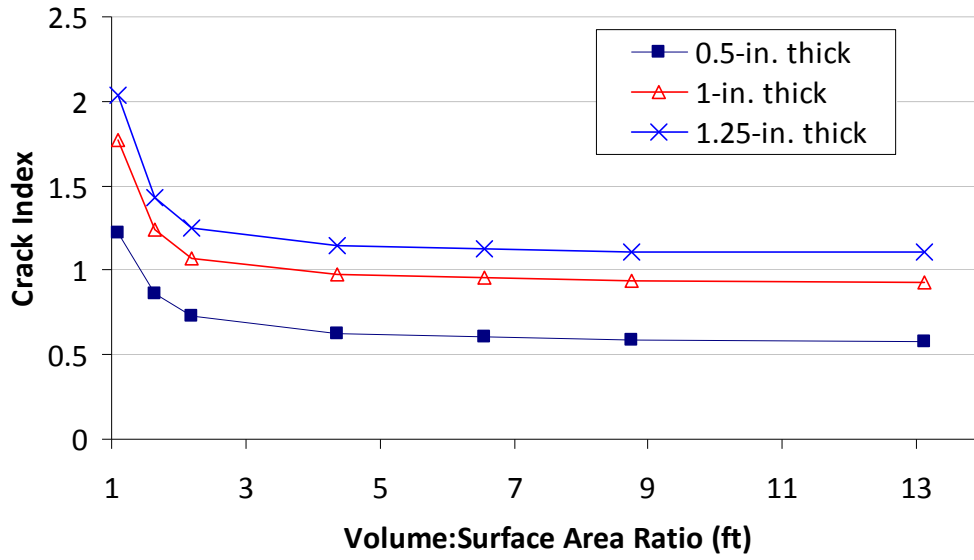
Figure 8-3. Crack Index in cubic footings.
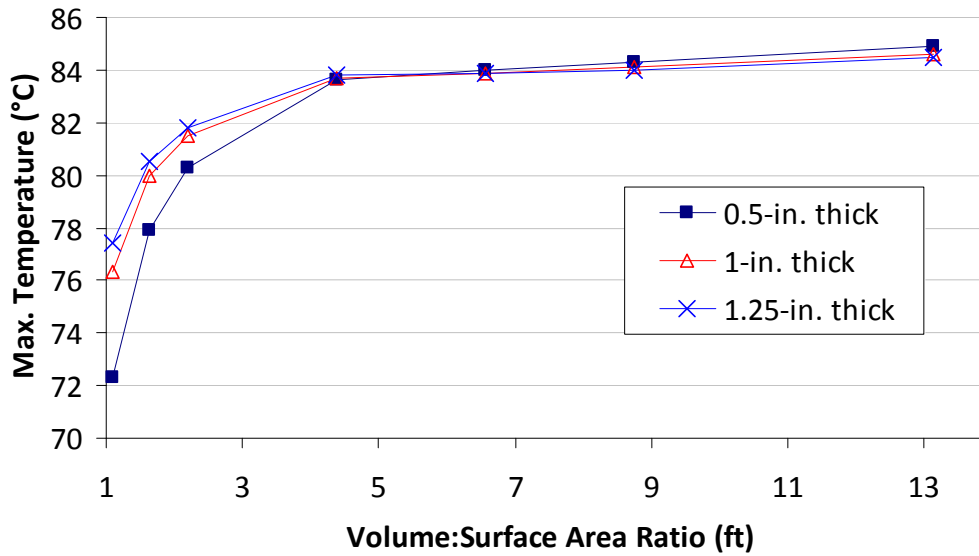
Figure 8-4. Maximum temperature in 4:4:1 footings.
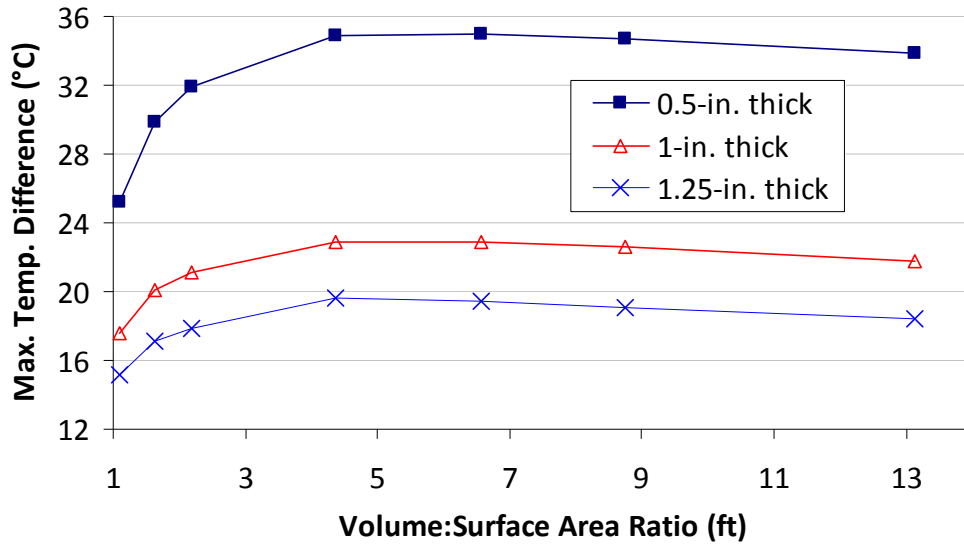
Figure 8-5. Maximum temperature difference in 4:4:1 footings.
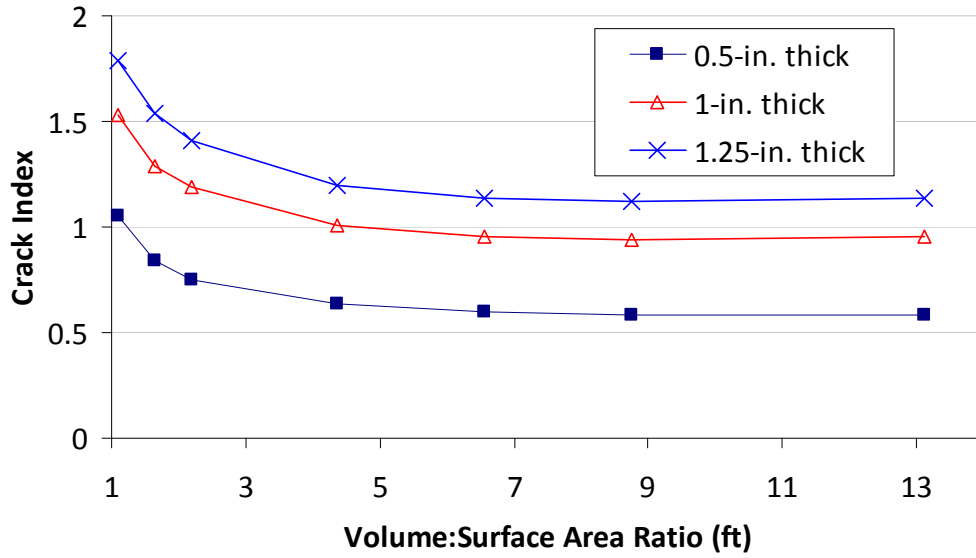
Figure 8-6. Crack Index in 4:4:1 footings.
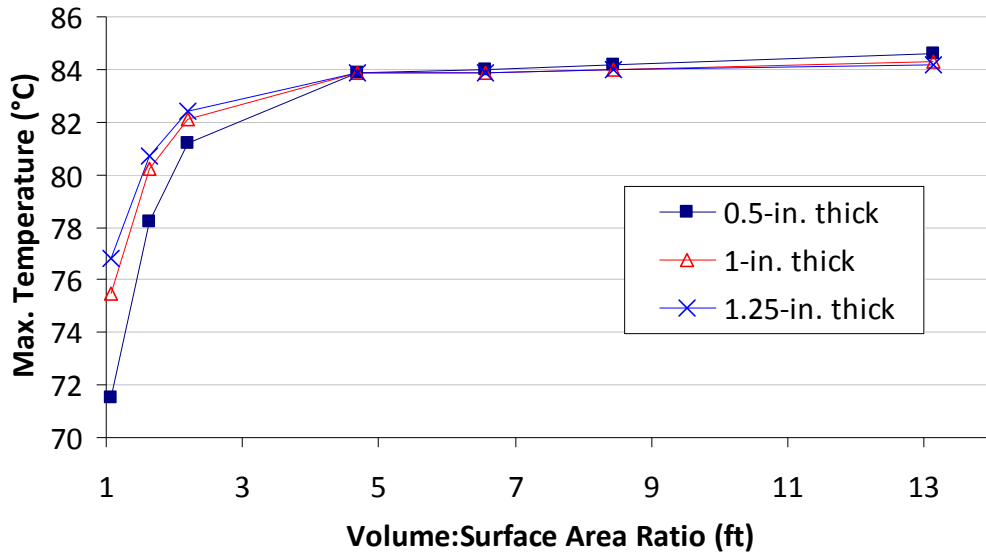
Figure 8-7. Maximum temperature in 4:2:1 footings.
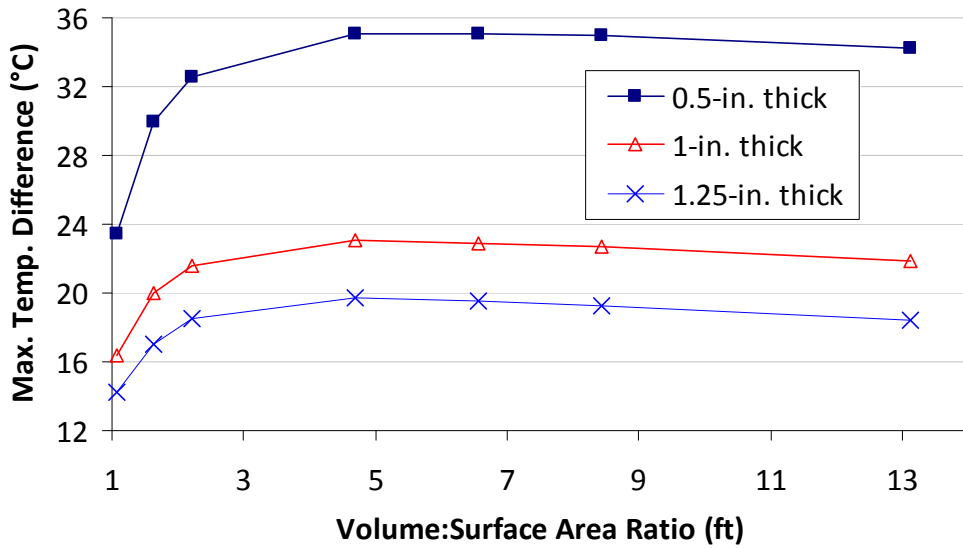
Figure 8-8. Maximum temperature difference in 4:2:1 footings.
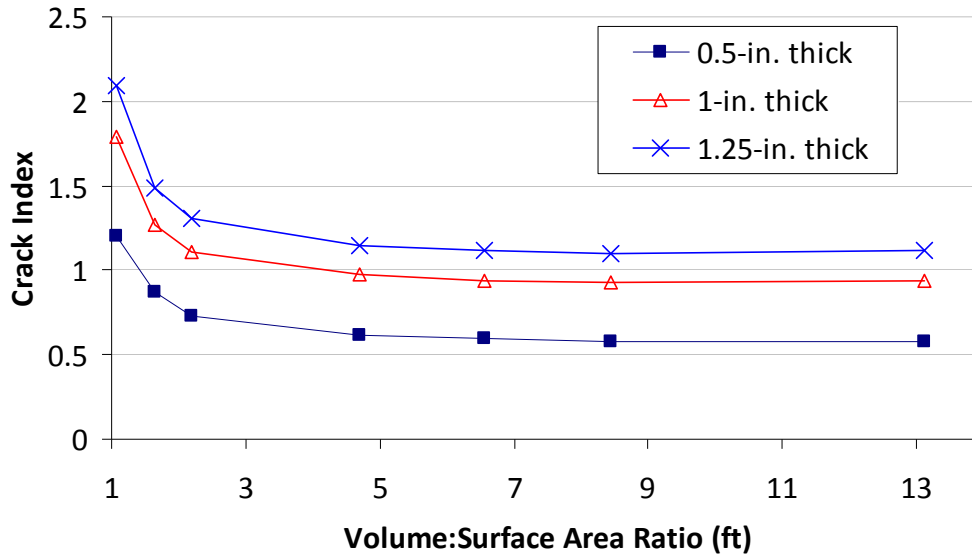
Figure 8-9. Crack Index in 4:2:1 footings.

8.3 Effects of Footing's Shape on Temperature Development and Cracking

The maximum temperatures, maximum temperature differences, and crack indices in all the modeled footings were then compared together for each insulation thickness level. Figures 8-10 through 8-12 show the maximum temperatures in footings fully insulated with 0.5 in., 1.0 in., and 1.25 in. of Styrofoam, respectively. For each insulation thickness level, the maximum temperatures that occurred in footings with the same V/A were very similar regardless of the footing's shapes. The difference in the maximum temperatures in the different footings having the same V/A did not exceed 2.3°C.

Figures 8-13 through 8-15 present the maximum temperature differences in the different footings fully insulated with 0.5 in., 1.0 in., and 1.25 in. of Styrofoam, respectively. For each insulation thickness level, the maximum temperature differences in footings that had the same V/A were very close to each other regardless of their shapes.

93

Figures 8-16 through 8-18 show the crack indices in the different footings for the cases of insulation with 0.5 in., 1.0 in., and 1.25 in. of Styrofoam, respectively. Again, for each insulation thickness level, the crack indices in footings that had the same V/A were very similar regardless of their shapes.

8.4 Determination of Required Insulation Thickness

In the analyses presented above, the insulation thickness was increased from 0.5 in. until it was adequate to prevent cracking in the concrete. Figure 8-16 shows the crack indices in all the footings insulated with 0.5 inch of Styrofoam. Beginning from a value slightly above 1.0 at a V/A of 1.09 ft, the crack index dropped sharply to below 1.0 as the V/A increased. Therefore, 0.5 inch of Styrofoam did not provide adequate insulation for footings with a V/A of greater than 1.09 ft to prevent cracking.

As shown in Figure 8-17, the crack index in a footing insulated with 1.0 in. of Styrofoam was greater than 1.0 at a V/A in the range of 1.0 ft and 4.0 ft, and was slightly below 1.0 as the V/A became larger. Hence, one inch of Styrofoam was adequate for footings with a V/A of 4.0 ft or smaller to insure no occurrence of cracking in the concrete.

Figure 8-18 shows the crack index in footings insulated with 1.25 inches of insulation. There was a sharp drop in the crack index as the V/A increased from 1.0 ft to 2.5 ft. The crack index then remained almost constant at a value of 1.1 when the V/A became larger than 4.0 ft. Therefore, an insulation thickness of 1.25 inches was adequate for footings with a V/A up to 13.0 ft to prevent cracking in the concrete induced by thermal contraction.
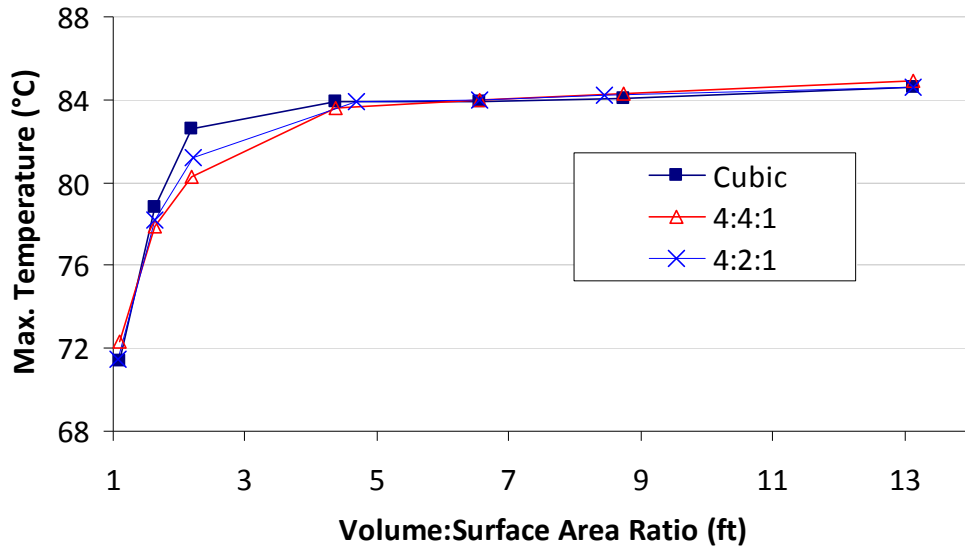
Figure 8-10. Maximum temperature in footings insulated with 0.5-in Styrofoam.
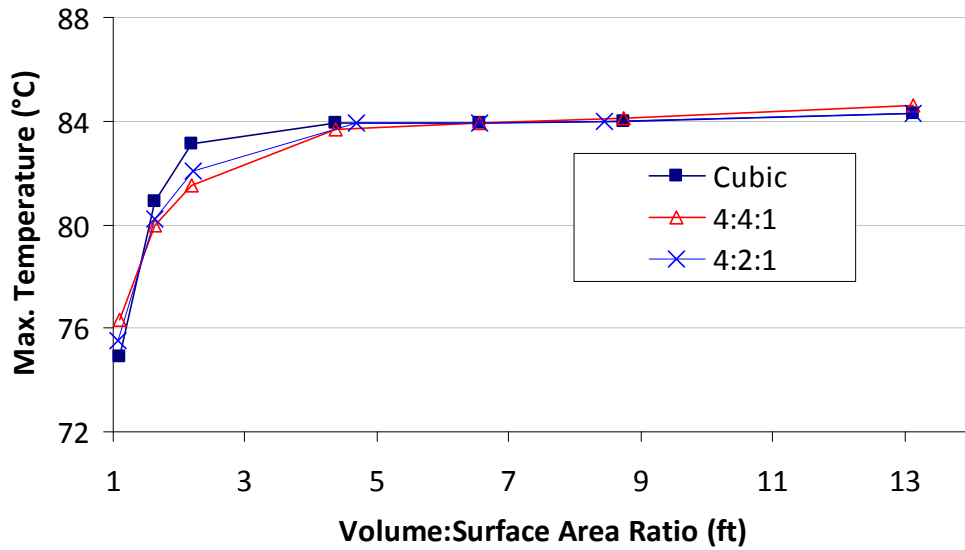
Figure 8-11. Maximum temperature in footings insulated with 1-in Styrofoam.
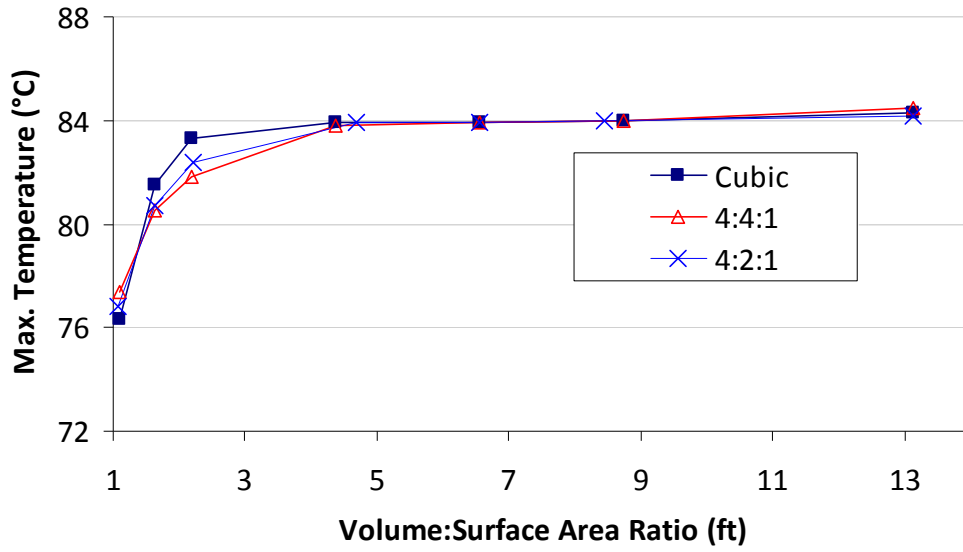
Figure 8-12. Maximum temperature in footings insulated with 1.25-in Styrofoam.
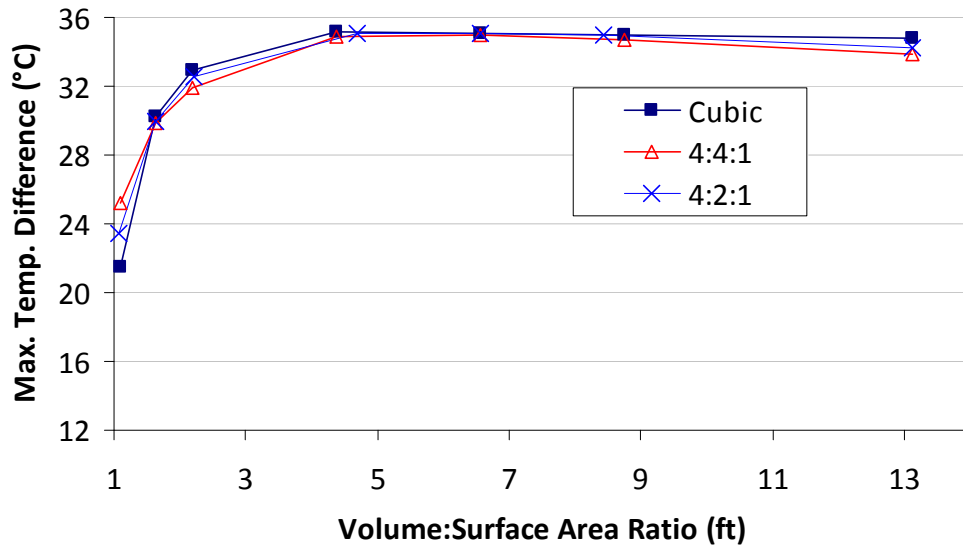
Figure 8-13. Maximum temperature difference in footings insulated with 0.5-in Styrofoam.
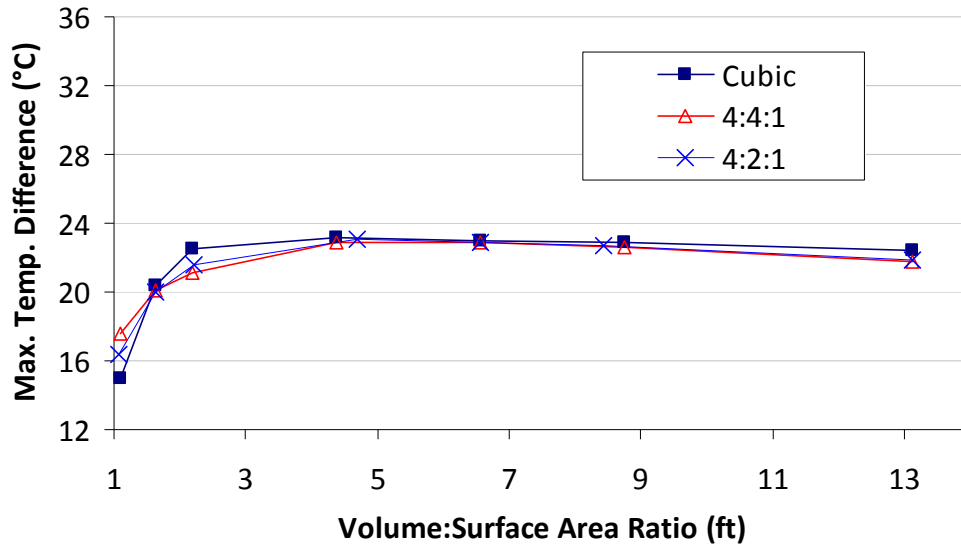
Figure 8-14. Maximum temperature difference in footings insulated with 1-in Styrofoam.
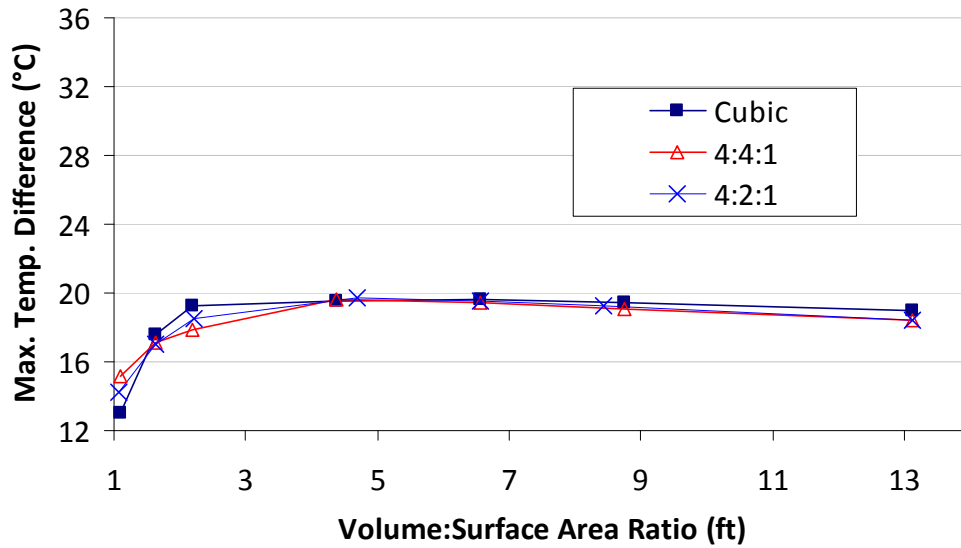
Figure 8-15. Maximum temperature difference in footings insulated with 1.25-in Styrofoam.

97
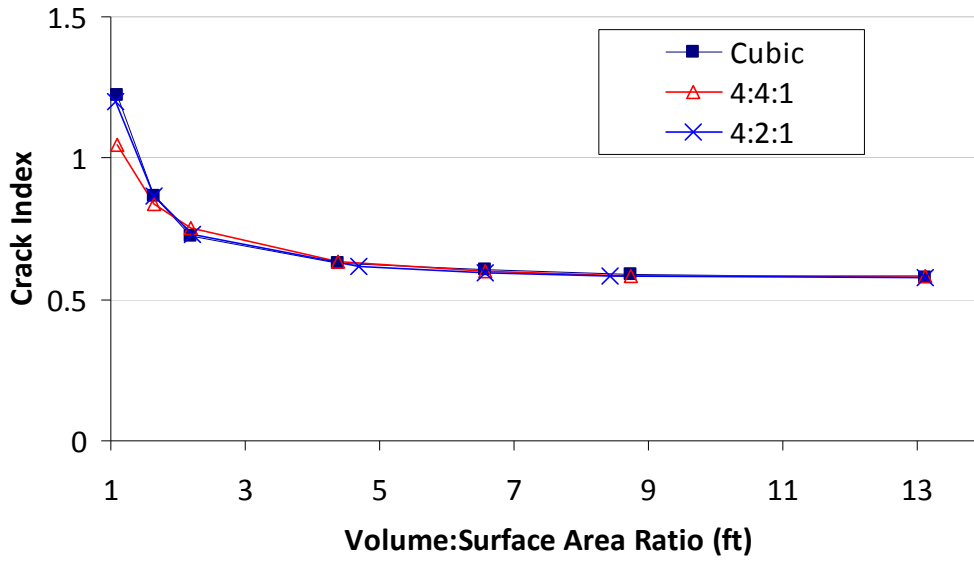
Figure 8-16. Crack Index in footings insulated with 0.5-in Styrofoam.
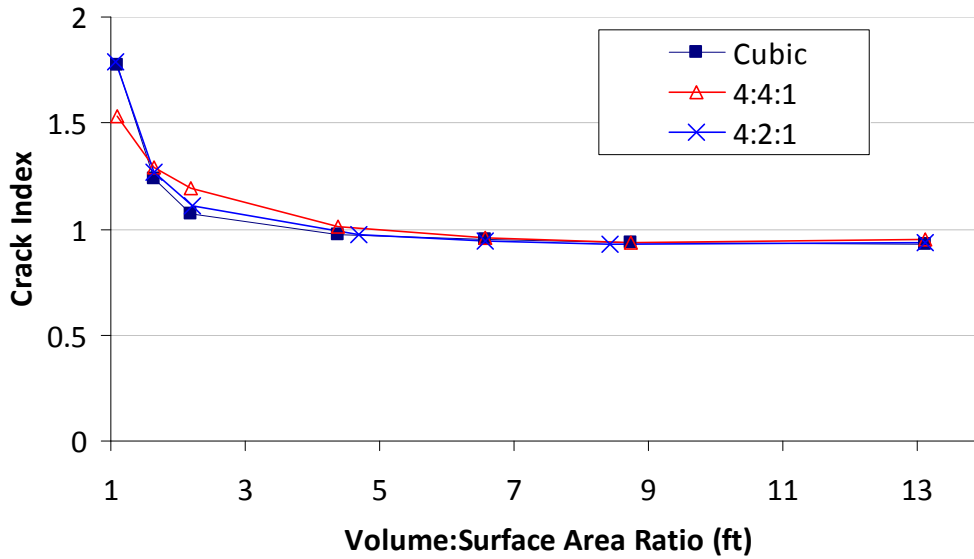
Figure 8-17. Crack Index in footings insulated with 1-in Styrofoam.
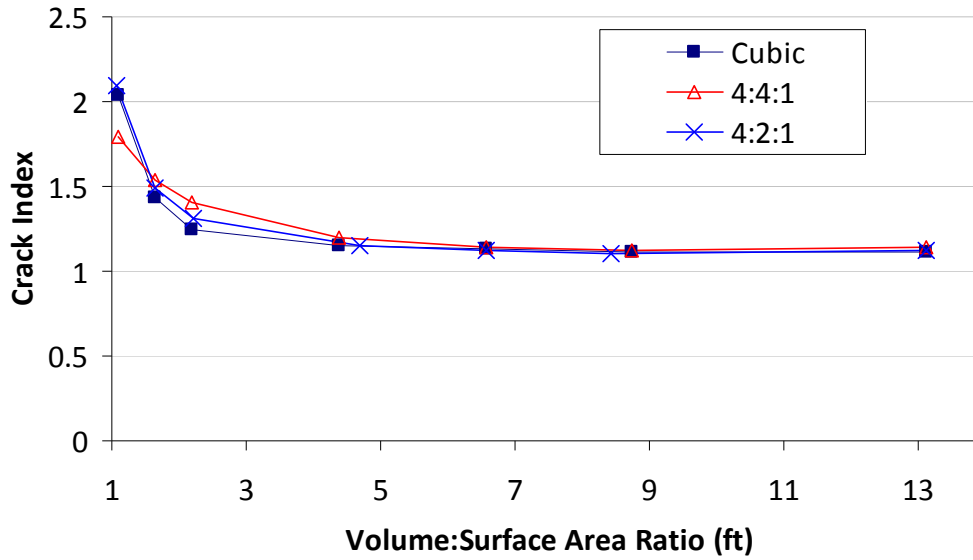
Figure 8-18. Crack Index in footings insulated with 1.25-in Styrofoam.

Table 8-10 shows the required insulation thickness to prevent cracking and the maximum temperature differentials for the footings (using concrete of Mix 1) with V/As ranging from 1.1 to 13.1. It was found that the maximum temperature differentials varied according to the size of the mass concrete footings especially for V/As less than 4.5 ft.

Table 8-10. Required insulation thickness and maximum temperature differential for different V/As

V/A (ft)	R-value per in.	Required Insulation Thickness (in.)	Maximum Temperature Differential (°C)
1.1	5.0	0.5	25.2
1.6	5.0	0.7	25.4
2.2	5.0	1.0	22.5
4.4	5.0	1.1	21.6
6.6	5.0	1.2	20.8
8.8	5.0	1.2	20.3
13.1	5.0	1.2	20.1

8.5 Summary of Findings

The main findings from the parametric study in this chapter can be summarized as

follows:

- The maximum temperature developed in a rectangular footing with a V/A of less than 4.5 ft was higher if insulated with thicker insulation. In a footing with a V/A of 4.5 ft or greater, however, it was not dependent on insulation thickness.

- The temperature differential in a concrete footing decreased with the increase in insulation thickness.

- With a V/A of less than 4.5 ft, under the same insulation condition and using the same concrete mix, a larger footing had a higher maximum temperature difference, and lower crack index. However, with a V/A of 4.5 ft or greater, a larger footing had a similar or slightly smaller maximum temperature difference, and an almost constant crack index. Thus, cracking potential was not dependent on how large a footing was when its V/A was 4.5 ft or greater.

- Rectangular footings that had the same V/A but different shapes (dimensional proportions) would develop a similar maximum temperature, a similar maximum temperature difference, and a similar crack index under the same insulation condition.

- Smaller footings allow slightly higher maximum temperature differential before thermal cracking would occur.

- When Styrofoam with an R-value of 5.0 per inch was used, 0.5 inch would provide adequate insulation for a footing with a V/A of around 1.0 ft; 1.0 inch would provide adequate insulation for a footing with a V/A less than 4.0 ft; 1.25 inches would provide adequate insulation for a footing with a V/A up to 13.0 ft. If another type of insulating material is used, an equivalent insulation thickness can be determined from the material's R-value.

CHAPTER 9
DEVELOPMENT OF SOFTWARE FOR GENERATING DIANA INPUT FILES

9.1 Overview

DIANA (DIsplacement ANAlyzer) is an extensive multi-purpose finite element software package that is dedicated, but not exclusive, to a wide range of problems arising in civil engineering. However, it does not have available templates for prompt analysis of mass concrete structures such as footings, columns, and pier caps. It is therefore needed to develop a user-friendly computer program so as to aid users to easily create a mass concrete model, and to minimize time for constructing geometry of mass concrete structures with typical shapes and various options of insulation.

9.2 DIANA Input File Generator

User-friendly software named "DIANA Input File Generator" (DIFG) was developed using the Delphi programming language to provide prompt input files for DIANA before performing an analysis of mass concrete. The software interface is shown in Figure 9-1.
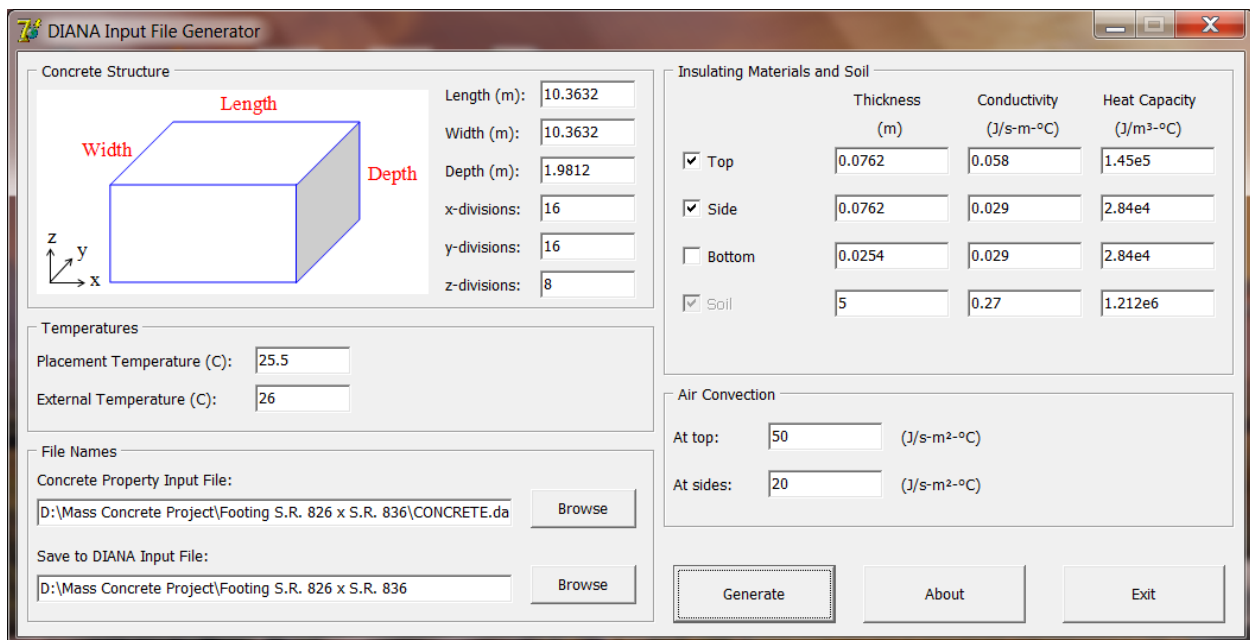
Figure 9-1. Software for generating DIANA input files.

The software can produce DIANA input files for rectangular footings as shown in the figure under "Concrete Structure" on its interface. In this group box, the user must enter dimensions of a footing in x, y and z-directions as well as a division (number of elements) in each direction. The program will create a model of one-quarter of the whole structure, that means the x and y dimensions of the actual structure will be reduced to a half in the finite element model.

In the group box "Temperatures", the user must enter the placement temperature of concrete (initial temperature) and external temperature. The "Insulating Materials and Soil" group box provides options of insulation at the top, sides and bottom of the footing. A soil layer beneath the footing will be automatically included to the model as a default. The user must enter the thickness, thermal conductivity and heat capacity for each of insulating layers and the soil layer. In the "Air Convection" group box, boundary air convection coefficients at the top and sides of the footing must be entered.

Finally, the user must specify the input file name of concrete properties being modeled and the input file name for DIANA in the "File Names" group box. These file names are in the extension of ".dat". The pre-created concrete property input file must include the thermal and mechanical properties of the concrete. The user can browse the concrete property input file using the "Browse" button as illustrated in Figure 9-2.
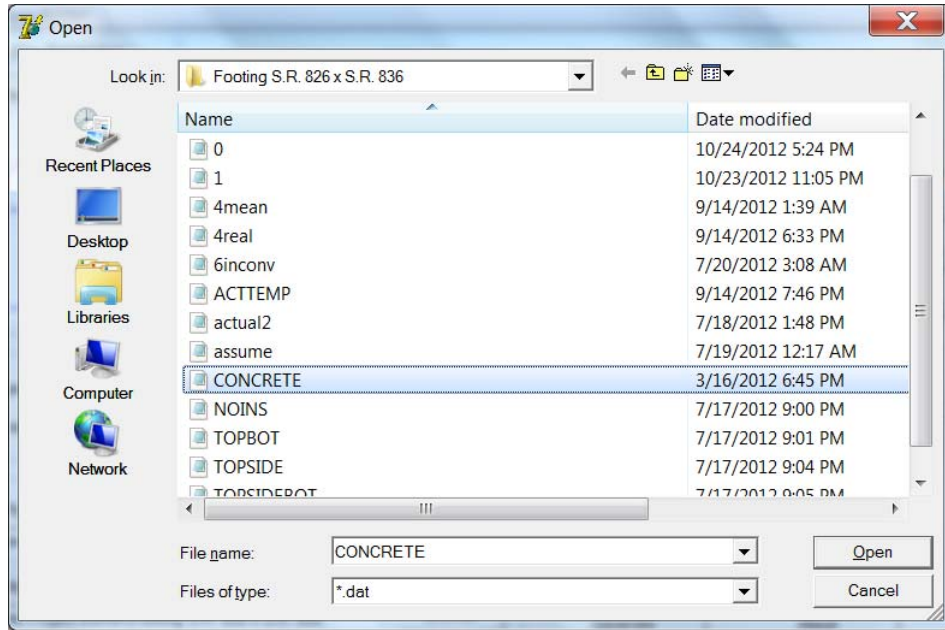
Figure 9-2. Browsing a concrete property file.

After all the parameters are determined and entered, the user may click the "Generate" button to start the generating process of DIANA input file. DIANA Input File Generator will set up the Diana 9.4.4 Environment and automatically create a .dat file by running iDIANA (pre- and post-processing of DIANA) (iDIANA Release 9.4.4., 2012) in silent mode as shown in Figure 9-3. If the generating process is successfully completed, a message will be shown by the software as illustrated in Figure 9-4.
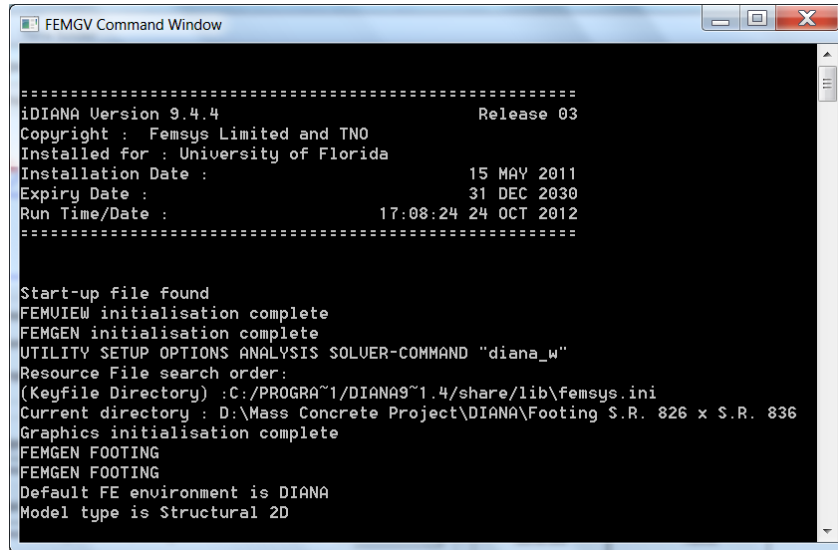
Figure 9-3. Generating process.
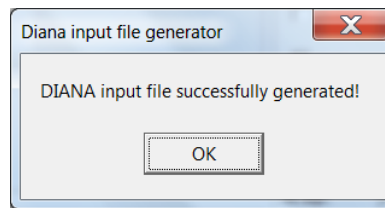
Figure 9-4. Message indicating the process is completed.

9.3 Running DIANA

Once the DIANA input file is generated, it is ready to be used in DIANA. The user

should run the DIANA software using the following steps:

- Choose Working directory (see Figure 9-5)
- Select "Initialize new"
- Click "Add" and select the DIANA input file that has been generated, then click "OK"
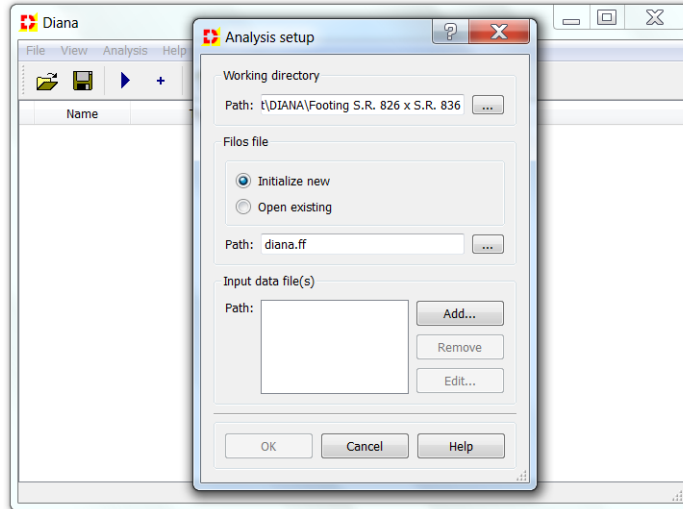
Figure 9-5. DIANA analysis setup.

- After reading input is completed, click "OK".
- ADINA will then show a window asking for analysis type as illustrated in Figure 9-6. Click "Cancel", DIANA will appear as shown in Figure 9-7.
- Open command file (i.e., "Command.dcf") and run.
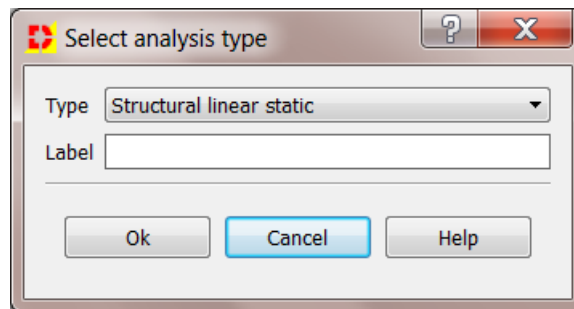
Figure 9-6. Selecting analysis type.
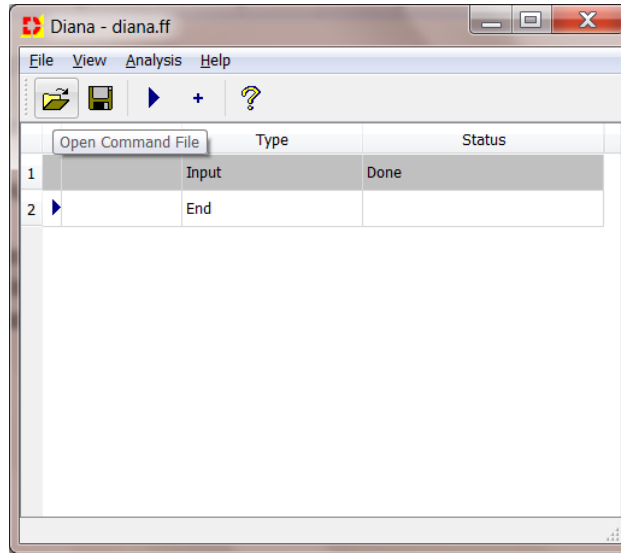
Figure 9-7. Open command file.

There are two types of output files created during running of DIANA that have the

following names:

- FLOW.* (.V72 and .G72): stores thermal results of the finite element thermal model
- STRUC.* (.V72 and .G72): stores stress results of the finite element structural model

Note: These files should be renamed prior to running another model, otherwise they will

be overwritten.

9.4 Example

9.4.1   Creating a Model Using DIFG

A mass concrete footing is to be modeled and analyzed to illustrate the use of DIFG and

DIANA. The footing has the dimensions of 10.36 m × 10.36 m × 1.98 m. The steps to create the

finite element model using DIFG are as follows:
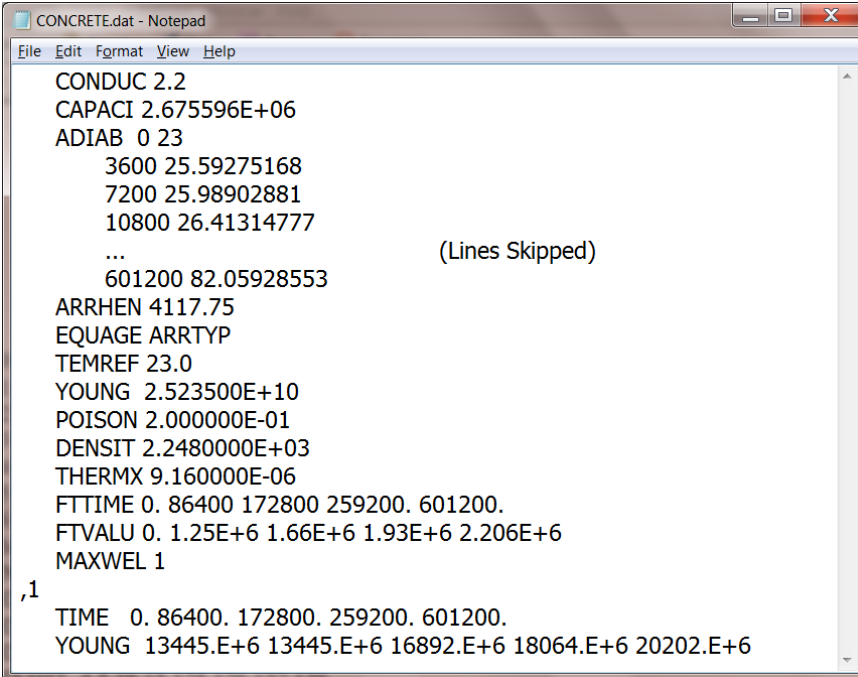
- Step 1: Enter a length of 10.36 m (in x-direction), a width of 10.36 m (in y-direction), and a depth of 1.98 m (in z-direction) in Box A (see Figure 9-8). Note: these numbers are the full dimensions of the footing. DIFG will generate a model of one-quarter of the whole footing, thus the finite element model of the concrete will have dimensions of 5.18 m × 5.18 m × 1.98 m.

- Step 2: Enter 16, 16, and 8 for divisions in x, y, and z-directions in Box B. This will create 16 × 16 × 8 = 2048 elements for the concrete.

- Step 3: In Box C, enter 25.5 (°C) for the placement temperature, 26 (°C) for the ambient temperature.

Figure 9-8. Input parameters for DIFG.

- Step 4: Enter or browse a file name of concrete properties in Box D. A concrete property file named "CONCRETE.dat" was created for the concrete used in the footing. Detailed contents of this file are shown in Figure 9-9.

- Step 5: Enter a name for the file to be generated in Box E. For instance, enter "footing.dat" with a full path.

- Step 6: Select "Top" and "Side" for top and side insulation in Box F. Enter 0.0762 m (3 inch) of thickness for each of them. Enter Conductivity and Heat Capacity values for each of insulating materials.

- Step 7: A soil layer is selected by default. Enter thickness (i.e., 5 m), Conductivity and Heat Capacity values for the soil layer in Box G.

- Step 8: Enter air convection coefficients for the top and side boundary surfaces. For instance, enter 30 for top and 20 for sides.

- Step 9: Click the "Generate" button. DIFG will call and run iDIANA to create the "footing.dat" file. Contents of this file type are given in Appendix B of "Development of

design parameters for mass concrete using finite element analysis" - Final Report (Tia et al., 2010). Run DIANA and follow the steps described in Section 8.3.

Figure 9-9. Detailed contents of "CONCRETE.dat" file.

9.4.2 Results and Post-Processing Commands in iDIANA

9.4.2.1 Thermal Results

To view thermal results from the thermal analysis, the user should run iDIANA (iDIANA Release 9.4.4., 2012) and open the "FLOW.V72" file (see Figure 9-10). The sketch of the model will appear as shown in Figure 9-11. The user then should interact with iDIANA by entering command lines. The following are standard commands to post-process the results (DIANA, 2012c).
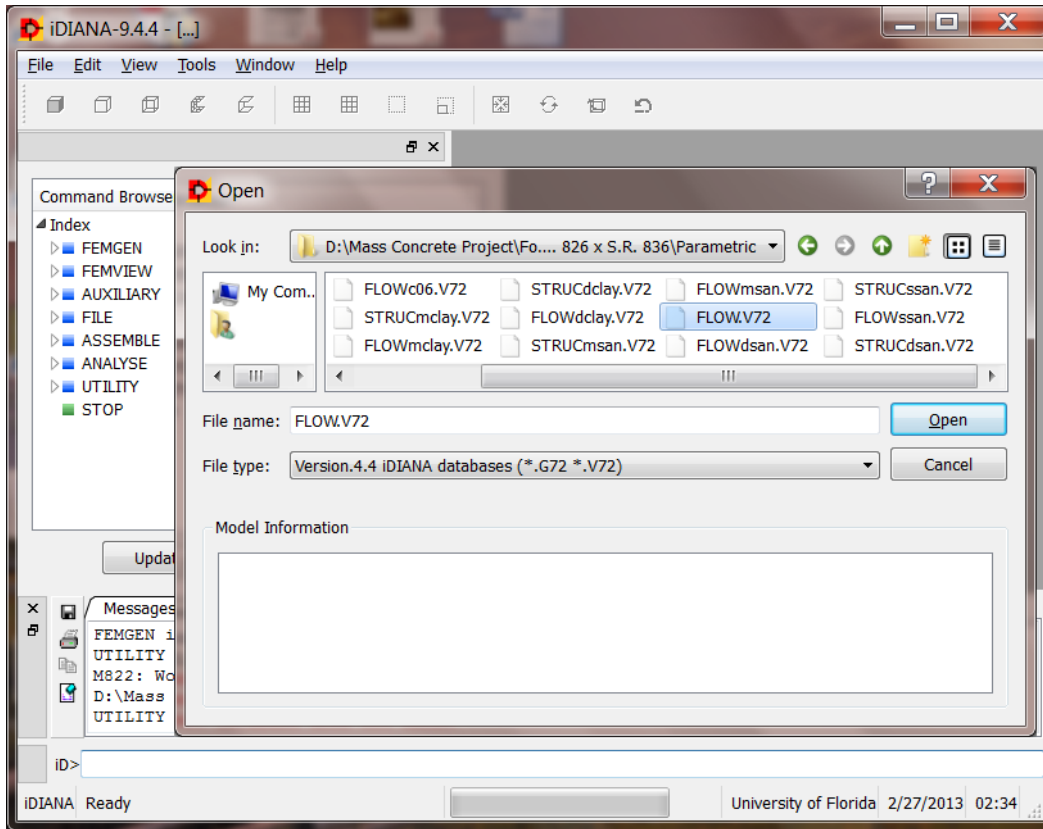
Figure 9-10. Open FLOW.V72 for thermal results.
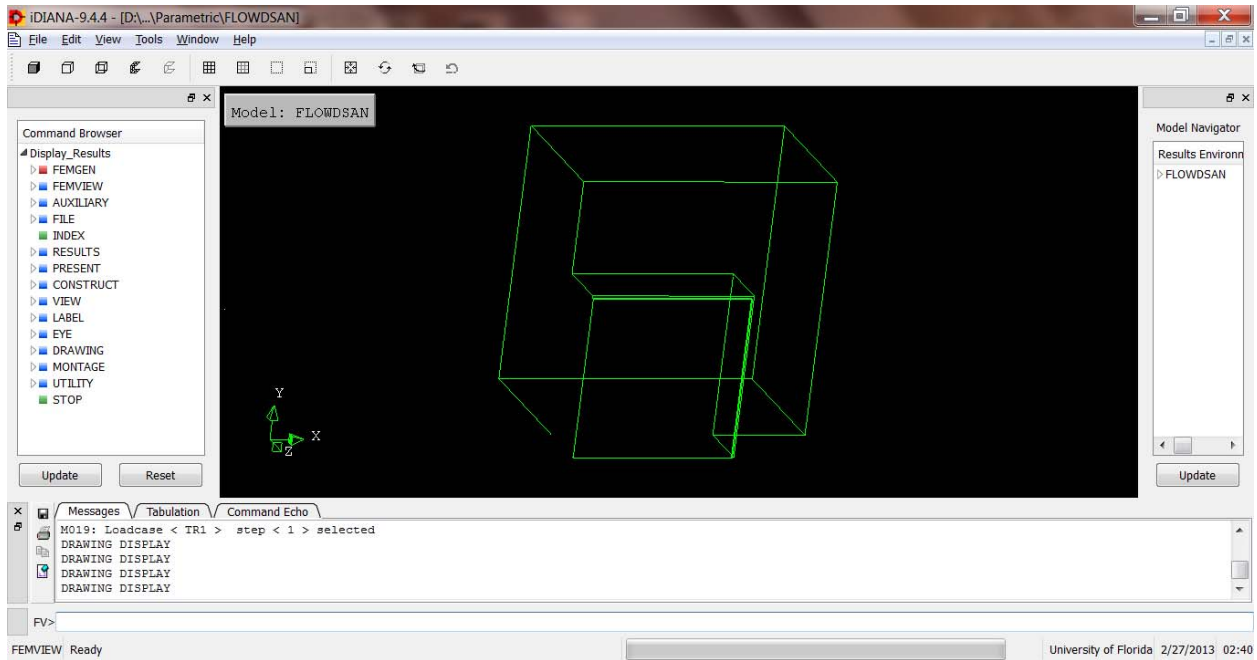
Figure 9-11. Sketch of model.

- View model:

VIEW MESH ALL (to view all the meshes of model)

VIEW MESH BLOCK (to view the concrete mesh)

VIEW MESH SOIL (to view the soil mesh)

VIEW MESH TOPINS (or BOTINS, SIDEINS: to view top, bottom, or side insulation mesh)

VIEW MESH +BLOCK (to add (+) the concrete mesh to the current mesh)

LABEL MESH NODES (iDIANA will label all the node names of current mesh)

LABEL MESH ELEMENTS (iDIANA will label all the element names of current mesh)

VIEW HIDDEN FILL (to provide a hidden surface representation of the model)

For instance, the following commands will generate Figure 9-12:

VIEW MESH SOIL

VIEW MESH +BLOCK

To turn off the transparent view as shown in Figure 9-13, use:

VIEW HIDDEN FILL

To rotate the model to a position as illustrated in Figure 9-14, use:

EYE ROTATE TO 30 45 45 (30, 45, and 45 are the rotation angles about the screen X , Y , Z axes, respectively)
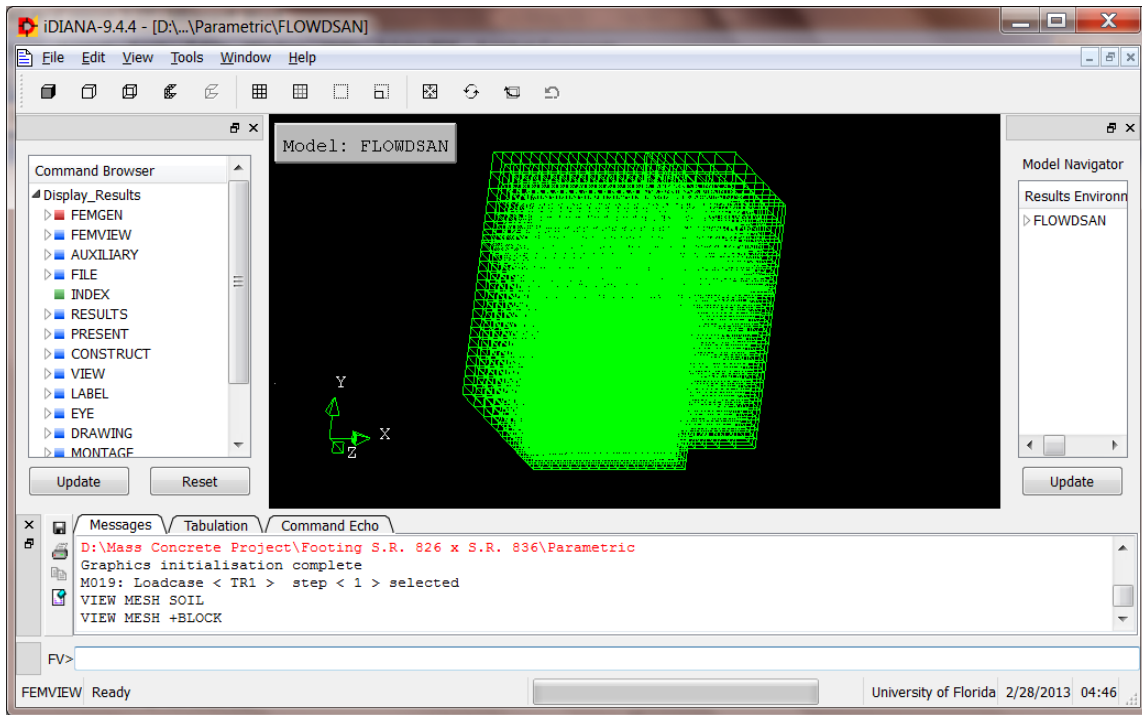
Figure 9-12. Transparent mesh view of concrete and soil.
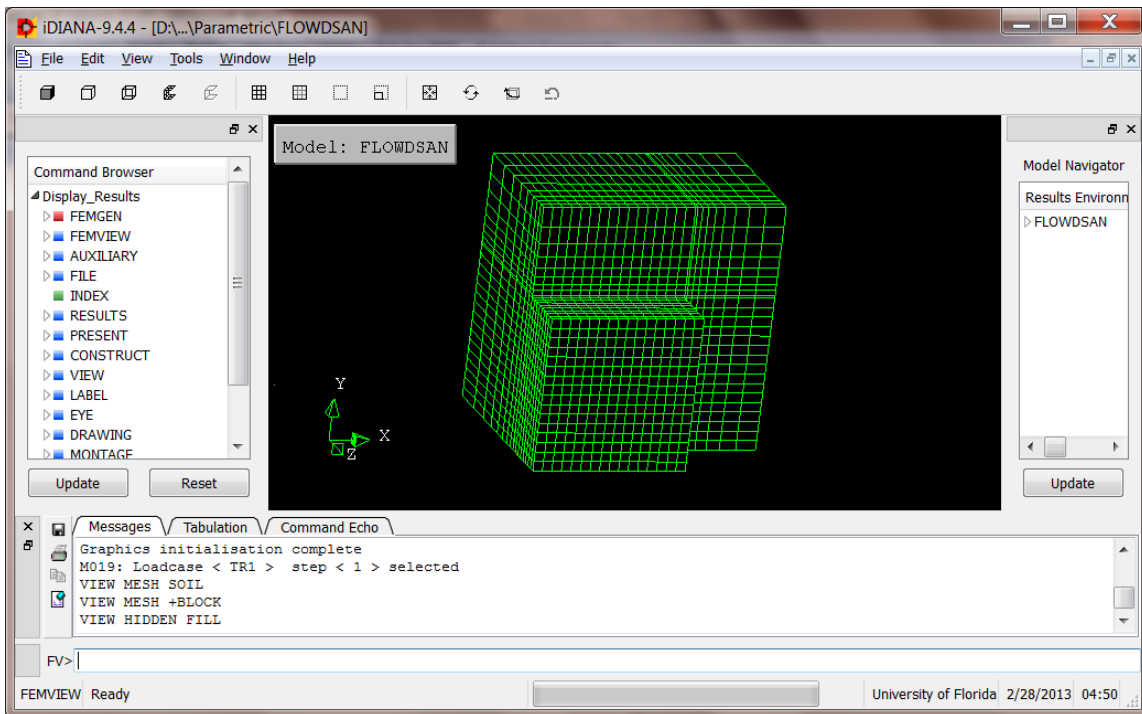
Figure 9-13. Hidden-fill view of concrete and soil.
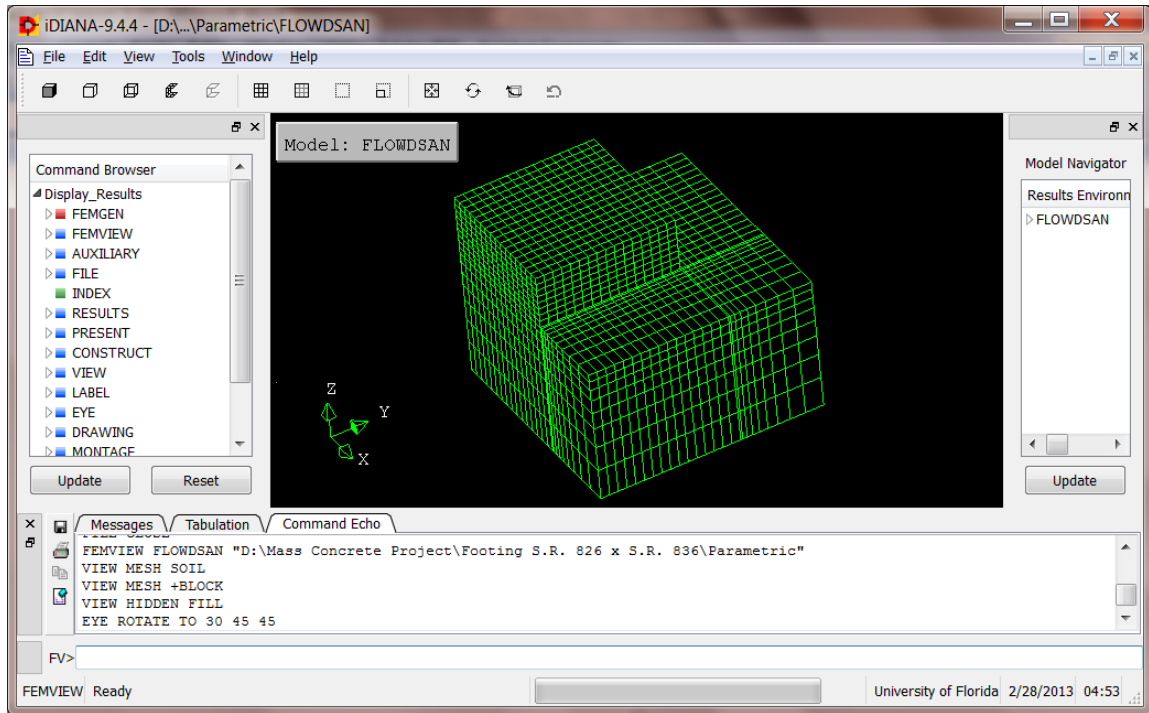
Figure 9-14. Another view using eye-rotation of 30, 45 and 45 degrees.

To see all the node names as shown in Figure 9-15, use:

LABEL MESH NODES
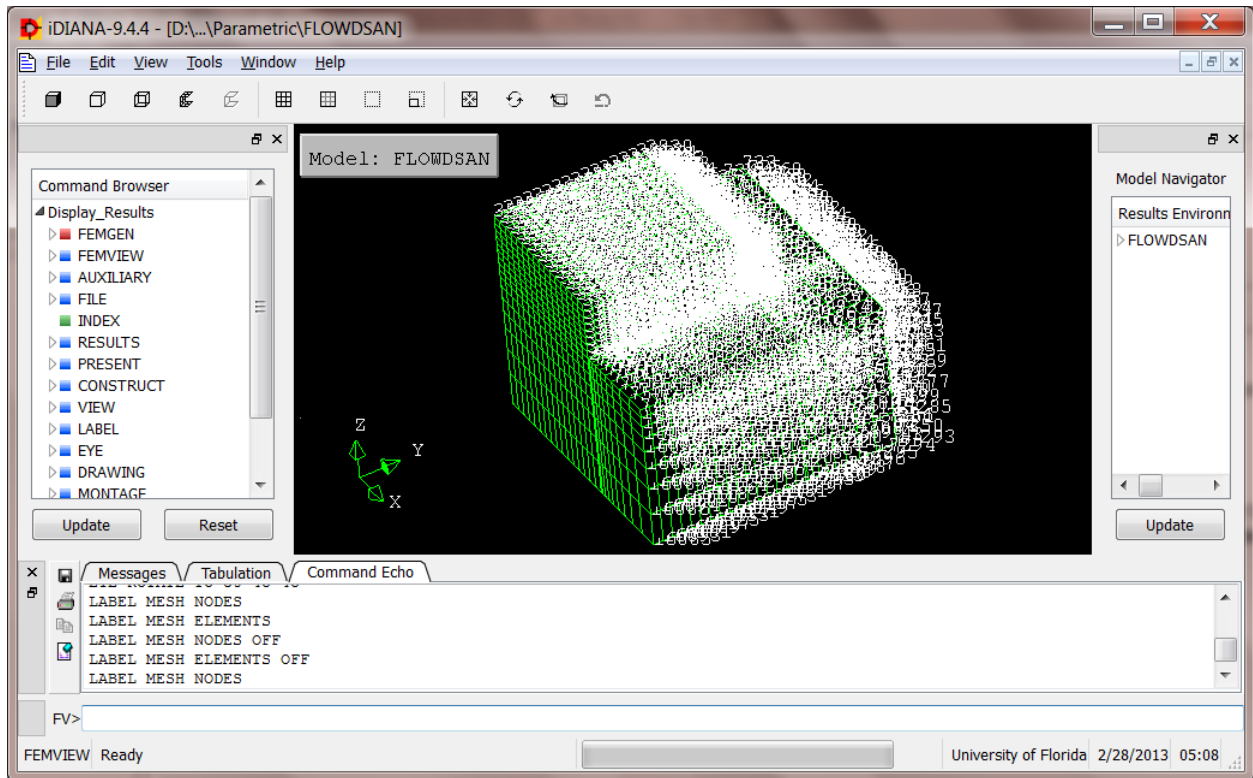
Figure 9-15. Labeling node names of current mesh.

- Display temperature graph:

To plot a graph of temperatures vs. time of 3 nodes: 3850 (concrete center), 957 (concrete bottom center), and 1245 (concrete bottom corner) as shown in Figure 9-16, enter:

RESULTS LOADCASE ALL (to choose all the time steps to be plotted (1-167))

RESULTS NODAL PTE….S PTE (to choose temperature to be plotted)

PRESENT GRAPH NODE 3850 957 1245 (to plot the graph of 3 specific nodes)
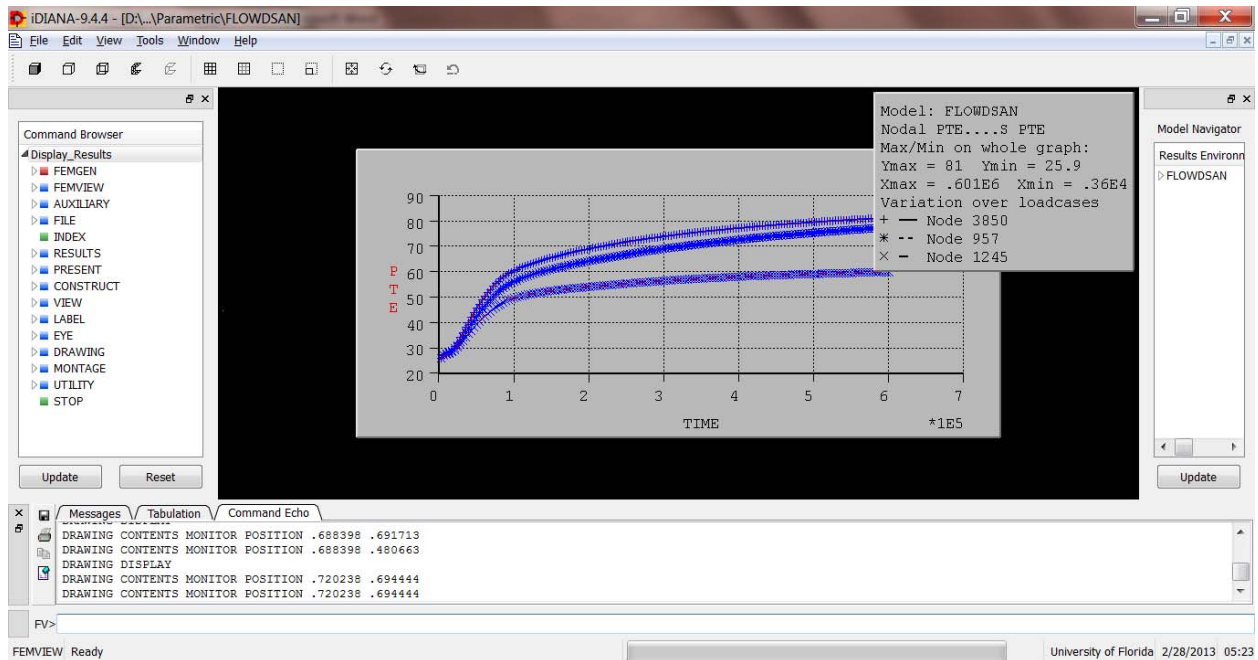
Figure 9-16. Temperature graph vs. time at Nodes 3850, 957, and 1245.

- Display temperature contour (as shown in Figure 9-17):

    RESULTS NODAL PTE….S PTE (to choose temperature to be plotted)

    RESULTS LOADCASE TR1 100 (to set time step at 100 hour)

    PRESENT CONTOUR LEVELS (to plot temperature contour of model (at 100 hour))
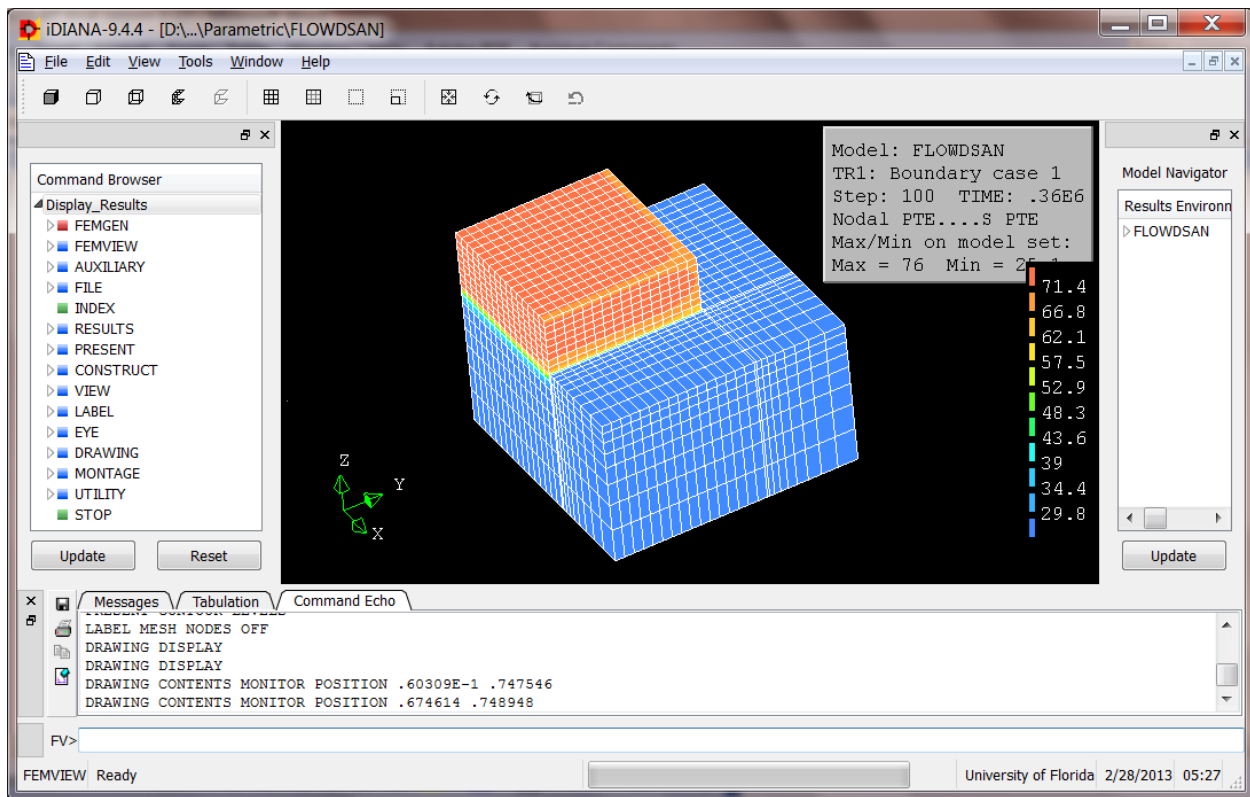
Figure 9-17. Temperature contour in concrete and soil at 100th hour.

9.4.2.2   Stress Results

To view stress results from the structural analysis, the user should open the

"STRUC.V72" file.

- Display First Principal Stress graph (as shown in Figure 9-18):

    VIEW MESH BLOCK

    VIEW HIDDEN FILL

    RESULTS LOADCASE ALL (to choose all the time steps to be plotted (1-167))

    RESULTS ELEMENT EL.S1 S1 (to calculate First Principal Stresses)

    PRESENT GRAPH ELEMENT 4961 NODE 957 (to plot graph of node "957" of element
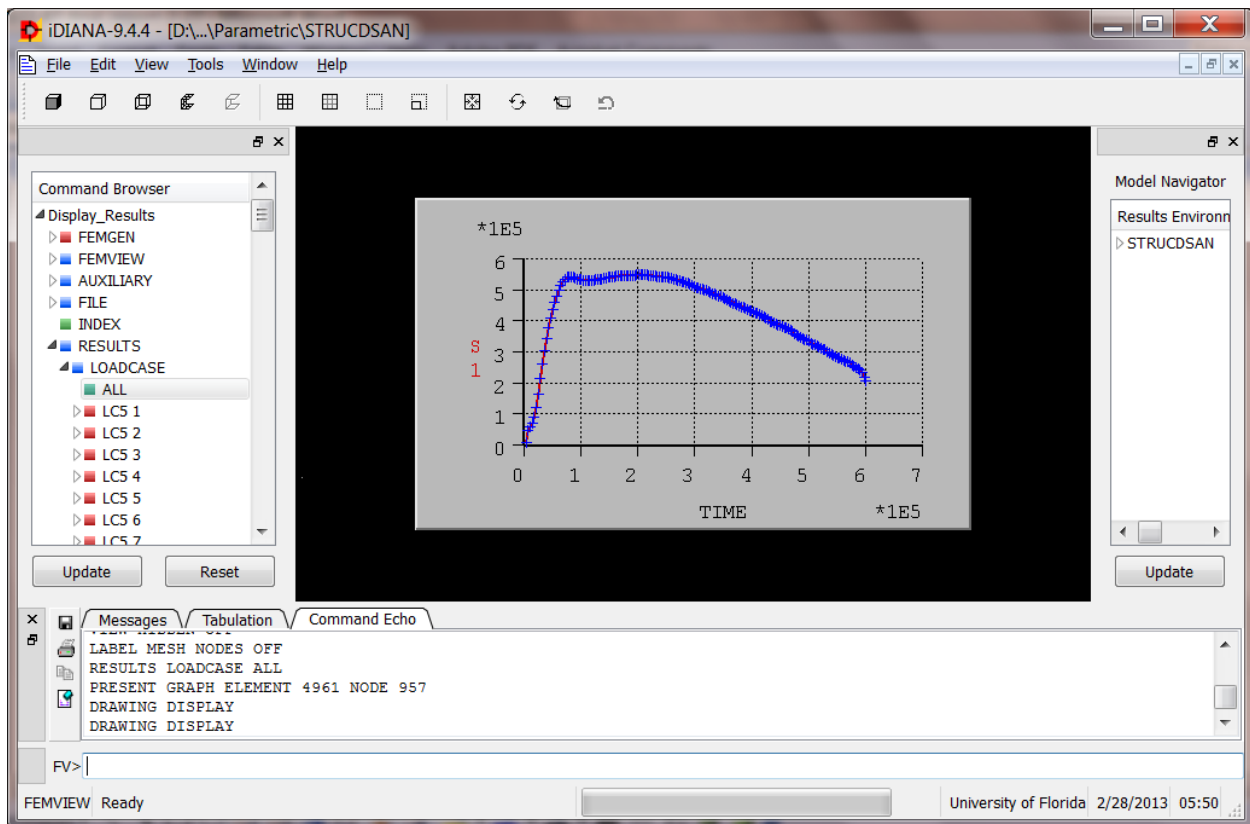
"4961")

Figure 9-18. First principal stress graph vs. time of node "957" of element "4961".

- Display First Principal Stress contour (as shown in Figure 9-19):

  RESULTS LOADCASE LC5 24 (to set time step = 24 hour, LC5 = gravity load)

  RESULTS ELEMENT EL.S1 S1

  PRESENT CONTOUR LEVELS (to plot First Principal Stress contour of model)

- Calculate crack index and display contour levels (as shown in Figure 9-20):

  RESULTS LOADCASE LC5 167 (to set time step = 167 hour)

  RESULTS ELEMENT EL.ICR.S ICR

  PRESENT CONTOUR FROM .9 TO 1 LEVELS 8 (to display crack index contour of model

with 8 levels from .9 to 1)
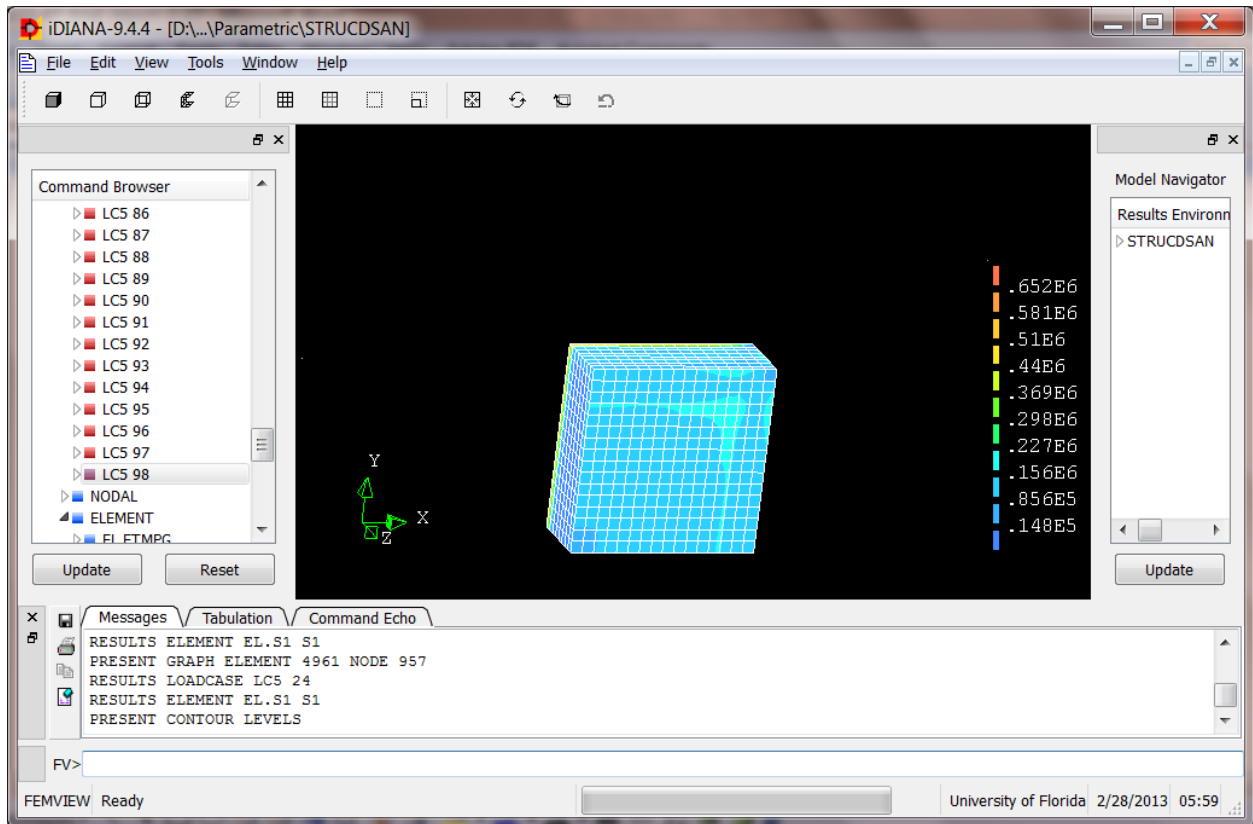
Figure 9-19. Crack index contour of concrete at 167th hour.
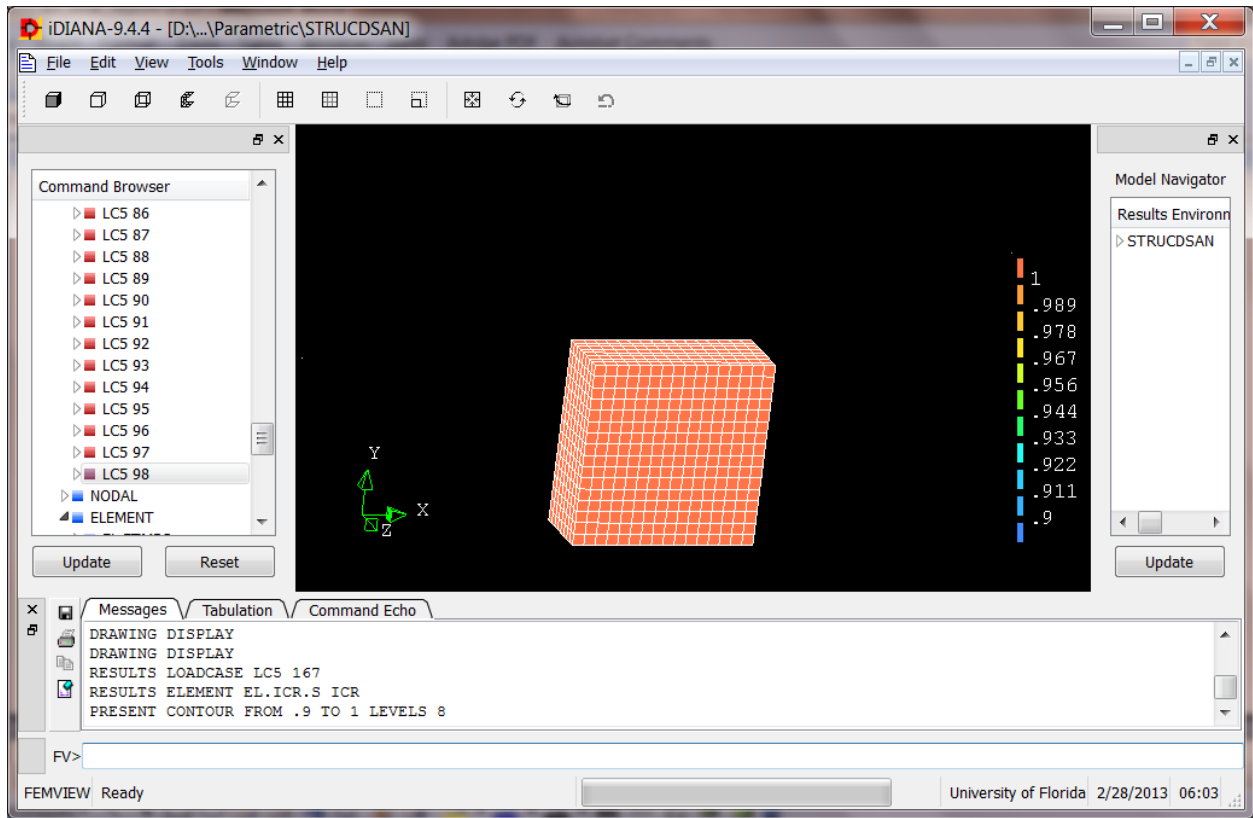
Figure 9-20. First principal stress contour of concrete at 24th hour.

CHAPTER 10
FINDINGS AND RECOMMENDATIONS

10.1 Summary of Findings

A finite element model using the commercially available TNO DIANA 9.4.4 software package was developed for the prediction of temperatures and cracking potential of mass concrete footings placed on soil. To evaluate the effectiveness of the temperature predictions from the model, three different bridge pier footings and one pier cap in Florida were monitored for temperature developments. The measured temperatures were compared with the results obtained from the model. Isothermal calorimetry testing was done on the cementitious materials of the concrete mixtures to determine the energy released during hydration, which was then converted to temperature rise as inputs for the finite element model. Analysis of influences of thermal properties of soil on temperature development and cracking in mass concrete footings was conducted. A parametric study on the effects of dimensions of three types of rectangular footings on the maximum allowable temperature differential to prevent cracking in concrete was conducted. A user-friendly computer program called "DIANA Input File Generator" was developed to provide the needed input files to the TNO DIANA software for modeling of typical mass concrete structures such as rectangular footings and columns.

The main findings from this study can be summarized as follows:

(1) The temperature predictions from the finite element model showed fair agreement with those measured in the field. The predicted temperatures tended to rise higher than the measured ones in Footing 3. This difference can be explained by the fact that there were variables affecting the actual temperature development in the concrete in the field, which were not accounted for in the model. First, the time of placement of the top insulation was delayed after concrete placement due to strike-off of the concrete surface, resulting in heat loss in the concrete which was not considered in the finite element model. The second reason is that the formwork used for this footing was a steel formwork and it was in direct contact with the concrete surface (Styrofoam was placed outside of the steel formwork), causing more rapid heat transfer from the concrete to the steel formwork and thus more rapid heat dissipation, while the steel formwork was not modeled for temperature predictions.

119

(2) The in situ condition of the soil upon which a concrete footing is directly placed affects the temperature development of the footing and determines whether or not an insulation layer would be needed to reduce the temperature difference in the mass concrete and the likelihood for cracking.

(3) At the contact surface between the mass concrete footing and soil, dry soil had higher temperatures than wet or saturated soil. This was because wet soil allowed the heat of hydration generated from the concrete to transfer to a greater depth than dry soil did.

(4) Dry sand and dry clay provided good insulation at the bottom of mass concrete footing as indicated from the crack indices obtained from the thermal cracking analysis performed.

(5) Soil with an R-value of 0.41 or greater (or thermal conductivity of 0.35 J/sec-m-°C or lower) would provide adequate insulation at the bottom of concrete footing using Mix 1 with a V/A of 13 ft or less to prevent thermal cracking. Thus, an insulating layer between the mass concrete and the soil would not be needed in such situation.

(6) With a V/A of less than 4.5 ft, under the same insulation condition and using the same concrete mix, a larger footing had a higher maximum temperature difference, and lower crack index. However, with a V/A of 4.5 ft or greater, a larger footing had a similar or slightly smaller maximum temperature difference, and an almost constant crack index. Thus, cracking potential was not dependent on how large a footing was when its V/A was 4.5 ft or greater.

(7) Rectangular footings that had the same V/A but different shapes (dimensional proportions) would develop a similar maximum temperature, a similar maximum temperature difference, and a similar crack index under the same insulation condition.

(8) When the concrete of Mix 1 was used, footings with a V/A from 1.1 ft to 1.6 ft reached a maximum temperature differential of 25.2°C before cracking. Footings with a V/A from 1.7 ft to 4.4 ft reached a maximum temperature differential of 21.6°C, and footings with a V/A from 4.5 ft to 13.1 ft reached a maximum temperature differential of 20.1°C before cracking. Thus, setting the maximum allowable temperature differential of 20 °C in mass concrete appears to be a conservative and appropriate criterion.

(9) When Styrofoam with an R-value of 5.0 per inch was used, 0.5 inch would provide adequate insulation for a footing with a V/A of around 1.0 ft; 1.0 inch would provide adequate insulation for a footing with a V/A less than 4.0 ft; 1.25 inches would provide adequate insulation for a footing with a V/A up to 13.0 ft. If another type of insulating material is used, an equivalent insulation thickness can be determined from the material's R-value.

(10) The development of the user-friendly software "DIFG" provides a convenient tool for generating the needed input files to the TNO DIANA software for analysis of

typical mass concrete structures of rectangular footings and columns. It allows engineers and contractors who are not familiar with the detailed inputs to the TNO DIANA software to use this software conveniently and efficiently.

10.2 Recommendations

Based on the findings from this study, the following recommendations are made:

(1) Bottom insulation should be used in concrete footing for the following cases: (a) there is water at the bottom of footing. (b) footings with a V/A of 2.0 ft or less are placed on soil that has an R-value of less than 0.29 per in., and (c) footings with a V/A of greater than 2.0 ft are placed on soil that has an R-value of less than 0.41 per in.

(2) The required insulation thickness method presented in this report should be used for footings to be constructed in the field.

(3) A database of rate of heat production of different cement blends should be developed. Isothermal calorimetry testing should be performed on the cementitious materials used in typical FDOT mass concrete mix designs to build a database of adiabatic temperature rise tables that can be used in the DIANA software for the modeling of mass concrete structures. The concrete mix designs that are to be analyzed consist of Type I/II Portland cement, ground-granulated blast furnace slag, Class F fly ash, ultra-fine fly ash, and silica fume, in various combinations and proportions.

(4) Thermal properties of soil in different in situ conditions should be evaluated and monitoring of footings directly placed on soil is needed to evaluate the predicted results. Since the properties of the soil upon which a mass concrete footing is placed greatly influence the thermal behavior of the concrete footing, further investigation needs to be conducted to determine the R-values for different types of soil and under different in situ conditions.

(5) Further development of the user-friendly software for mass concrete analysis should be made. The present developed software is capable of generating input files of rectangular footings on soil with options of insulation and with concrete properties loaded from a file. Additional capabilities with further development of the software can provide input files for pier caps and columns with rectangular or octagonal shape. It should also have the capability of inputting the concrete properties from the database to be developed.

LIST OF REFERENCES

Ali, W. and Urgessa, G. (2012). "Numerical prediction model for temperature distributions in concrete at early ages." *American Journal of Engineering and Applied Sciences*, Vol. 5, No. 4, pp. 282-290.

ACI Committee 207. (2005). *Guide to mass concrete* (207.1R-05), Farmington Hills, MI.

ACI Committee 207. (2007). *Report on thermal and volume change effects on cracking of mass concrete* (207.2R-07), Farmington Hills, MI.

Ayotte, E., Massicotte, B., Houde, J., and Gocevski, V. (1997). "Modeling of thermal stresses at early ages in a concrete monolith." *ACI Mater. J.*, Vol. 94, No. 6, pp. 577–587.

De Schutter, G. (2002). "Finite element simulation of thermal cracking in massive hardening concrete elements using degree of hydration based material laws." *Comput. Struct.*, Vol. 80, No. 27–30, pp. 2035–2042.

DIANA: Displacement Analyzer Version 9.4.4. (2012a). [Computer software]. *TNO DIANA BV*, Delft, Netherlands.

DIANA. (2012b). "Finite Element Analysis User's Manual Material Library Release 9.4.4." *TNO DIANA BV*, Delft, Netherlands.

DIANA. (2012c). "Finite Element Analysis User's Manual Pre- and Postprocessing Release 9.4.4." *TNO DIANA BV*, Delft, Netherlands.

Evju, C. (2003). "Initial hydration of cementitious systems using a simple isothermal calorimeter and dynamic correction." *J. Therm. Anal. Calorim.*, Vol. 71, No. 3, pp. 829–840.

Faria, R., Azenha, M., and Figueiras, J. (2006). "Modeling of concrete at early ages: Application to an externally restrained slab." *Cem. Concr. Compos.*, Vol. 28, No. 6, pp. 572–585.

Ferraro, C. C. (2009). "Determination of test methods for the prediction of the behavior of mass concrete." Ph.D. dissertation, Univ. of FL, Gainesville, FL.

Florida Department of Transportation. (2007). *Standard specifications for road and bridge construction*. Florida Department of Transportation (FDOT), Tallahassee, FL.

Florida Department of Transportation. (2009). *FDOT Structures Manual*, Florida Department of Transportation, Tallahassee, FL.

Florida Department of Transportation. (2010). *Standard specifications for road and bridge construction*. Florida Department of Transportation, Tallahassee, FL.

Florida Department of Transportation. (2013). *Structures Design Guidelines: FDOT Structures Manual Volume 1*, Florida Department of Transportation, Tallahassee, FL.

iDIANA Release 9.4.4. (2012). [Computer software]. *TNO DIANA BV*, Delft, Netherlands.

Kim, J. K., Kim, K. H., Yang, J. K. (2001). "Thermal analysis of hydration heat in concrete structures with pipe-cooling system." *Computers & Structures*, Vol. 79, No. 2, pp. 163-171.

Lawrence, A. M. (2009). "A Finite Element Model for the Prediction of Thermal Stresses in Mass Concrete." Ph.D. dissertation, Univ. of FL, Gainesville, FL.

Lawrence, A. M., Tia, M., Ferraro, C., and Bergin, M. (2012). "Effect of Early Age Strength on Cracking in Mass Concrete Containing Different Supplementary Cementitious Materials: Experimental and Finite-Element Investigation." *Journal of Materials in Civil Engineering*, Vol. 24, No. 4, pp. 362–372.

Machida, N., and Uehara, K. (1987). "Nonlinear Thermal Stress Analysis of a Massive Concrete Structure." *Comput. Struct.*, Vol. 26, pp. 287-296.

Mehta, P.K., and Monteiro, P. J. M. (2006). *Concrete – Microstructure, Properties and Materials*. 3rd Edition. McGraw-Hill.

Mills, A.F. (1995). *Heat and Mass Transfer*. Richard D. Irwin, Concord, MA.

Radovanovic, S. (1998). "Thermal and structural finite element analysis of early age mass concrete structures." Masters thesis, Univ. of Manitoba, Winnipeg, Manitoba, Canada.

Tanabe, T., Kawasumi, M., and Yamashita, Y. (1986). "Thermal Stress Analysis of Massive Concrete," Seminar Proceedings For Finite Element Analysis of Reinforced Concrete Structures, Tokyo, Japan, May 21-24, 1985, ASCE, New York, NY.

Thomas, L.C. (1980). *Fundamentals of Heat Transfer*. Prentice-Hall. NJ.

Tia, M., Lawrence, A., Ferraro, C., Smith, S., Ochiai, E. (2010). "Development of design parameters for mass concrete using finite element analysis." Final Report, Dept. of Civil and Coastal Engineering, Univ. of FL, Gainesville, FL.

APPENDIX A
iDIANA INPUT COMMANDS OF A FULLY INSULATED CONCRETE MODEL

femgen Footing

property fe-prog diana htstag_3d

yes

utility setup units length meter

utility setup units mass kilogram

utility setup units force newton

utility setup units time second

utility setup units temperature celsius

geometry point coord P1 0 0 0

geometry point coord P2 4.00E+0000 0.00E+0000 0.00E+0000

geometry point coord P3 0.00E+0000 4.00E+0000 0.00E+0000

geometry point coord P4 4.00E+0000 4.00E+0000 0.00E+0000

geometry surface 4points p1 p2 p4 p3

construct set botInBot append all

construct set xline append lines l1 l3

construct set yline append lines l2 l4

meshing division line xline 16

meshing division line yline 16

construct space tolerance off

geometry sweep botInBot SoilBot 408 translate 0 0 -5.00E+0000

construct set Soil append bodies b1

construct set SoilY1 append surfaces s5

construct set SoilX1 append surfaces s4

geometry sweep botInBot BlockBot 1 translate 0 0 3.175E-0002

construct set botIns append bodies b2

meshing types botIns he8 hx8ht

geometry sweep BlockBot BlockTop 8 translate 0 0 2.00E+0000

construct set fBlock append bodies b3

meshing types all he8 hx8ht

geometry copy fBlock Block translate 0 0 0

construct set xline2 append lines l29 l31 l33 l35

construct set yline2 append lines l30 l32 l34 l36

construct set zline2 append lines l37 l38 l39 l40

meshing division line xline2 32

meshing division line yline2 32

meshing division line zline2 16

meshing types Block he20 chx60

construct set InsY1 append surfaces s10

construct set InsX1 append surfaces s9

construct set InsY1 append surfaces s15

construct set InsX1 append surfaces s14

geometry sweep SoilY1 SoilY2 1 translate 0 3.17500000000000E-0002 0

geometry sweep InsY1 InsY2 1 translate 0 3.17500000000000E-0002 0

construct set SoilX1 append surfaces s24

construct set InsX1 append surfaces s30

construct set InsX1 append surfaces s34

construct set Soil append bodies b5

construct set SideIns append bodies b6

construct set SideIns append bodies b7

geometry sweep SoilX1 SoilX2 1 translate 3.17500000000000E-0002 0 0

geometry sweep InsX1 InsX2 1 translate 3.17500000000000E-0002 0 0

construct set Soil append bodies b8 b9

construct set sideIns append bodies b10 b12

construct set sideIns append bodies b11 b13

construct set SoilY2 append surfaces s45

construct set InsY2 append surfaces s59

construct set InsY2 append surfaces s61

meshing types sideIns he8 hx8ht

geometry sweep SoilY2 SoilY 408 translate 0 3.00E+0000 0

construct set SoilX2 append surfaces s70

geometry sweep SoilX2 SoilX 408 translate 3.00E+0000 0 0

construct set SoilY append surfaces s83

construct set Soil append bodies b14 b15 b16 b17 b18

construct set soilBot append surfaces s27 s42 s44 s67 s69 s77 s79 s82

meshing types Soil he8 hx8ht

construct set soilTop append surfaces s65 s68 s75 s78 s81

geometry sweep BlockTop Top 1 translate 0 0 3.17500000000000E-0002

construct set topIns append bodies b19

meshing types topIns he8 hx8ht

construct set sideSur append surfaces InsX2 InsY2

construct set topSur append surfaces Top

geometry copy topSur topExt translate 0 0 0

meshing types topExt qu4 bq4ht

geometry copy sideSur sideExt translate 0 0 0

meshing types sideExt qu4 bq4ht

geometry copy soilTop soilExt translate 0 0 0

meshing types soilExt qu4 bq4ht

construct set soilFix append surfaces SoilX SoilY SoilBot

```
meshing generate
meshing merge all 0.001


property material concrete external external "CONCRETE.dat"
property material topBo flow boundary convecti  5.00E+0001 0
property material sideBo flow boundary convecti  2.00E+0001 0
property material soilBo flow boundary convecti  2.00E+0001 0
property material topMat flow isotrop  2.90E-0002  2.84E+0004
property material sideMat flow isotrop  2.90E-0002  2.84E+0004
property material botMat flow isotrop  2.90E-0002  2.84E+0004
property material SoilMat flow isotrop  2.70E-0001  1.21200000000000E+0006


property attach fBlock concrete
property attach Block concrete
property attach topExt topBo
property attach sideExt sideBo
property attach soilExt soilBo
property attach topIns topMat
property attach sideIns sideMat
property attach botIns botMat
property attach Soil SoilMat


property loads exttemp 1 sideExt  2.60E+0001
property loads exttemp 2 topExt  2.60E+0001
property loads exttemp 3 soilExt  2.60E+0001
property loads fixtemp 4 soilFix  2.60E+0001
property loads gravity 5 Block -9.81 3
construct tcurve tcdum list 0 1 601200 1


property attach loadcase 1 tcdum
property attach loadcase 2 tcdum
```

property attach loadcase 3 tcdum

property attach loadcase 4 tcdum

property attach loadcase 5 tcdum

property boundary constraint s17 z

property boundary constraint s22 x

property boundary constraint s19 y

property initial initemp all 2.55E+0001

eye frame

utility write diana Footing

yes

APPENDIX B
CONTENTS OF CONCRETE PROPERTY FILE "CONCRETE.DAT"

CONDUC 2.2

CAPACI 2.675596E+06

ADIAB 0 23

  3600 25.42679371

  7200 25.71257944

  10800 26.04072774

  14400 26.51625577

  18000 27.23067965

  21600 28.23307206

  25200 29.52351384

  28800 31.07516457

  32400 32.82326773

  36000 34.68964656

  39600 36.59175871

  43200 38.46492849

  46800 40.26881443

  50400 41.99678727

  54000 43.66679452

  57600 45.25854419

  61200 46.75441214

  64800 48.18317906

  68400 49.50046125

  72000 50.7506424

  75600 51.93388422

  79200 53.00556046

  82800 54.01021652

  86400 54.94785239

  90000 55.77392269

  93600 56.53297279

97200 57.20277045

100800 57.82786103

104400 58.38601226

108000 58.89945643

111600 59.39066832

115200 59.83717314

118800 60.26136484

122400 60.66316259

126000 61.04272807

129600 61.42229354

133200 61.75715195

136800 62.09201035

140400 62.4269496

144000 62.73949489

147600 63.02972707

151200 63.31995924

154800 63.61019142

158400 63.87811048

162000 64.14594869

165600 64.41386775

169200 64.6594737

172800 64.90507965

176400 65.15060475

180000 65.37389758

183600 65.61950353

187200 65.84271552

190800 66.06600835

194400 66.26690722

198000 66.49020005

201600 66.69109893

205200 66.8919978

208800 67.09297752

212400 67.29387639

216000 67.47246215

219600 67.67344187

223200 67.85202763

226800 68.03061339

230400 68.20919915

234000 68.38786575

237600 68.56645151

241200 68.72272415

244800 68.90130991

248400 69.05758256

252000 69.23616832

255600 69.39252181

259200 69.54879445

262800 69.7050671

266400 69.86133974

270000 70.01761239

273600 70.17388503

277200 70.33015767

280800 70.46411721

284400 70.62038985

288000 70.77666249

291600 70.91062203

295200 71.04458156

298800 71.2008542

302400 71.33481373

306000 71.46877326

309600 71.60273279

313200 71.73669232

316800 71.87065185

320400 72.00461138

324000 72.13849007

327600 72.2724496

331200 72.40640913

334800 72.51805555

338400 72.65201508

342000 72.78597461

345600 72.89762102

349200 73.00918659

352800 73.14314612

356400 73.25479254

360000 73.38875207

363600 73.50039849

367200 73.6120449

370800 73.72361048

374400 73.83525689

378000 73.94690331

381600 74.05854972

385200 74.1701153

388800 74.28176171

392400 74.39340813

396000 74.50505454

399600 74.61670096

403200 74.72826653

406800 74.83991295

410400 74.92924625

414000 75.04081182

417600 75.15245824

421200 75.24179154

424800 75.35343796

428400 75.44269041

432000 75.55433683

435600 75.64367013

439200 75.7552357

442800 75.844569

446400 75.93390231

450000 76.02315476

453600 76.13480118

457200 76.22413448

460800 76.31338694

464400 76.40272024

468000 76.4919727

471600 76.581306

475200 76.6706393

478800 76.78220487

482400 76.87153817

486000 76.96087148

489600 77.05012393

493200 77.13945724

496800 77.22879054

500400 77.31804299

504000 77.38506318

507600 77.47431564

511200 77.56364894

514800 77.6529014

518400 77.7422347

522000 77.80925489

525600 77.89850734

529200 77.98784065

532800 78.05477999

536400 78.14411329

540000 78.23336575

```
        543600 78.30038594

        547200 78.38971924

        550800 78.45665858

        554400 78.54599188

        558000 78.63524434

        561600 78.70226453

        565200 78.79151698

        568800 78.85853717

        572400 78.94778963

        576000 79.01480982

        579600 79.08174916

        583200 79.17108246

        586800 79.2380218

        590400 79.32735511

        594000 79.39429445

        597600 79.46131464

        601200 79.55064794

    ARRHEN 4117.75

    EQUAGE ARRTYP

    TEMREF 23.0

    YOUNG  2.523500E+10

    POISON 2.000000E-01

    DENSIT 2.2480000E+03

    THERMX 9.160000E-06

    FTTIME 0. 86400 172800 259200. 601200.

    FTVALU 0. 1.25E+6 1.66E+6 1.93E+6 2.206E+6

    MAXWEL 1

,1

    TIME   0. 86400. 172800. 259200. 601200.

    YOUNG  13445.E+6 13445.E+6 16892.E+6 18064.E+6 20202.E+6
```

APPENDIX C
FINITE ELEMENT ANALYSIS OF SEGMENTAL PIER SEGMENT

A segmental pier segment was modeled to determine the temperature differentials that would develop and any consequential cracking as a result of a segment with a volume to surface area ratio of slightly less than 1.0 ft. being placed using high strength concrete without the use of thermal protective measures. This question came about due to the real world placement of a pier segment that was not deemed as mass concrete in the project plans due to the fact that when the surface area of the post-tensioning ducts and other voids were accounted for, the volume to surface area (V/A) ratio was found to be 0.97 ft. However during the construction of the pier segment, significant thermal cracking developed. The concrete mix design used in the construction was a high-strength 8500 psi concrete mix. Figure C-1 shows the shape of a pier segment that was constructed in the field. The core of the segment was considered for calculating the volume to surface area ratio and for modeling. The eventual question that is hoped to be answered is whether the V/A threshold of 1.0 ft. should be reduced when high strength mixes are used, and what that threshold should be.
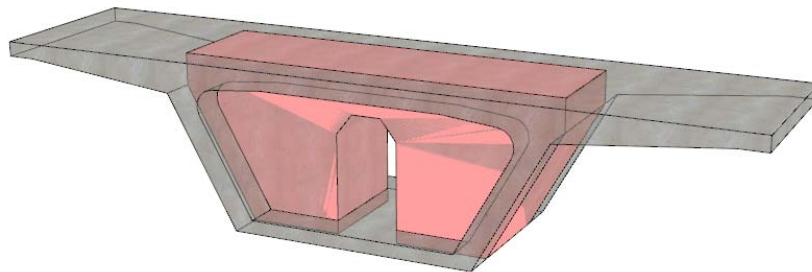
Figure C-1. Segmental pier segment.

135

Figure C-2 shows the finite element mesh of half of the segment core. Since the actual dimensions of the segment was not available, the dimensions of the segment model were assumed based on the proportioning of its shape. The core had a length of 18 ft., and a height of 6 ft. For the thickness of the core, the two cases were considered: 5 ft. and 4 ft. Its volume to surface area ratio was 0.97 ft. for the first case and 0.89 ft. for the second case.
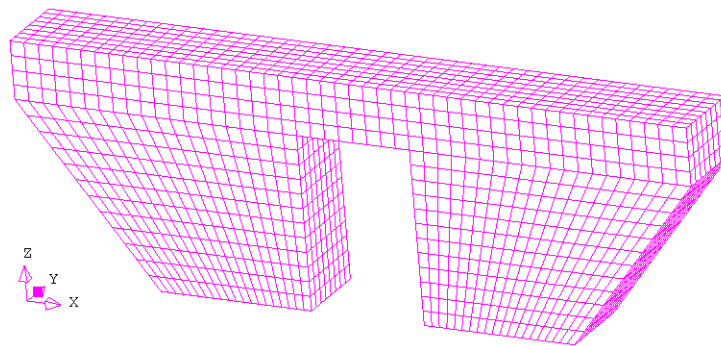
Figure C-2. Finite element mesh of half of the segment core.

Since there was no detailed information on the actual mix design used in the segment, the concrete properties that used in previous progress reports were used for the concrete in this finite element analysis. The segment was not insulated in this model.

Figure C-3 shows the temperature distribution in the model at 7 days. The finite element result reveals that the maximum temperature differential in the model was 28.4 °C (51 °F) corresponding to the volume to surface area ratio of 0.97 ft., and 26.2 °C (47 °F) corresponding to the volume to surface area ratio of 0.89 ft. These values are all higher than the FDOT maximum allowable value of 20 °C (35 °F). Due to the fact that the mix design used in this analysis produces less heat than the actual concrete mix design used in the pier segment, it can be reasonably assumed that an even higher temperature differential would have occurred in the pier

136

segment constructed in the field. It is therefore recommended that the laboratory tests be

conducted on the actual mix design of the segment to provide full input parameters for the finite

element model and therefore provide better temperature and cracking predictions for the pier

segment.
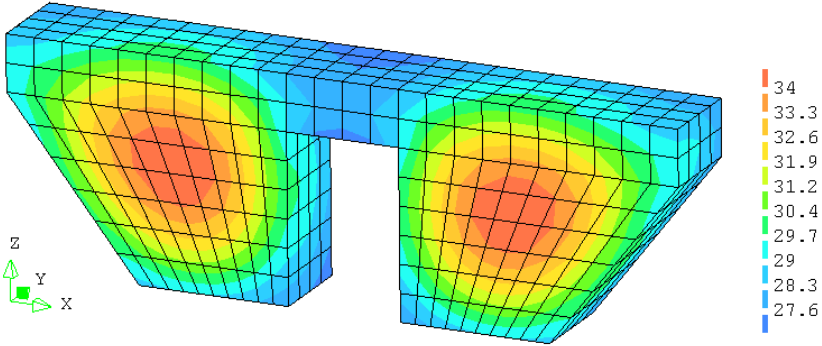
Figure C-3. Temperature distribution in the pier segment model at 7 days.

CODES OF "DIFG" IN DELPHI PROGRAMMING LANGUAGE

Codes of "DianaGen.pas" file

```
unit DianaGen;

interface

uses
  Windows, Messages, SysUtils, Variants, Classes, Graphics, Controls, Forms,
  Dialogs, StdCtrls, ExtCtrls, ComObj, ShellApi;

type
  TForm1 = class(TForm)
    GroupBox1: TGroupBox;
    GroupBox2: TGroupBox;
    Edit1: TEdit;
    Label1: TLabel;
    Edit2: TEdit;
    Edit3: TEdit;
    Label2: TLabel;
    Label3: TLabel;
    Button1: TButton;
    GroupBox3: TGroupBox;
    Label4: TLabel;
    Label5: TLabel;
    Edit4: TEdit;
    Edit5: TEdit;
    OpenDialog1: TOpenDialog;
    GroupBox4: TGroupBox;
    Label7: TLabel;
    Label6: TLabel;
    Button2: TButton;
    Edit6: TEdit;
    Edit7: TEdit;
    Button3: TButton;
    SaveDialog1: TSaveDialog;
    CheckBox1: TCheckBox;
    Edit8: TEdit;
    Edit9: TEdit;
    Edit10: TEdit;
    Label8: TLabel;
    Label9: TLabel;
    Label10: TLabel;
```

```
    Label11: TLabel;
    Label12: TLabel;
    Label13: TLabel;
    CheckBox2: TCheckBox;
    Edit11: TEdit;
    Edit12: TEdit;
    Edit13: TEdit;
    CheckBox3: TCheckBox;
    Edit14: TEdit;
    Edit15: TEdit;
    Edit16: TEdit;
    CheckBox4: TCheckBox;
    Edit17: TEdit;
    Edit18: TEdit;
    Edit19: TEdit;
    GroupBox5: TGroupBox;
    Label14: TLabel;
    Label15: TLabel;
    Edit20: TEdit;
    Edit21: TEdit;
    Label16: TLabel;
    Label17: TLabel;
    Button4: TButton;
    Button5: TButton;
    Label18: TLabel;
    Label19: TLabel;
    Label20: TLabel;
    Edit22: TEdit;
    Edit23: TEdit;
    Edit24: TEdit;
    Panel1: TPanel;
    Image1: TImage;
    procedure Button1Click(Sender: TObject);
    procedure Button2Click(Sender: TObject);
    procedure Button3Click(Sender: TObject);
    procedure Button4Click(Sender: TObject);
    procedure Button5Click(Sender: TObject);

  private
    { Private declarations }
  public
    { Public declarations }
  end;

var
  Form1: TForm1;
```

```
length, width, depth, a, b, c, IniTemp, ExtTemp,
ttop, tside, tbot, contop, conside, conbot, heattop, heatside, heatbot,
tsoil, wsoil, consoil, heatsoil, TopConv, SideConv: Real;
Px,Py,Pz: array[1..100] of Real;
ConcFName, BatFName, DatFName, ShortName, WDir: string;
TopInd, BotInd, SideInd, SoilInd, xdiv, ydiv, zdiv, Soildiv,SoilWdiv: Integer;

implementation

{$R *.dfm}

procedure ExecuteShellCommand(cmdline: string; hidden: Boolean);
const
  flags: array[Boolean] of Integer = (SW_SHOWNORMAL, SW_HIDE);
var
  cmdbuffer: array[0..MAX_PATH] of Char;
begin
  GetEnvironmentVariable('COMSPEC', cmdBUffer, SizeOf(cmdBuffer));
  ShellExecute(0,'open',cmdbuffer, PChar('/k' + cmdline), nil, flags[hidden]);
end;

procedure iDianaRun;
var
  Txt: Text;
  SEInfo: TShellExecuteInfo;
  ExitCode: DWORD;
  ExecuteFile, ParamString, StartInString, Name: string;
begin
  Form1.Enabled:=False;

  Assign(Txt,'dianagen.bat');
  Rewrite(Txt);
  WriteLn(Txt,'rem === Diana Environment Setup ===');
  WriteLn(Txt,'call "C:\Program Files\Diana 9.4.4\dialogin.bat"');
  WriteLn(Txt,'set FGVSTR=.');

  WriteLn(Txt,'copy "',BatFName,'" fgvstr.str');
  WriteLn(Txt,'idiana -alpha');
  WriteLn(Txt,'del fgvstr.str');
  WriteLn(Txt,'del dianagen.bat');
  Close(Txt);

  ExecuteFile:='dianagen.bat';
  FillChar(SEInfo, SizeOf(SEInfo), 0);
  SEInfo.cbSize := SizeOf(TShellExecuteInfo);
  with SEInfo do
```

```
  begin
    fMask := SEE_MASK_NOCLOSEPROCESS;
    Wnd := Application.Handle;
    lpFile := PChar(ExecuteFile);
    //lpParameters := PChar(ParamString);
       {ParamString can contain the application parameters.}
    //lpDirectory := PChar(StartInString);
       {StartInString specifies the name of the working directory.
        If ommited, the current directory is used.}
    nShow := SW_HIDE;
  end;
  if ShellExecuteEx(@SEInfo) then
  begin
    repeat
      Application.ProcessMessages;
      GetExitCodeProcess(SEInfo.hProcess, ExitCode);
    until (ExitCode <> STILL_ACTIVE) or Application.Terminated;
    ShowMessage('DIANA input file successfully generated!');

  end
  else
    ShowMessage('Error running iDIANA!');
  Form1.Enabled:=True;
end;

procedure Generate;
var
  Txt: Text;
  i: Integer;

begin
  Assign(Txt,BatFName);
  Rewrite(Txt);
  WriteLn(Txt,'utility setup directory "',WDir,'"');
  WriteLn(Txt,'femgen Footing');
  WriteLn(Txt,'property fe-prog diana htstag_3d');
  WriteLn(Txt,'yes');
  WriteLn(Txt,'utility setup units length meter');
  WriteLn(Txt,'utility setup units mass kilogram');
  WriteLn(Txt,'utility setup units force newton');
  WriteLn(Txt,'utility setup units time second');
  WriteLn(Txt,'utility setup units temperature celsius');
  WriteLn(Txt);
  WriteLn(Txt,'geometry point coord P1 0 0 0');

  WriteLn(Txt,'geometry point coord P2 ',Px[2],' ',Py[2],' ',Pz[2]);
```

```
WriteLn(Txt,'geometry point coord P3 ',Px[3],' ',Py[3],' ',Pz[3]);
WriteLn(Txt,'geometry point coord P4 ',Px[4],' ',Py[4],' ',Pz[4]);
WriteLn(Txt,'geometry surface 4points p1 p2 p4 p3');
WriteLn(Txt);
WriteLn(Txt,'construct set botInBot append all');
WriteLn(Txt,'construct set xline append lines l1 l3');
WriteLn(Txt,'construct set yline append lines l2 l4');
WriteLn(Txt,'meshing division line xline ',xdiv);
WriteLn(Txt,'meshing division line yline ',ydiv);
WriteLn(Txt);
WriteLn(Txt,'geometry sweep botInBot SoilBot ',Soildiv,' translate 0 0 ',-tsoil);
WriteLn(Txt,'construct set Soil append bodies b1');
WriteLn(Txt,'construct set SoilY1 append surfaces s5');
WriteLn(Txt,'construct set SoilX1 append surfaces s4');
WriteLn(Txt);

if Form1.CheckBox3.Checked then
  begin
    WriteLn(Txt,'geometry sweep botInBot BlockBot 1 translate 0 0 ',tbot);
    WriteLn(Txt,'construct set botIns append bodies b',1+BotInd);
    WriteLn(Txt,'meshing types botIns he8 hx8ht');
  end
else WriteLn(Txt,'geometry copy botInBot BlockBot translate 0 0 0');
WriteLn(Txt,'geometry sweep BlockBot BlockTop ',zdiv,' translate 0 0 ',c);
WriteLn(Txt);
WriteLn(Txt,'construct set fBlock append bodies b',1+BotInd+1);
WriteLn(Txt,'meshing types all he8 hx8ht');
WriteLn(Txt);
WriteLn(Txt,'construct space tolerance off');
WriteLn(Txt,'geometry copy fBlock Block translate 0 0 0');
i:=8*BotInd;
WriteLn(Txt,'construct set xline2 append lines l',21+i,' l',23+i,' l',25+i,' l',27+i);
WriteLn(Txt,'construct set yline2 append lines l',22+i,' l',24+i,' l',26+i,' l',28+i);
WriteLn(Txt,'construct set zline2 append lines l',29+i,' l',30+i,' l',31+i,' l',32+i);
WriteLn(Txt,'meshing division line xline2 ',xdiv*2);
WriteLn(Txt,'meshing division line yline2 ',ydiv*2);
WriteLn(Txt,'meshing division line zline2 ',zdiv*2);

WriteLn(Txt,'meshing types Block he20 chx60');
WriteLn(Txt);
WriteLn(Txt,'construct set InsY1 append surfaces s10');
WriteLn(Txt,'construct set InsX1 append surfaces s9');
if Form1.CheckBox3.Checked then
  begin
    WriteLn(Txt,'construct set InsY1 append surfaces s15');
    WriteLn(Txt,'construct set InsX1 append surfaces s14');
```

```
      end;

  if Form1.CheckBox2.Checked then
    begin
      WriteLn(Txt,'geometry sweep SoilY1 SoilY2 1 translate 0 ',tside,' 0');
      WriteLn(Txt,'geometry sweep InsY1 InsY2 1 translate 0 ',tside,' 0');
      WriteLn(Txt,'construct set SoilX1 append surfaces s',19+5*BotInd);
      WriteLn(Txt,'construct set InsX1 append surfaces s',24+6*BotInd);
      if BotInd=1 then WriteLn(Txt,'construct set InsX1 append surfaces s34');
      WriteLn(Txt,'construct set Soil append bodies b',4+BotInd);
      WriteLn(Txt,'construct set SideIns append bodies b',5+BotInd);
      if BotInd=1 then WriteLn(Txt,'construct set SideIns append bodies b7');

      WriteLn(Txt,'geometry sweep SoilX1 SoilX2 1 translate ',tside,' 0 0');
      WriteLn(Txt,'geometry sweep InsX1 InsX2 1 translate ',tside,' 0 0');
      WriteLn(Txt,'construct set Soil append bodies b',6+2*BotInd,' b',7+2*BotInd);
      WriteLn(Txt,'construct set sideIns append bodies b',8+2*BotInd,' b',9+3*BotInd);
      if BotInd=1 then WriteLn(Txt,'construct set sideIns append bodies b11 b13');

      WriteLn(Txt,'construct set SoilY2 append surfaces s',36+9*BotInd);
      WriteLn(Txt,'construct set InsY2 append surfaces s',45+14*BotInd);
      if BotInd=1 then WriteLn(Txt,'construct set InsY2 append surfaces s61');

      WriteLn(Txt,'meshing types sideIns he8 hx8ht');
    end
  else
    begin
      WriteLn(Txt,'geometry copy InsX1 InsX2 translate 0 0 0');
      WriteLn(Txt,'geometry copy InsY1 InsY2 translate 0 0 0');
      WriteLn(Txt,'geometry copy SoilX1 SoilX2 translate 0 0 0');
      WriteLn(Txt,'geometry copy SoilY1 SoilY2 translate 0 0 0');
    end;

  WriteLn(Txt,'geometry sweep SoilY2 SoilY ',SoilWdiv,' translate 0 ',wsoil,' 0');
  WriteLn(Txt,'construct set SoilX2 append surfaces
s',23+31*sideInd+7*BotInd+9*(sideInd and botInd));
  WriteLn(Txt,'geometry sweep SoilX2 SoilX ',soilWdiv,' translate ',wsoil,' 0 0');
  WriteLn(Txt,'construct set SoilY append surfaces
s',36+31*sideInd+7*BotInd+9*(sideInd and botInd));


  if (Boolean(botInd) and Boolean(sideInd)) then WriteLn(Txt,'construct set Soil append
bodies b14 b15 b16 b17 b18')
  else if Boolean(sideInd) then WriteLn(Txt,'construct set Soil append bodies b10 b11
b12 b13 b14')
  else if Boolean(botInd) then WriteLn(Txt,'construct set Soil append bodies b5 b6 b7')
```

143

```
      else WriteLn(Txt,'construct set Soil append bodies b4 b5 b6');

      if (Boolean(botInd) and Boolean(sideInd)) then
        WriteLn(Txt,'construct set soilBot append surfaces s27 s42 s44 s67 s69 s77 s79 s82')
      else if Boolean(sideInd) then WriteLn(Txt,'construct set soilBot append surfaces s22 s33
s35 s51 s53 s61 s63 s66')
      else if Boolean(botInd) then WriteLn(Txt,'construct set soilBot append surfaces s33 s39
s42')
      else WriteLn(Txt,'construct set soilBot append surfaces s26 s32 s35');

      WriteLn(Txt,'meshing types Soil he8 hx8ht');

      if (Boolean(botInd) and Boolean(sideInd)) then
        WriteLn(Txt,'construct set soilTop append surfaces s65 s68 s75 s78 s81')
      else if Boolean(sideInd) then WriteLn(Txt,'construct set soilTop append surfaces s49
s52 s59 s62 s65')
      else if Boolean(botInd) then WriteLn(Txt,'construct set soilTop append surfaces s31 s37
s40')
      else WriteLn(Txt,'construct set soilTop append surfaces s24 s30 s33');

      if Form1.CheckBox1.Checked then
        begin
          WriteLn(Txt,'geometry sweep BlockTop Top 1 translate 0 0 ',ttop);
          i:=7+botInd+8*sideInd+3*(sideInd and botInd);
          WriteLn(Txt,'construct set topIns append bodies b',i);
          WriteLn(Txt,'meshing types topIns he8 hx8ht');
        end
      else WriteLn(Txt,'geometry copy BlockTop Top translate 0 0 0');

      WriteLn(Txt,'construct set sideSur append surfaces InsX2 InsY2');
      WriteLn(Txt,'construct set topSur append surfaces Top');
      WriteLn(Txt,'geometry copy topSur topExt translate 0 0 0');
      WriteLn(Txt,'meshing types topExt qu4 bq4ht');
      WriteLn(Txt,'geometry copy sideSur sideExt translate 0 0 0');
      WriteLn(Txt,'meshing types sideExt qu4 bq4ht');
      WriteLn(Txt,'geometry copy soilTop soilExt translate 0 0 0');
      WriteLn(Txt,'meshing types soilExt qu4 bq4ht');
      WriteLn(Txt,'construct set soilFix append surfaces SoilX SoilY SoilBot');

      WriteLn(Txt,'meshing generate ');
      WriteLn(Txt,'meshing merge all 0.001');

      WriteLn(Txt,'property material concrete external external "',ConcFName,'"');
      WriteLn(Txt,'property material topBo flow boundary convecti ',topconv,' 0');
      WriteLn(Txt,'property material sideBo flow boundary convecti ',sideconv,' 0');
      WriteLn(Txt,'property material soilBo flow boundary convecti ',sideconv,' 0');
```

```
if Form1.CheckBox1.Checked then
  WriteLn(Txt,'property material topMat flow isotrop ',contop,' ',heattop);
if Form1.CheckBox2.Checked then
  WriteLn(Txt,'property material sideMat flow isotrop ',conside,' ',heatside);
if Form1.CheckBox3.Checked then
  WriteLn(Txt,'property material botMat flow isotrop ',conbot,' ',heatbot);
if Form1.CheckBox4.Checked then
  WriteLn(Txt,'property material SoilMat flow isotrop ',consoil,' ',heatsoil);

WriteLn(Txt,'property attach fBlock concrete');
WriteLn(Txt,'property attach Block concrete');
WriteLn(Txt,'property attach topExt topBo');
WriteLn(Txt,'property attach sideExt sideBo');
WriteLn(Txt,'property attach soilExt soilBo');
if Form1.CheckBox1.Checked then
  WriteLn(Txt,'property attach topIns topMat');
if Form1.CheckBox2.Checked then
  WriteLn(Txt,'property attach sideIns sideMat');
if Form1.CheckBox3.Checked then
  WriteLn(Txt,'property attach botIns botMat');
if Form1.CheckBox4.Checked then
  WriteLn(Txt,'property attach Soil SoilMat');

WriteLn(Txt,'property loads exttemp 1 sideExt ',ExtTemp);
WriteLn(Txt,'property loads exttemp 2 topExt ',ExtTemp);
WriteLn(Txt,'property loads exttemp 3 soilExt ',ExtTemp);

WriteLn(Txt,'property loads fixtemp 4 soilFix ',ExtTemp);
WriteLn(Txt,'property loads gravity 5 Block -9.81 3');
WriteLn(Txt,'construct tcurve tcdum list 0 1 601200 1');
for i:=1 to 5 do WriteLn(Txt,'property attach loadcase ',i,' tcdum');

WriteLn(Txt,'property boundary constraint s',12+5*BotInd,' z');
WriteLn(Txt,'property boundary constraint s',17+5*BotInd,' x');
WriteLn(Txt,'property boundary constraint s',14+5*BotInd,' y');

WriteLn(Txt,'property initial initemp all ',IniTemp);

WriteLn(Txt,'eye frame');
WriteLn(Txt,'utility write diana ',ShortName);
WriteLn(Txt,'yes');
WriteLn(Txt,'stop');
WriteLn(Txt,'yes');
WriteLn(Txt,'no');
Close(Txt);
```

```
   iDianaRun;
end;


procedure TForm1.Button1Click(Sender: TObject);
var
 i: Integer;
begin
 try
    a:=StrToFloat(Form1.Edit1.Text);
    b:=StrToFloat(Form1.Edit2.Text);
    c:=StrToFloat(Form1.Edit3.Text);
    IniTemp:=StrToFloat(Form1.Edit4.Text);
    ExtTemp:=StrToFloat(Form1.Edit5.Text);

    TopInd:=Integer(Form1.CheckBox1.Checked);
    SideInd:=Integer(Form1.CheckBox2.Checked);
    BotInd:=Integer(Form1.CheckBox3.Checked);
    SoilInd:=Integer(Form1.CheckBox4.Checked);

    if Form1.CheckBox1.Checked then
      begin
    ttop:=StrToFloat(Form1.Edit8.Text);
    contop:=StrToFloat(Form1.Edit9.Text);
    heattop:=StrToFloat(Form1.Edit10.Text);
      end
    else ttop:=0;
    if Form1.CheckBox2.Checked then
      begin
    tside:=StrToFloat(Form1.Edit11.Text);
    conside:=StrToFloat(Form1.Edit12.Text);
    heatside:=StrToFloat(Form1.Edit13.Text);
      end
    else tside:=0;
    if Form1.CheckBox3.Checked then
      begin
    tbot:=StrToFloat(Form1.Edit14.Text);
    conbot:=StrToFloat(Form1.Edit15.Text);
    heatbot:=StrToFloat(Form1.Edit16.Text);
      end
    else tbot:=0;
    if Form1.CheckBox4.Checked then
      begin
    tsoil:=StrToFloat(Form1.Edit17.Text);
    wsoil:=3;
    consoil:=StrToFloat(Form1.Edit18.Text);
```

```
      heatsoil:=StrToFloat(Form1.Edit19.Text);
        end
      else tsoil:=0;

      TopConv:=StrToFloat(Form1.Edit20.Text);
      SideConv:=StrToFloat(Form1.Edit21.Text);

      xdiv:=StrToInt(Form1.Edit22.Text);
      ydiv:=StrToInt(Form1.Edit23.Text);
      zdiv:=StrToInt(Form1.Edit24.Text);

      Soildiv:=408;
      SoilWdiv:=408;


      if FileExists(Edit6.Text) then ConcFName:=Edit6.Text
      else ShowMessage('Please check Concrete Property Input File!');
      WDir:=ExtractFileDir(Edit7.Text);

      for i:=1 to 4 do Pz[i]:=0;
      Px[1]:=0;
      Py[1]:=0;
      Px[2]:=a/2;
      Py[2]:=0;
      Px[3]:=0;
      Py[3]:=b/2;
      Px[4]:=a/2;
      Py[4]:=b/2;

      Generate;
   except

     ShowMessage('Please check numbers or file names!');
   end
end;

procedure TForm1.Button2Click(Sender: TObject);
begin
  OpenDialog1.InitialDir:=GetCurrentDir;
  //OpenDialog1.InitialDir:=Edit6.Text;
  if OpenDialog1.Execute then
  if FileExists(OpenDialog1.FileName) then
     Edit6.Text:=OpenDialog1.FileName;
end;

procedure TForm1.Button3Click(Sender: TObject);
```

```
begin
  //SaveDialog1.InitialDir:=Edit7.Text;
  SaveDialog1.InitialDir:=GetCurrentDir;
  if SaveDialog1.Execute then
  if not FileExists(SaveDialog1.FileName) then
    begin
      BatFName:=SaveDialog1.FileName+'.txt';
      DatFName:=SaveDialog1.FileName+'.dat';
      Edit7.Text:=DatFName;
      ShortName:=ExtractFileName(SaveDialog1.FileName);
    end
  else ShowMessage('File already exists, choose another name!');
end;


procedure TForm1.Button4Click(Sender: TObject);
begin
  ShowMessage('DIANA Input File Generator developed by Tu Anh Do, University of
Florida');
end;


procedure TForm1.Button5Click(Sender: TObject);
begin
  Close;
end;



end.
```

Codes of "DIFG.dpr" file

```
program DInterface;

uses
  Forms,
  DianaGen in 'DianaGen.pas' {Form1};

{$R *.res}

begin
  Application.Initialize;
  Application.CreateForm(TForm1, Form1);
  Application.Run;
end.
```